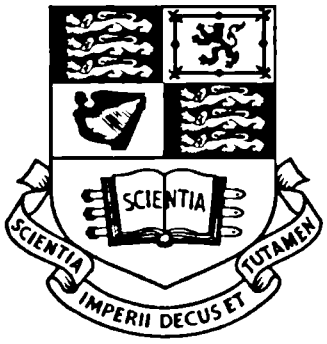
UNIVERSITY OF LONDON
IMPERIAL COLLEGE OF SCIENCE, TECHNOLOGY AND MEDICINE
DEPARTMENT OF ELECTRICAL AND ELECTRONIC ENGINEERING



THE DAMPING OF INTER-AREA OSCILLATIONS IN POWER SYSTEMS WITH CONTROLLABLE PHASE SHIFTERS

by

Ping Lam So, B. Eng. (Hons)

Thesis submitted for the Degree of
Doctor of Philosophy and the Diploma of
Imperial College in the Faculty of Engineering

April 1997

BIBL.
LONDIN
UNIV

ABSTRACT

Dynamic instability in the form of inter-area oscillations has been observed in many power systems. These low frequency (0.1-0.8 Hz) electromechanical oscillations can occur as a result of one group of generators swinging against another, or they can arise from a non-linear interaction among the power system natural modes of oscillation which can threaten the secure operation of the power system. The characteristics of these inter-area modes, and the factors influencing them, are not well understood. The analysis and control of these modes is often difficult as they can involve many generators in a complex interconnected system.

The factors affecting the damping characteristics of low frequency inter-area oscillations in an interconnected system have been investigated. The effects of system running arrangements, operating conditions, excitation systems, load characteristics and in particular the level of power transfer across the tie lines and machine loadings are examined. An understanding of their occurrence has been sought and alternative practical remedies have been tried in order to improve system damping. It is shown that a fast, fully controllable phase shifter (CPS) can damp the inter-area modes in an interconnected system. Inter-area oscillatory modes were identified and stabilized using a CPS. A decentralized control scheme, using tie-line power deviation as the feedback signal for the CPS controller, is shown to be effective in damping inter-area modes of oscillation under dynamic or transient disturbance conditions. Application of eigenvector (mode shape) analysis to identify the machines causing instability was examined. The best location for a CPS was identified using participation factors and the mode controllability. Based on the analysis of eigenvalue sensitivity, the CPS control parameters for damping inter-area modes of oscillation were determined. Computer simulation of an interconnected 8-machine 112-bus study system was used to validate the effectiveness of the proposed CPS controller. It is shown that with proper selection of CPS location and controller, just one CPS would suffice to introduce sufficient damping. The controller designed is found to be robust over a wide range of power transfers across the tie lines, thereby allowing the interconnected system to operate securely at higher power transfer levels.

A compensation-based phase shifter model is developed and included in the transmission system model. With the addition of appropriate control systems, the combined models can be used for power flow, dynamic (small disturbance) stability and transient (large disturbance) stability studies with no modification of the bus admittance matrix required at each iteration. This compensation method has the advantages of fast computational speed and low computer storage compared with that of modifying the bus admittance matrix method.

ACKNOWLEDGEMENTS

The work presented in this thesis has been carried out under the supervision of Dr. D.C. Macdonald, B.Sc.(Eng.), Ph.D., ACGI, C.Eng., FIEE, MIEEE, Senior Lecturer in the Department of Electrical and Electronic Engineering, Imperial College. I wish to thank Dr. Macdonald for his constant encouragement, keen interest and valuable guidance during the course of this research work.

I am especially indebted to Dr. B.J. Cory, Senior Research Fellow, Imperial College for his useful advice and valuable assistance.

Support from the Overseas Research Students Awards Scheme for the last two years of my research is gratefully acknowledged.

I must thank Dr. J.L. Jardim, Dr. A. Roman-Messina, Dr. C.A. Roa-Sepulveda and Dr. P.D.C. Wijayatunga for their helpful discussions and suggestions in the early stages of my research.

I would like to thank all members of the Energy and Electromagnetics Section for all the assistance they have provided to me during my three years at Imperial College.

Finally, my wife Cindy deserves special thanks for her great patience and support.

CONTENTS

		Page
ABSTRACT		2
ACKNOWLEDGEMENTS		4
CONTENTS		5
LIST OF FIGURES		8
LIST OF TABLES		12
NOMENCLATURE		13
CHAPTER ONE:	**INTRODUCTION**	
1.1	Inter-area oscillation problems	16
1.2	Review of inter-area oscillation problems	17
1.3	Analysis of inter-area oscillation problems	19
1.4	FACTS devices and mitigation of inter-area oscillation problems	20
1.5	Objectives	22
1.6	Original contributions	23
CHAPTER TWO:	**CONCEPTS OF A CONTROLLABLE PHASE SHIFTER (CPS) ON SYSTEM DAMPING ENHANCEMENT**	
2.1	Introduction	25
2.2	Principle of operation of a CPS	26
2.3	Dynamic power flow control	29
2.4	Concepts on system damping enhancement	32

Page

CHAPTER THREE: POWER SYSTEM MODELLING

3.1	Introduction	36
3.2	Power system representation	37
	3.2.1 Free response, mode shape and eigenvectors	39
	3.2.2 Participation factors	40
	3.2.3 Damping ratio	41
3.3	Synchronous machine model	42
3.4	Excitation system models	49
3.5	Speed-governing system model	52
3.6	Compensation-based controllable phase shifter model	53
	3.6.1 Steady-state power flow studies	56
	3.6.2 Dynamic stability studies	58
	3.6.3 Transient stability studies	63
3.7	Load models	64
	3.7.1 Static load models	64
	3.7.2 Dynamic load model	66
3.8	Network representation	69
3.9	Complete model of the interconnected system	71

CHAPTER FOUR: ANALYSIS OF INTER-AREA OSCILLATIONS

4.1	Introduction	74
4.2	Interconnected 8-machine system	74
4.3	Identification of machines causing instability	76
4.4	Analysis of factors affecting the damping of the inter-area mode	78
	4.4.1 Effect of tie-line flow	78
	4.4.2 Effect of tie-line impedance	80
	4.4.3 Effect of excitation systems	80
	4.4.4 Effect of load characteristics	81
	4.4.5 Effect of machine loadings	82
	4.4.6 Effect of generation rescheduling	83
4.5	Time simulation results	84

Page

CHAPTER FIVE: DAMPING INTER-AREA OSCILLATION USING A CONTROLLABLE PHASE SHIFTER

5.1 Introduction 110
5.2 Selection of a FACTS device 110
5.3 Selection of a feedback signal 111
5.4 Selection of CPS location 112
5.5 Design of CPS controller 118
5.6 Performance evaluation 123

CHAPTER SIX: CONCLUSIONS

6.1 General conclusions 132
6.2 Suggestions for future work 137

APPENDICES

Appendix A: Synchronous machine and controllers representation 139
A.1 Synchronous machine model 139
A.2 Excitation system models 143
A.3 Speed-governing system model 145

Appendix B: Controllable phase shifter representation 146

Appendix C: Load representation 152
C.1 Static load models 152
C.2 Induction motor model 153

REFERENCES 155

LIST OF FIGURES

		Page
2.1	Single-phase representation of a typical CPS	27
2.2	Phasor diagram for one phase of the CPS	28
2.3	Symbolic representation of a CPS	28
2.4	Block diagram for one phase of the CPS control system	28
2.5	Phase shifter equivalent circuit	29
2.6	Phase diagram of the phase shifter equivalent circuit	29
2.7	Typical control block diagram of a CPS	32
2.8	Simple single-machine infinite bus system with a CPS	33
3.1	Power system configuration showing two main subsystems	37
3.2	d-q axis synchronous machine model	42
3.3	Reference frame transformation	44
3.4	Structure of the complete power system model	46
3.5a	Fast-acting exciter model	49
3.5b	Slow-acting exciter model	50
3.6	Speed-governor model	52
3.7	Phase shifter equivalent circuit	54
3.8	Representation of a phase shifter in the transmission network	55
3.9	Equivalent circuit of a compensation-based phase shifter model	56
3.10	Phase shifter power injection model	57
3.11	Functional block diagram of the CPS with tie-line power feedback	59
3.12	Control system diagram of the CPS	60
4.1	Interconnected 8-machine 112-bus system under study	75
4.2	Inter-area mode shape with respect to rotor speed	77
4.3	Speed participation factors of the inter-area mode	78
4.4	Angle difference for a 2-bus system	79
4.5a	Rotor angle swings following a large disturbance	86
4.5b	Tie-line active power, voltage and current responses to a large disturbance	87
4.5c	Generators' active power output responses to a large disturbance	88

Page

4.5d Generators' terminal voltage responses to a large disturbance 89
4.6a Dynamic responses of rotor angle swings following a 1% step small disturbance 90
4.6b Dynamic responses of tie-line active power, voltage and current following a 1% step small disturbance 91
4.6c Dynamic responses of generators' active power output following a 1% step small disturbance 92
4.6d Dynamic responses of generators' terminal voltage following a 1% step small disturbance 93
4.7a Dynamic responses of rotor angle swings following a small disturbance of line switching 94
4.7b Dynamic responses of tie-line active power, voltage and current following a small disturbance of line switching 95
4.7c Dynamic responses of generators' active power output following a small disturbance of line switching 96
4.7d Dynamic responses of generators' terminal voltage following a small disturbance of line switching 97
4.8a Rotor angle swings following a large disturbance with reduction of G1 exciter gain by 33% 98
4.8b Tie-line active power, voltage and current responses to a large disturbance with reduction of G1 exciter gain by 33% 99
4.8c Generators' active power output responses to a large disturbance with reduction of G1 exciter gain by 33% 100
4.8d Generators' terminal voltage responses to a large disturbance with reduction of G1 exciter gain by 33% 101
4.9a Dynamic responses of rotor angle swings following a 1% step small disturbance with reduction of G1 exciter gain by 33% 102
4.9b Dynamic responses of tie-line active power, voltage and current following a 1% step small disturbance with reduction of G1 exciter gain by 33% 103
4.9c Dynamic responses of generators' active power output following a 1% step small disturbance with reduction of G1 exciter gain by 33% 104

Page

4.9d Dynamic responses of generators' terminal voltage following a 1% step small disturbance with reduction of G1 exciter gain by 33% 105
4.10a Dynamic responses of rotor angle swings following a small disturbance of line switching with reduction of G1 exciter gain by 33% 106
4.10b Dynamic responses of tie-line active power, voltage and current following a small disturbance of line switching with reduction of G1 exciter gain by 33% 107
4.10c Dynamic responses of generators' active power output following a small disturbance of line switching with reduction of G1 exciter gain by 33% 108
4.10d Dynamic responses of generators' terminal voltage following a small disturbance of line switching with reduction of G1 exciter gain by 33% 109
5.1 CPS damping controller circuit 113
5.2 Interconnected 8-machine 112-bus system with CPS 115
5.3 Performance of the CPS on the 132 kV tie line following a large disturbance 116
5.4 Performance of the CPS on the 66 kV tie line following a large disturbance 116
5.5 Performance of the CPS on the 132 kV tie line following a small disturbance of line switching 117
5.6 Performance of the CPS on the 66 kV tie line following a small disturbance of line switching 117
5.7 Decentralized output feedback CPS controller 120
5.8 Rotor speed mode shape of the inter-area mode with CPS 121
5.9 Variation of frequency and damping ratio when tie-line power transfer is increased from 110 MW to 190 MW 122
5.10 Rotor angle swings following a large disturbance with CPS 124
5.11 Tie-line active power and voltage responses to a large disturbance with CPS 125
5.12 Generators' active power output responses to a large disturbance with CPS 126

Page

5.13 Generators' terminal voltage responses to a large disturbance with CPS 127
5.14 Dynamic responses of rotor angle swings following a small disturbance of line switching with CPS 128
5.15 Dynamic responses of tie-line active power and voltage following a small disturbance of line switching with CPS 129
5.16 Dynamic responses of generators' active power output following a small disturbance of line switching with CPS 130
5.17 Dynamic responses of generators' terminal voltage following a small disturbance of line switching with CPS 131

LIST OF TABLES

		Page
4.1	Operating condition of the machines	75
4.2	System eigenvalues of the 8-machine system	76
4.3	Mode shape and participation factors of the inter-area mode	77
4.4	Effect of tie-line flow on the inter-area mode	79
4.5	Effect of tie-line impedance on the inter-area mode	80
4.6	Effect of excitation systems on the inter-area mode	81
4.7	Effect of load characteristics on the inter-area mode	82
4.8	Effect of machine G1 loadings on the inter-area mode	83
4.9	Effect of generation rescheduling on the inter-area mode	84
5.1	Base CPS control setting	114
5.2	Participation factors and controllability of CPS to the inter-area mode	114
5.3	Sensitivity coefficients of the inter-area mode	119
5.4	Summary of CPS control settings	120
5.5	Effect of CPS on the inter-area mode	120
5.6	Rotor speed mode shape of the inter-area mode with CPS	121
5.7	Effect of tie-line flow on the inter-area mode with CPS	122

NOMENCLATURE

A	system state matrix
AVR	automatic voltage regulator
b,c	mechanical torque equation constants
B	input matrix
c	subscript for CPS
CPS	controllable phase shifter
d-q	direct- and quadrature-axis in the machine reference frame
D	damping coefficient
D-Q	Direct- and Quadrature-axis in the network reference frame
e	error signal
E	magnitude of generator internal voltage
E'_q	quadrature-axis transient voltage
E''_d, E''_q	direct- and quadrature-axis subtransient voltages
E_{fd}	field voltage
E'_{mD}, E'_{mQ}	Direct- and Quadrature-axis transient voltages
EPRI	Electric Power Research Institute
f	frequency of oscillation in Hz
FACTS	Flexible AC Transmission Systems
g	subscript for generator
H	inertia constant
HVDC	high voltage direct current
I_c	vector of injected currents into the network due to CPS
I_d, I_q	direct- and quadrature-axis stator currents
I_g	vector of injected currents into the network due to generators
I_m	vector of injected currents into the network due to induction motor loads
J_1, J_2, J_3, J_4	submatrices of the Jacobian matrix
m	subscript for induction motor
max	maximum value
min	minimum value
n	number of generators in the power system
o	superscript for nominal value
p	number of CPS in the power system
P	tie-line active power

P_e	electrical power
P_{ki}	participation factor
P_m	mechanical power
P_{ref}	tie-line reference transfer power
PI	proportional plus integral controller
PSS	power system stabilizer
q	number of induction motors in the power system
R_a	armature resistance
R_1, R_2	stator and rotor resistances
S	slip
S_{ix}	real part of the relative sensitivity coefficient
SSR	subsynchronous resonance
STATCON	static condenser
SVC	static var compensator
t, t_{ik}	tap ratio magnitude
T	modal matrix, also superscript for transpose
T'_{do}	direct-axis transient open-circuit time constant
T''_{do}, T''_{qo}	direct- and quadrature-axis subtransient open-circuit time constants
T_e	electrical torque
T_m	mechanical torque
T'_o	rotor open-circuit time constant
TCPS	thyristor controller phase shifter
TCSC	thyristor controlled series capacitor
u	input vector
UPFC	unified power flow controller
v	right eigenvector of A
V	magnitude of the infinite bus voltage
V_c	vector of nodal voltages at CPS buses
V_d, V_q	direct- and quadrature-axis terminal voltages
V_g	vector of nodal voltages at generator buses
V_l	vector of nodal voltages at load buses
V_m	vectors of nodal voltages at induction motor load buses
$\overline{V}$	input voltage
$\overline{V}'$	output voltage
$\overline{V}_s$	quadrature voltage injection
w	left eigenvector of A
WSCC	Western Systems Coordinating Council

x	state variable vector
X_d, X_q	direct- and quadrature-axis synchronous reactances
X'_d, X'_q	direct- and quadrature-axis transient reactances
X''_d, X''_q	direct- and quadrature-axis subtransient reactances
X_o	open-circuit reactance
X_1, X_2	stator and rotor reactances
X_m	magnetizing reactance
X'	transient reactance
y	algebraic variable vector
$[Y_{bus}]$	bus admittance matrix
z	transformed state vector
α, α_{ik}	percentage of quadrature voltage injection, also damping factor
Δ	incremental deviation
δ	rotor angle, also angle between the rotor d-axis and the network D-axis reference frames
λ	eigenvalue (mode) of A
Λ	diagonal matrix of eigenvalues
ω	rotor speed, also frequency of oscillation in rad/s
ω_o	rated system frequency
ϕ	phase shift angle
ζ	damping ratio

CHAPTER ONE

INTRODUCTION

1.1 INTER-AREA OSCILLATION PROBLEMS

Power systems fall into natural areas in which load density and/or generation are high. Such areas are connected to each other by relatively weak tie-lines in order to deliver power and/or to provide more efficient operation and greater security.

System operators have usually been surprised when increasing spontaneous oscillations occurred in the level of power passing between areas accompanied by oscillations in frequency and voltage. The immediate response has usually been to reduce the power transfer and the oscillations then subsided. This is only an immediate solution and other methods have been sought to allow the tie lines to be used up to their full thermal limits. These instability problems have been experienced in many power systems [1-7]. Generator damper windings give a positive contribution to system damping but their effect at low frequencies is slight. Automatic voltage regulators (AVR) have the effect of increasing the synchronizing torque between interconnected generators but may contribute negative damping. Speed governors on generating units also can contribute negative damping, especially in hydro turbines. Large tie-line reactances (areas connected by weak tie-lines) and heavy tie-line power transfers result in large load angle differences between generators and can make negative damping more likely.

Inter-area mode oscillations occur at 0.1 to 0.8 Hz [8]. The analysis and control of these modes is very complex as they involve many generators in an interconnected system [9-11].

Inter-area mode oscillations are usually spontaneous [12] but they can be started by a small disturbance. When a small disturbance occurs, decaying oscillations usually follow. When system damping is inadequate or negative, even a minor disturbance may result in sustained or increasing oscillations. Such oscillations

are associated with the linear response of the system and represent natural modes of oscillation.

Inter-area mode oscillations have also been associated with the non-linear response of the system occurring when the system was subjected to large disturbances, such as the loss of a large load or a short-circuit on a transmission line. They may be caused by poorly tuned controls which act following large disturbances. Alternatively, they may be the result of a non-linear interaction of the natural modes of oscillation [13, 14].

The damping characteristics of inter-area mode oscillations are influenced by system structures, operating conditions, control effects and load characteristics [15-16].

Local mode oscillations involve a single generator, or a group of identical generators within a generation plant, swinging against the rest of the system. Local modes normally have frequencies in the range of 0.7 to 2.0 Hz [8]. Spontaneous local oscillations tend to occur when a very weak transmission link exists between a generator and its load centre, such as for an isolated generation plant sending power across a single long transmission line. Such system can usually be modelled by a single-machine infinite busbar. The characteristics of these local modes are well recognized and their stabilization through excitation control has been developed [17].

1.2 REVIEW OF INTER-AREA OSCILLATION PROBLEMS

A major inter-area oscillation was observed in 1964. A poorly damped inter-area mode gave 0.1 Hz oscillations in the Western U.S. power system (Western Systems Coordinating Council (WSCC)) [1]. These oscillations were primarily caused by the negative damping effect of hydro turbine governors on the inter-area mode between the Pacific Northwest (predominantly hydro) system and Pacific Southwest (predominantly steam) system, which were connected by weak (i.e. high impedance) 230 kV interties. In the first nine months of operation, over 100 tie-line separations occurred. Subsequent modification of hydro turbine governors provided damping to these oscillations but operation of the North-South ties was still limited. In 1968, a new 2000 MW 500 kV ac transmission

line and a new 1440 MW ±400 kV dc transmission line were installed. In service 1330 MW on the 500 kV ac line caused sustained oscillations at 0.33 Hz instead of 0.1 Hz previously. This new frequency was above the range that could be effectively controlled by governor action. Analysis showed that the AVR caused substantial negative damping. Power system stabilizers (PSS) were therefore installed on the AVR of all large generators. The frequency of oscillation of the WSCC system remained at 0.35 Hz and reasonably well damped by the PSS. During the 1980's, a new 0.7 Hz inter-area mode of oscillation was observed and is still present [7]. Increased intertie power transfers have contributed to the magnitude of oscillations and the poor damping of this new mode.

Other unstable inter-area oscillations have been reported [12]:

- Michigan-Ontario-Quebec 1959
- Saskatchewan-Manitoba-Ontario West 1962-1965
- Western U.S. (WSCC) 1964-1978
- Mid-Continent Area Power Pool (MAPP) 1971-1972
- Italy-Yugoslavia-Austria 1971-1974
- South East Australia 1975
- Scotland-England 1978
- Western Australia 1982-1983
- Taiwan 1984
- Hong Kong-South China 1984
- Ghana-Ivory Coast 1985
- Southern Brazil 1985-1987
- South Africa 1995

Inter-area oscillations have been accompanied by:

- High power flow over relatively weak interconnections
- High response excitation systems
- Light load conditions
- Heavy loading of particular machines for economic operation
- Depressed system voltage
- System loads of particular characteristics

The immediate remedial actions taken at the time when the oscillations occurred were:

- To reduce the tie-line flow
- To maintain the tie-line flow but relocate part of the generation from the highly loaded machines to others in the same area
- To open the interconnectors

Another interim measure was to reduce the AVR gain on the main generating units, but the inter-area oscillation problems have been largely overcome by the

- Addition of PSS on generating units
- Use of HVDC links instead of ac ties
- Installation of static Var compensators (SVC) at key locations

Utilities have recommended that [12]:

- Inter-area oscillation problems should be identified in planning and operating studies of the interconnected system
- PSS with high initial response excitation systems should be specified for all new generation plants
- Power system monitoring devices, designed to capture low frequency oscillations, should be installed throughout the system

1.3 ANALYSIS OF INTER-AREA OSCILLATION PROBLEMS

Analysis of global inter-area oscillation problems requires a detailed representation of the entire interconnected system [18]. In particular, accurate models are required for excitation systems and loads throughout the system. The analytical tools, in addition to determining the existence of problems, should be capable of identifying factors influencing these problems and providing information useful in developing control measures for their mitigation.

Inter-area oscillations that are essentially linear in nature can be analyzed using the linearized equations of the power system [6]. The technique is termed small disturbance or small signal stability analysis. Small signal stability is the ability

of the power system to maintain synchronism when subjected to small disturbances.

Small signal stability analysis is based on the linearization of the non-linear equations, which describe the dynamic behaviour of the power system, about a system operating point. The linearized system is then analyzed using eigenvalue techniques. Eigenvalue analysis is a powerful tool for analyzing the nature of oscillatory instability and providing information about the frequency and damping of each oscillation mode. Eigenvalue-based techniques can also provide information on damping ratios, mode shapes, participation factors, and eigenvalue sensitivities, which are useful in designing a controller to add damping to inter-area modes of oscillation. To verify the results obtained by eigenvalue analysis, the system dynamic performance can be checked using a fully non-linear transient stability model. With this complementary use of eigenvalue analysis and time domain simulation techniques, a better understanding of the nature of inter-area oscillation problems can be obtained.

A power system of n generators has (n-1) natural modes of oscillation, each with its own natural frequency and mode shape, that is the groups of generators acting together [19]. Most oscillatory modes between generators are positively damped and do not attract attention. Interest is centred on poorly damped inter-area modes which cause dynamic instability so that rotor oscillations may persist or increase in magnitude with time.

1.4 FACTS DEVICES AND MITIGATION OF INTER-AREA OSCILLATIONS PROBLEMS

System damping can be improved either by removing the causes of negative damping or by introducing positive damping to the system [20]. Measures taken to remove the causes of negative damping are usually expensive or severely restrict the operation of the power system. The reduction of power transfers across the tie lines as an emergency measure is economically undesirable. The reduction of gain on voltage regulators as an interim measure is at the expense of excitation system response. The building of new tie lines or the compensation of existing tie lines with series capacitors as a permanent solution to reduce tie-line reactances is very expensive and the latter can give

rise to other problems such as the excitation of torsional oscillations in turbine-generator shafts. Obviously, none of these measures are desirable and other measures are now taken to add positive damping to the system.

A number of power system devices have the potential of providing additional damping by supplementary control. The use of PSS has been recognized as an inexpensive means of enhancing the inter-area mode damping for interconnected systems [11, 21-25]. The PSS provides a supplementary stabilizing signal to control the excitation system of a generator in order to produce a positive damping torque [17]. Additionally, supplementary stabilizing signals can be used to modulate HVDC converter controls and SVC controls to enhance the damping of inter-area modes [26-27]. In today's power systems, many HVDC links and SVC installations are equipped with special modulation controls to stabilize inter-area oscillations.

In recent years, problems associated with environmental issues, right-of-way restrictions, regulatory pressures and high costs have delayed the construction of new transmission lines, while the demand for electric power has continued to grow. This trend has forced power utilities, manufacturers and researchers to re-evaluate their conventional reinforcement strategy. In order to achieve greater operating flexibility and better utilization of existing transmission systems, the concept of FACTS (Flexible AC Transmission Systems) was introduced in 1988 by Dr. N.G. Hingorani from the Electric Power Research Institute (EPRI) in the USA [28-30]. The philosophy of FACTS is to use power electronic controlled devices to control power flows in a transmission network, thereby allowing ac transmission lines to be loaded to their full capability [31]. The use of FACTS technology is attractive since FACTS devices can be retrofitted to existing ac transmission routes, holding out the possibility of an economic solution.

With the development of high power thyristors, fast and reliable control of FACTS devices have become feasible. Currently, the main control actions in a power system, such as changing transformer taps, switching series and shunt reactive compensation, are achieved through the use of mechanical devices, which impose a limit on the speed at which control action can be made. FACTS devices based on solid-state control are capable of control actions at much higher speed. The three parameters that control transmission line power flow are the transmission line impedance, the magnitude and phase angle of line end voltages.

Conventional control of these parameters, although adequate during steady state or slowly changing load conditions, cannot be achieved quickly enough to handle dynamic or transient system conditions. The ability of FACTS devices to control the power flow rapidly can considerably improve the dynamic and transient stability of power systems.

Power electronic controlled devices, such as SVC, have been used for many years in transmission networks for voltage control and stability enhancement [32]. Other main FACTS devices, which are in advanced stages of development and/or implementation, are the thyristor controlled series capacitor (TCSC) [33], the thyristor controlled phase shifter (TCPS) [34], the unified power flow controller (UPFC) [35] and the static condenser (STATCON) [36]. FACTS devices, such as SVC, TCSC, TCPS and UPFC, can be effectively controlled to damp power system oscillations [37-41] and, depending on the power system configuration and nature of the inter-area oscillations, can be used as cost-effective measures to mitigate inter-area oscillation problems [42].

1.5 OBJECTIVES

The objectives of this research were:

(i) to analyse the factors affecting the damping characteristics of low frequency inter-area oscillations in an interconnected system. The effects of system running arrangements, operating conditions, excitation systems, load characteristics and in particular power transfers across the tie lines and machine loadings were examined. The analysis attempts to develop a better understanding of their occurrence and hence alternative practical remedies are investigated in order to improve system damping.

(ii) to design a damping controller for a fast, fully controllable phase shifter (CPS) to stabilize poorly damped or unstable inter-area oscillatory modes in an interconnected system. A decentralized control scheme using tie-line power deviation as the feedback signal for the CPS controller was proposed.

(iii) to develop techniques for the analysis and control of inter-area oscillations in an interconnected multimachine system. Eigenvalue techniques based on small signal stability analysis were utilized to analyze problems associated with spontaneous inter-area oscillations, and design a supplementary stabilizing loop for the CPS controller to add damping to inter-area oscillations. A linearized interconnected system model equipped with CPS was derived. Inter-area modes were first identified for an oscillatory incident and then stabilization of these modes using a CPS was obtained. Application of eigenvector (mode shape) analysis to identify the machines involved in the instability was examined. The optimum location for installing a CPS was identified using participation factors and the mode controllability. By using eigenvalue sensitivity analysis techniques, the CPS control parameters for damping inter-area modes of oscillation were determined. The effectiveness of the CPS controller for damping inter-area oscillations caused by small and large disturbances was verified by computer simulation of an interconnected 8-machine 112-bus study system.

1.6 ORIGINAL CONTRIBUTIONS

The original contributions of this thesis are thought to be:

(i) An analytical investigation of factors influencing the damping characteristics of low frequency inter-area oscillations in an interconnected system was reported. The findings give an insight into the nature of these oscillations, leading to the understanding of their characteristics and the development of remedial actions.

(ii) A linearized state-space model of an interconnected system was developed to analyze the dynamic interactions of its various components across the interconnected network. The model includes a detailed description of the synchronous machines with their associated controls, the interconnected network and the loads. It also considers the representation of synchronous machines and CPS as dynamic subsystems which interact through the interconnected network.

(iii) The application and development of eigenvalue analysis to analyze the system oscillation behaviour and design a stabilizing control function for the CPS controller was accomplished. A successful simulation of such a controller to enhance the dynamic stability of an interconnected system was made.

(iv) A compensation-based phase shifter model was introduced and included in the transmission system model. By using compensation injected currents at terminal buses to simulate a phase shifter the symmetry property of the bus admittance matrix was maintained. This compensation method has the advantages of fast computational speed and low computer storage compared with that of modifying the bus admittance matrix method.

(v) A clear concept of how a CPS functions to increase system damping was developed. This can be illustrated by using a simplified single-machine infinite bus system model to study the dynamic interaction between generator and CPS states.

(vi) A CPS equipped with a feedback controller using tie-line power deviation was designed. The scheme was found to be effective in damping inter-area oscillations. This type of decentralized controller is of practical interest as the feedback control signal is locally available and no remote data transmission is required.

(vii) A method for locating a CPS was proposed. This method, based on participation factor and mode controllability analysis, identifies the most effective location for controlling the critical inter-area mode.

(viii) A systematic procedure for the design of a FACTS controller to add damping to inter-area oscillations was established. The tasks include:

- Selection and modelling of a FACTS device
- Development of control strategies
- Selection of controller location and feedback signal(s)
- Determination of the controller parameters
- Simulation

CHAPTER TWO

CONCEPTS OF A CONTROLLABLE PHASE SHIFTER (CPS) ON SYSTEM DAMPING ENHANCEMENT

2.1 INTRODUCTION

For many years phase shifters (quadrature boosters) have been used in power systems as control equipment to regulate power flows [43-45]. In the UK, for example, the National Grid Company has installed seven 2000 MVA 400 kV quadrature boosters to control power sharing in the lines between the North and Midlands, with an additional three quadrature boosters to be installed over the next two-three years [46]. In the USA, from 1965 to 1991 phase shifters were installed at about eighteen sites within the WSCC region to control transmission line flows [47]. A very comprehensive description of conventional (mechanical) phase-angle regulating transformers can be found in [48]. Operation of a conventional phase shifter is characterized by [34]

(i) low response time as a result of the inertia of moving parts, and

(ii) high level of maintenance due to mechanical contacts and oil deterioration.

The slow-speed action of the on-line tap changer precludes the use of phase shifters for improving the dynamic and transient stability of power systems. So far, phase shifters are limited to control of the power flow distribution in a network.

Recently, the advent of high power thyristors has led to the development of controllable (thyristor controlled) phase shifters (discussed in Section 1.4). The above mentioned drawbacks of a conventional phase shifter can be overcome by the replacement of mechanical switches with thyristor valves, thereby increasing the response speed of the phase shifter. This leads to the further consideration and application of phase shifters in power systems.

Over the last two decades, considerable research effort has been devoted to the use of controllable phase shifters (CPS) to improve the power system performance during steady state, dynamic state and transient state conditions. References [49-53] discuss the applications of CPS in steady state power flow control, line loss reduction and alleviation of line overloads. Many authors have demonstrated that electromechanical oscillations resulting from small or large disturbances can be effectively damped using additional stabilizing loops in CPS control systems [10, 38-41, 52, 54-61]. In [62], a systematic procedure for the control design of a multimachine power system including CPS is provided. This method is suitable for assessing transient stability because it includes the phase-shifter dynamics and the main system non-linearities. In [57, 59, 63-64], the simulation of a CPS for damping torsional oscillations of subsynchronous resonance (SSR) which may occur in machines connected to long series capacitor compensated transmission lines is presented. The high speed response of CPS can also be utilized to improve power system transient stability [54, 58, 59, 65-67].

2.2 PRINCIPLE OF OPERATION OF A CPS

Figure 2.1 shows the schematic diagram of one phase of a typical CPS [68]. The excitation transformer is connected in delta on the primary and has four secondary windings whose voltages are in the ratio of 1 : 3 : 9 : 27. These windings feed the associated sub-converters Z1, Z3, Z9 and Z27. Each sub-converter is a bridge circuit with anti-parallel thyristors in each arm of the bridge. The function of the sub-converters is of changeover switches that connect the input through to the output of the converter either

- direct (valve pairs 1 and 2 conducting), or
- with reversed polarity (valve pairs 3 and 4 conducting),
- or it is prevented from reaching the output which is short-circuited (valve pairs 1 and 4 or 3 and 2 conducting).

Depending on the mode of operation (boosting or bucking), the resultant output voltage of the converter can be adjusted in 40 equal steps from zero to either the positive or negative maximum value.

The delta-star transformer gives the voltage $\overline{E}$ 90^{o} out of phase with the system line-neutral voltage $\overline{V}$. The former is then injected, via the converter and boosting transformer, into the line as a quadrature voltage $\overline{V}_s$, which causes a phase shift ϕ of the output voltage $\overline{V}'$ with respect to the input voltage $\overline{V}$ (Figure 2.2). The direction of the phase shift depends upon whether the injected quadrature voltage $\overline{V}_s$ is leading or lagging of the system voltage $\overline{V}$. The converter controls the magnitude and lead-lag of the injected quadrature voltage $\overline{V}_s$.

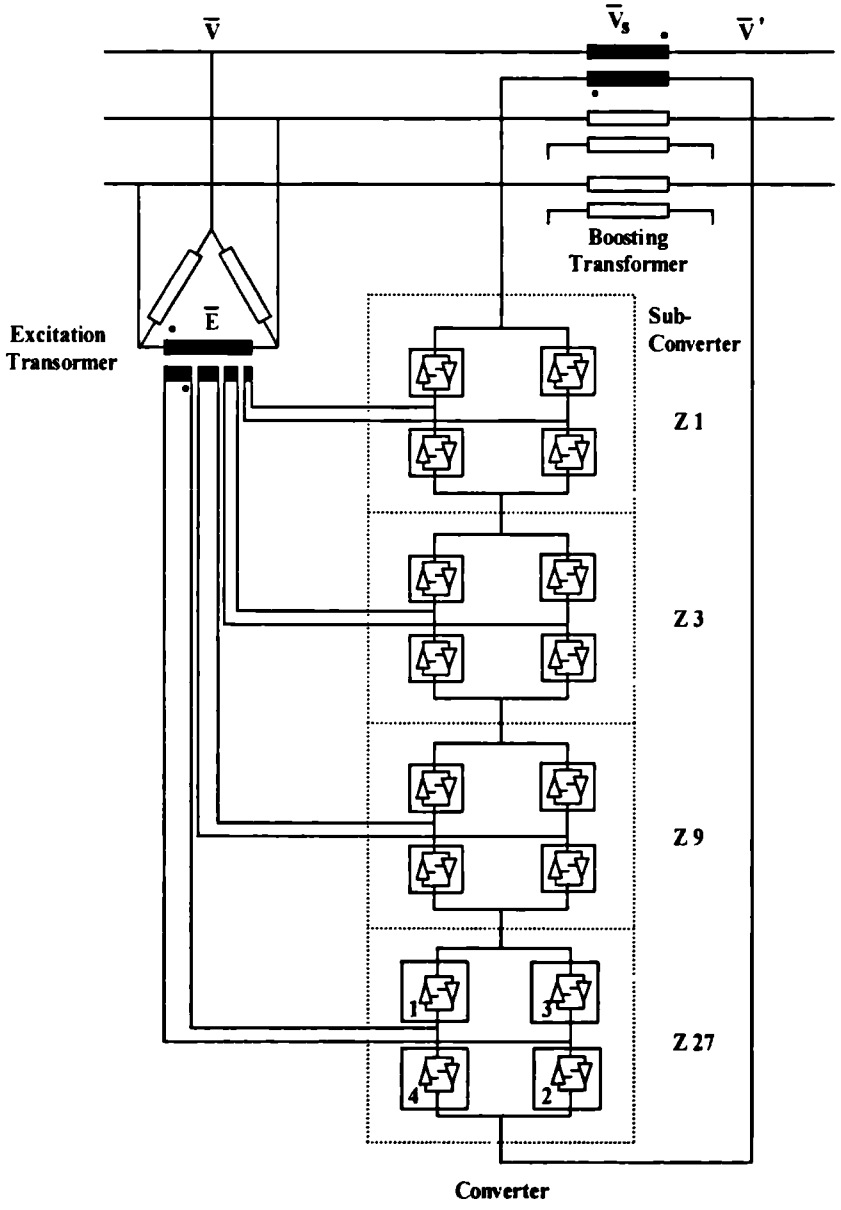


Figure 2.1 Single-phase representation of a typical CPS

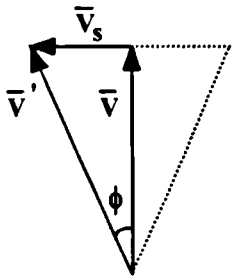


Figure 2.2 Phasor diagram for one phase of the CPS

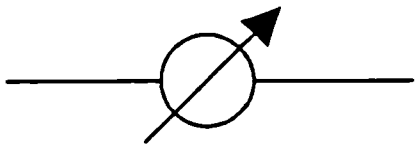


Figure 2.3 Symbolic representation of a CPS

Figure 2.4 shows the block diagram of the control system of one phase of a CPS. The measured feedback signal(s) and system variables are fed into the controller block and firing control circuits respectively. The controller block determines the magnitude and lead-lag of the injected quadrature voltage $\bar{V}_s$. Based on the signal from the controller block, the firing control circuits generate the gate pulses for the thyristor valves.

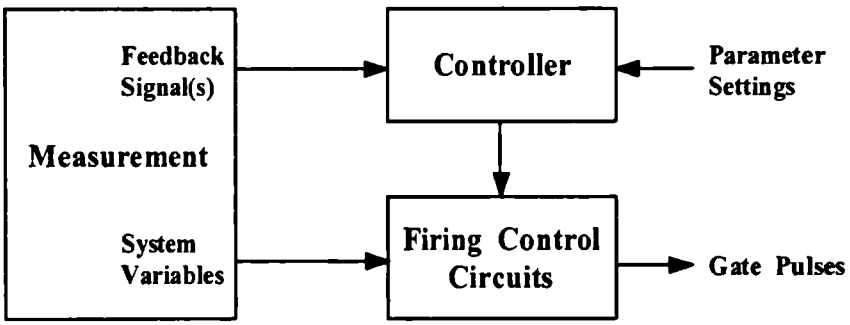


Figure 2.4 Block diagram for one phase of the CPS control system

2.3 DYNAMIC POWER FLOW CONTROL

The function of a fast-acting phase shifter is to control the phase angle of line end voltages in real time by injecting a continuously adjustable quadrature voltage in the line. A phase shifter connected between nodes i and k with a complex tap ratio $1 : t_{ik}\, e^{j\phi}$ in series with its reactance jx can be represented by the equivalent circuit, as shown in Figure 2.5.

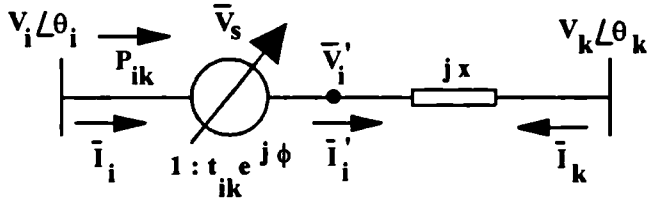


Figure 2.5 Phase shifter equivalent circuit

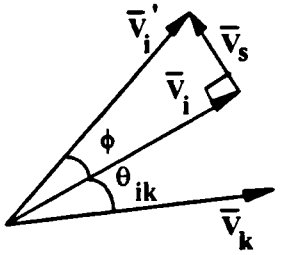


Figure 2.6 Phase diagram

$\bar{I}_i$ and $\bar{I}_k$ are the complex phase shifter currents at nodes i and k, $\bar{V}_i$ and $\bar{V}_k$ are the complex voltages at nodes i and k, and $\bar{V}_i'$ is the virtual voltage behind the series reactance. The phasor diagram of the phase shifter equivalent circuit is shown in Figure 2.6.

From Figures 2.5 and 2.6, it can be shown that

$$\begin{aligned} \bar{V}_i' &= \bar{V}_i + \bar{V}_s \\ &= t_{ik}\, e^{j\phi}\, \bar{V}_i \\ &= (1 + j\alpha_{ik})\, \bar{V}_i \end{aligned} \tag{2.1}$$

where $t_{ik} = \sqrt{1+\alpha_{ik}^2}$ is the tap ratio magnitude and $\phi = \tan^{-1}\alpha_{ik}$ is the phase shift angle. This means that the output voltage $\bar{V}_i'$ is equal to the input voltage $\bar{V}_i$ plus a voltage $\bar{V}_s$ in quadrature with and proportional to the input voltage $\bar{V}_i$. The constant of proportionality is α_{ik} limited to $-\alpha_{ik(\min)} \le \alpha_{ik} \le \alpha_{ik(\max)}$. A CPS is modelled by inserting a controllable quadrature voltage $\bar{V}_s = j\alpha_{ik}\, \bar{V}_i$ (its

magnitude equal to $\alpha_{ik} V_i$) in the line. If V_i is equal to the rated voltage (i.e. $V_i = 1.0$ p.u.), the magnitude of the injected quadrature voltage would be controlled by α_{ik}.

Neglecting the power losses in the phase shifter and according to the energy conservation law, the following equation holds

$$\bar{V}_i \bar{I}_i^* = \bar{V}_i' \bar{I}_i'^* \tag{2.2}$$

or

$$\bar{I}_i = \frac{\bar{V}_i'^*}{\bar{V}_i^*} \bar{I}_i' \tag{2.3}$$

The current $\bar{I}_i'$ is

$$\bar{I}_i' = \frac{(\bar{V}_i' - \bar{V}_k)}{jx} = -\bar{I}_k \tag{2.4}$$

$$= \frac{(t_{ik} e^{j\phi} \bar{V}_i - \bar{V}_k)}{jx} = -\bar{I}_k$$

Substituting equations (2.1) and (2.4) into (2.3) gives

$$\bar{I}_i = t_{ik} e^{-j\phi} \frac{(t_{ik} e^{j\phi} \bar{V}_i - \bar{V}_k)}{jx} \tag{2.5}$$

$$= \frac{(t_{ik}^2 \bar{V}_i - t_{ik} e^{-j\phi} \bar{V}_k)}{jx}$$

Considering equations (2.4) and (2.5), the following two-terminal network equation in the matrix form can be obtained:

$$\begin{bmatrix} \bar{I}_i \\ \bar{I}_k \end{bmatrix} = \frac{1}{jx} \begin{bmatrix} t_{ik}^2 & -t_{ik}\, e^{-j\phi} \\ -t_{ik}\, e^{j\phi} & 1 \end{bmatrix} \begin{bmatrix} \bar{V}_i \\ \bar{V}_k \end{bmatrix} \tag{2.6}$$

The complex power at node i is given by

$$\bar{S}_i = \bar{V}_i \bar{I}_i^* \tag{2.7}$$

$$= j \frac{(t_{ik}^2 V_i^2 - V_i V_k t_{ik} e^{j(\theta_{ik}+\phi)})}{x}$$

The real part of $\bar{S}_i$ corresponds to

$$P_{ik} = \frac{V_i V_k t_{ik}}{x} \sin(\theta_{ik} + \phi) \tag{2.8}$$

$$= \frac{V_i V_k}{x} (\sin\theta_{ik} + \alpha_{ik} \cos\theta_{ik})$$

where P_{ik} is the controllable power flow through the line and $\theta_{ik} = \theta_i - \theta_k$. Since the output voltage phasor $\bar{V}_i'$ can be moved with respect to the input voltage phasor $\bar{V}_i$ by inserting a controllable quadrature voltage phasor $\bar{V}_s$ (see Figure 2.6), the phase shift angle ϕ can be adjusted and thus the transmitted power P_{ik} can be controlled (see Equation 2.8).

Figure 2.7 shows a typical block representation of the controllers used for the CPS. During steady state conditions, the main (power flow) controller uses active power P_m as the feedback signal. The measured power signal is compared with the reference transfer power signal P_{ref}, and the error signal Δe

is generated. The magnitude of the injected quadrature voltage α is determined based on the error signal Δe. Hence, the PI controller can dynamically regulate the power flow across the device and then through the equipped line by forcing and keeping the power error to zero.

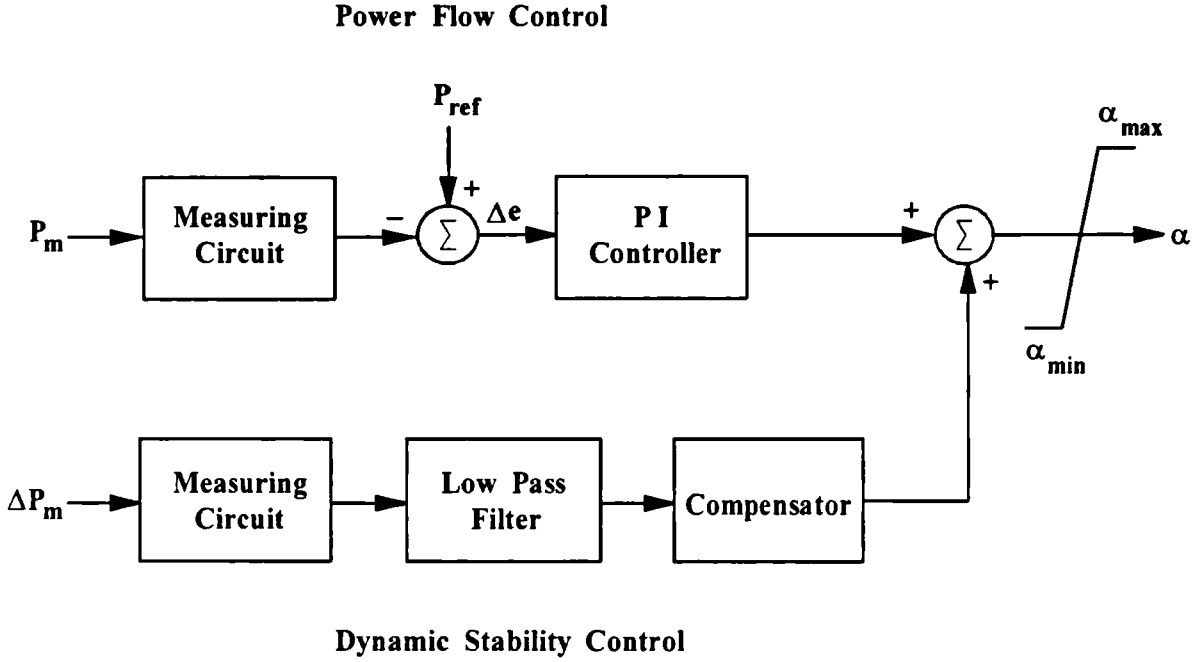


Figure 2.7 Typical control block diagram of a CPS

2.4 CONCEPTS ON SYSTEM DAMPING ENHANCEMENT

The idea of using a CPS to provide system damping is based on its capability to modulate the power flow on the transmission line. It is generally assumed that this power modulation can cause a corresponding variation of the torques of the connected generators. If the prime movers of the generators have constant torques, this assumption is obviously correct [69].

Consider the simple model of a single-machine infinite bus system with a CPS shown in Figure 2.8. On the basis of this model, the additional damping contributed by the CPS to the system is analysed.

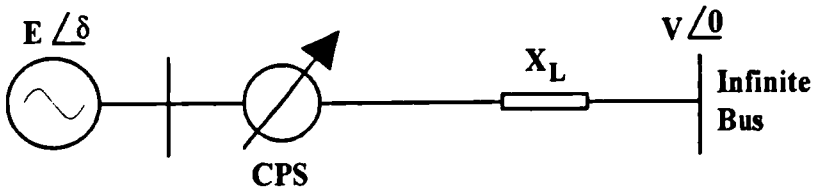


Figure 2.8 Simple single-machine infinite bus system with a CPS

As shown in Section 2.3, the controllable power flow through the transmission line is given by

$$P_e = \frac{EVt}{X_L}\sin(\delta + \phi) \tag{2.9}$$

$$= \frac{EV}{X_L}(\sin\delta + \alpha\cos\delta)$$

where E is the magnitude of the generator internal voltage, V is the magnitude of the infinite bus voltage, X_L is the transmission line reactance, t is the tap ratio magnitude, ϕ is the phase shift angle, α is the magnitude of injected quadrature voltage, and δ is the generator rotor angle (the power angle between the generator internal voltage and the infinite bus voltage).

The dynamic behaviour of the system can be described by

$$\frac{2H}{\omega_o}\frac{d^2\delta}{dt^2} = P_m - P_e(\alpha,\delta) \tag{2.10}$$

$$= P_m - \frac{EV}{X_L}(\sin\delta + \alpha\cos\delta)$$

where H is the generator inertia constant, ω_o is the rated system frequency, P_m is the mechanical power input to the generator, and P_e is the electrical power (controllable) transfer to the infinite bus. It is assumed that the mechanical

power input P_m remains constant during periods of CPS control action since the response of the latter is high speed compared to the prime mover governor.

For small disturbances, assuming constant mechanical power (P_m = constant) and expressing the change in electrical power P_e in terms of the (controllable) magnitude of the injected quadrature voltage α and the rotor angle δ (refer to Equation (2.9)), equation (2.10) can be written as [70]

$$\frac{2H}{\omega_o}\frac{d^2(\Delta\delta)}{dt^2} + \frac{\partial P_e}{\partial \alpha}\Delta\alpha + \frac{\partial P_e}{\partial \delta}\Delta\delta = 0 \tag{2.11}$$

Inspection of equation (2.11) indicates that, if the magnitude of the injected quadrature voltage is constant (α = constant and $\Delta\alpha = 0$), the rotor angle $\Delta\delta$ would oscillate undamped with a frequency of

$$\omega_n = \sqrt{\frac{\omega_o}{2H}\frac{\partial P_e}{\partial \delta}} \tag{2.12}$$

In order to provide damping, the magnitude of the injected quadrature voltage must be varied as a function of the rate of change of the rotor angle $d(\Delta\delta)/dt$, that is

$$\Delta\alpha = K\frac{d(\Delta\delta)}{dt} \tag{2.13}$$

where K is a constant.

Rotor angle changes, of course, result in frequency and real power variations. The usual suggestion has been that the variation of the system frequency or the transmitted real power is measured and used as the feedback signal for the CPS controller. A typical damping control scheme that utilizes an additional

stabilizing loop in the CPS control system is shown in Figure 2.7. The auxiliary (dynamic stability) controller uses line power deviation ΔP_m as the feedback signal. The signal is passed through a measuring circuit, a low pass filter, and then its phase shift is adjusted by the compensator to produce the required α to modulate the line power flow so as to aid system damping.

In this study, a control strategy that utilizes line power deviation feedback and a CPS to continuously modulate the line power flow by injecting a controllable quadrature voltage in the system is adopted. The control policies are

(i) During periods when the generator is accelerating (i.e. detecting that $d\delta/dt > 0$), the phase shift angle ϕ is made more positive (refer to Equation 2.9) thus increasing the line power transfer in order to compensate for the excess mechanical power and thereby to oppose the acceleration of the generator.

(ii) Similarly, during periods when the generator is decelerating (i.e. detecting that $d\delta/dt < 0$), the phase shift angle ϕ is made smaller (or negative) (refer to Equation 2.9) thus decreasing the line power transfer in order to cater for a decrease in mechanical power and thereby to oppose the deceleration of the generator.

Control action of this nature (i.e. the phase shift angle ϕ swings between its positive and negative ranges) will inherently damp rotor oscillations and thus reduce the risk of dynamic instability.

CHAPTER THREE

POWER SYSTEM MODELLING

3.1 INTRODUCTION

The aim here in modelling a power system is to provide a facility with which the performance of the system can be evaluated and to provide a basis from which controllers can be designed. For more than 30 years, many methods [71-80] have been proposed to represent the synchronous machines with their associated controls, the power network and the loads.

Eigenvalue analysis in the frequency domain, using modal techniques [81], has been widely employed for the study of inter-area oscillations and the design of controls to aid in the damping of these oscillations. This technique [82, 83] can show

(i) All modes clearly separated and identified by the eigenvalues.

(ii) The eigenvalue associated with each mode giving the characteristic frequency and the damping factor.

(iii) The mode shapes, participation factors, mode controllability and eigenvalue sensitivities, which are useful for control design.

For the analysis and control of inter-area oscillations, a linearized model of an interconnected system with CPS is developed by using small signal linearization around a nominal operating point. This model is convenient for the evaluation of system dynamic performance and stability studies when conventional forms of control are utilized and it also enables new forms of controllers to be developed using concepts of modern control theory.

Non-linear time domain simulations, using the implicit trapezoidal integration method, are utilized to verify the results obtained by eigenvalue analysis. The implicit trapezoidal method of integration has been recognized as being very

powerful for solving the differential equations due to its speed, numerical stability, accuracy and ease of implementation [84].

3.2 POWER SYSTEM REPRESENTATION

A linearized state-space model of an interconnected multimachine system is developed to analyze the dynamic interactions of its various components across the interconnected network. The model includes a detailed description of the synchronous machines with their excitation and governor controls, the CPS, the static and dynamic loads, and the interconnected network. It also considers the representation of synchronous machines and CPS as dynamic subsystems which interact with one another through the interconnected network (see Figure 3.1). The nature of interaction between dynamic subsystems is used to describe the impact of CPS on system damping enhancement [85]. In the development of this model, emphasis is placed on the systematic formulation of the complex interconnected system model from the basic subsystem equations.

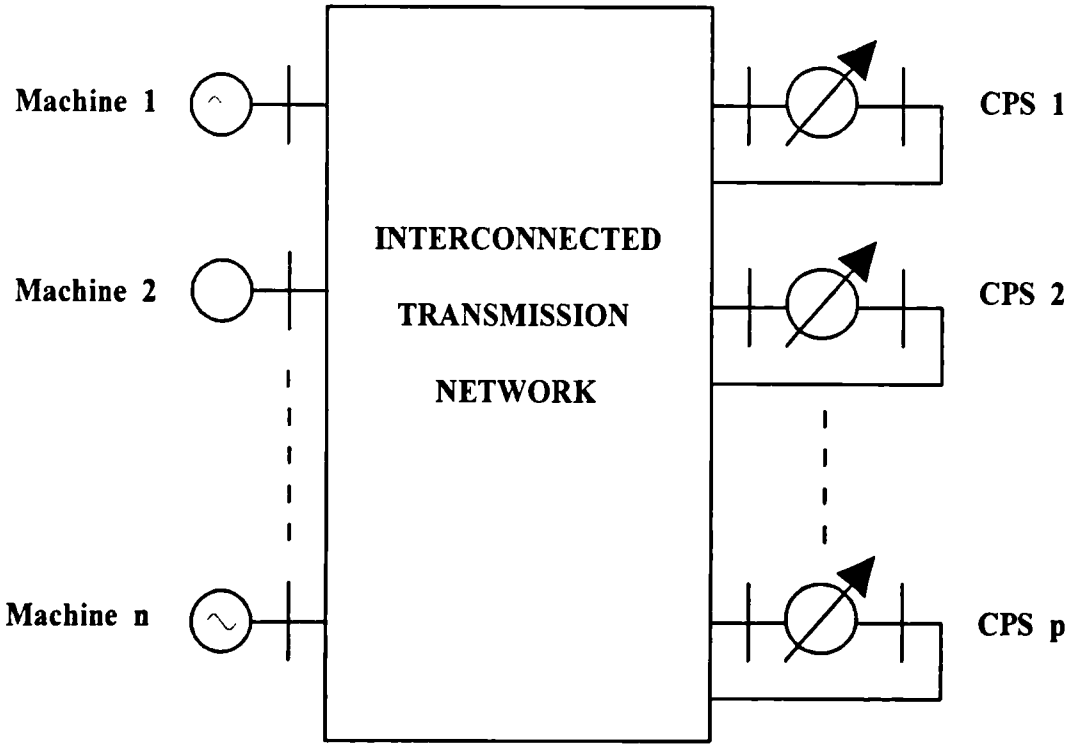


Figure 3.1 Power system configuration showing two main subsystems

For this dynamic stability study, machine stator, CPS and network transients are neglected. The entire interconnected system can be represented by a set of differential equations together with a set of algebraic equations [86]

$$\dot{x} = f(x, y, u) \tag{3.1}$$

$$0 = g(x, y, u) \tag{3.2}$$

where x is a vector of state variables, y is a vector of algebraic variables and u is the control input vector. Small signal stability analysis involves the linearization of equations (3.1) and (3.2) around a system operating point

$$\begin{bmatrix} \Delta \dot{x} \\ 0 \end{bmatrix} = \begin{bmatrix} J_1 & J_2 \\ J_3 & J_4 \end{bmatrix} \begin{bmatrix} \Delta x \\ \Delta y \end{bmatrix} + \begin{bmatrix} B_1 \\ B_2 \end{bmatrix} \Delta u \tag{3.3}$$

where J_1, J_2, J_3 and J_4 are submatrices of the Jacobian matrix. The linearized dynamic system can be obtained by eliminating the vector of algebraic variables Δy in equation (3.3)

$$\Delta \dot{x} = A \Delta x + B \Delta u \tag{3.4}$$

where $A = J_1 - J_2 J_4^{-1} J_3$ and $B = B_1 - J_2 J_4^{-1} B_2$. When no phase shifting action of a CPS is considered ($\Delta u = 0$), A represents the open-loop system state matrix, whose eigenvalues determine the stability of the non-linear system. When a CPS design is to be considered, the input vector is given by the CPS control variable to modulate the line power flow in order to enhance system damping. The phase shift angle ϕ of the CPS is taken as a control variable. In order to include the dynamic of the CPS in the controller design, the change in the phase shift angle $\Delta\phi$ is also considered as a state variable. For low frequency oscillation studies, matrix A is real-valued, non-symmetric and exhibits some degree of sparsity [86]. Matrix B defines the impact of phase shifting

action on the generator states, and depends on (i) CPS location, (ii) CPS size, (iii) system operating conditions. The state and input vectors in equation (3.4) are given by

$$x = [x_{g1}^T, x_{g2}^T, \ldots, x_{gi}^T, \ldots, x_{gn}^T, x_{c1}^T, x_{c2}^T, \ldots, x_{ci}^T, \ldots, x_{cp}^T]^T \tag{3.5}$$

$$u = [\phi_{c1}, \phi_{c2}, \ldots, \phi_{ci}, \ldots, \phi_{cp}]^T \tag{3.6}$$

The vectors x_{gi} and x_{ci} include the state variables of the i-th machine and i-th CPS respectively. The element ϕ_{ci} of the input vector u represents the control variable of the i-th CPS.

3.2.1 FREE RESPONSE, MODE SHAPE AND EIGENVECTORS

The free motion (with zero input) is given by the reduced state equation (3.4):

$$\Delta \dot{x} = A \Delta x \tag{3.7}$$

The nature of the free motion of the system described by equation (3.7) following a disturbance can be described in terms of the eigenvalues, and the right and left eigenvectors of the system matrix A [87]. It is well-known [87] that if A has N distinct eigenvalues λ_i $(i = 1,2,\ldots..,N)$, then equation (3.7) has a solution of the form

$$x(t) = \sum_{i=1}^{N} e^{\lambda_i t} v_i w_i x(0) \tag{3.8}$$

where λ_i is the i-th eigenvalue

v_i is the i-th right eigenvector of the system matrix A satisfying

$$A v_i = \lambda_i v_i \tag{3.9}$$

w_i is the i-th left eigenvector of the system matrix A satisfying

$$w_i A = \lambda_i w_i \tag{3.10}$$

Equation (3.8) clearly shows that the free motion time response of the system governed by equation (3.7) is a linear combination of N functions of the form $e^{\lambda_i t} v_i$ $(i = 1,2,\ldots..,N)$ which describe the N natural modes of the system. Thus, the "shape" of a mode is described by its associated right eigenvector v_i and its time domain characteristics by its associated eigenvalue λ_i. Mode shape analysis is useful in identifying the machines involved in a particular oscillation mode.

3.2.2 PARTICIPATION FACTORS

In [88] a dimensionless measure of state variable participation in a mode i is obtained by examining the right eigenvector v_i, and the associated left eigenvector w_i. The participation of the k-th state variable x_k in the i-th mode can be measured through its "participation factor"

$$P_{ki} = v_{ki} w_{ki} \tag{3.11}$$

where v_{ki} and w_{ki} are the k-th elements of v_i and w_i. Participation factors are used to determine the degree of participation of various machines in a particular mode of oscillation as well as to identify the optimum site for a CPS.

3.2.3 DAMPING RATIO

For a complex pair of eigenvalues

$$\lambda_{1,2} = \alpha \pm j\omega \tag{3.12}$$

the real component α of the eigenvalues gives the damping, and the imaginary component ω gives the frequency of oscillations in rad/s. The damped frequency of oscillation in Hz is given by

$$f = \frac{\omega}{2\pi} \tag{3.13}$$

The damping ratio is given by

$$\zeta = \frac{-\alpha}{\sqrt{\alpha^2 + \omega^2}} \tag{3.14}$$

The damping ratio ζ determines the rate of decay of the amplitude of the oscillation. The time constant of amplitude decay is $1/|\alpha|$. It is known [89] that if

$\zeta > 0.25$, the system is well damped

$\zeta = 0.1$, the system is damped

$\zeta < 0.03$, the system is weakly damped

$\zeta \leq 0$, the system is unstable

3.3 SYNCHRONOUS MACHINE MODEL

Each synchronous machine is represented by a subtransient fifth-order model. This model uses the two-axis theory based on Park's transformation [90, 91], in which the three phase windings on the stator are replaced by two armature phase windings, one D winding on the d-axis and one Q winding on the q-axis. The machine rotor circuit is modelled by one field winding F and one damper winding KD on the d-axis and one damper winding KQ on the q-axis. This is represented diagrammatically in Figure 3.2. In this model, machine saturation and stator transients are ignored.

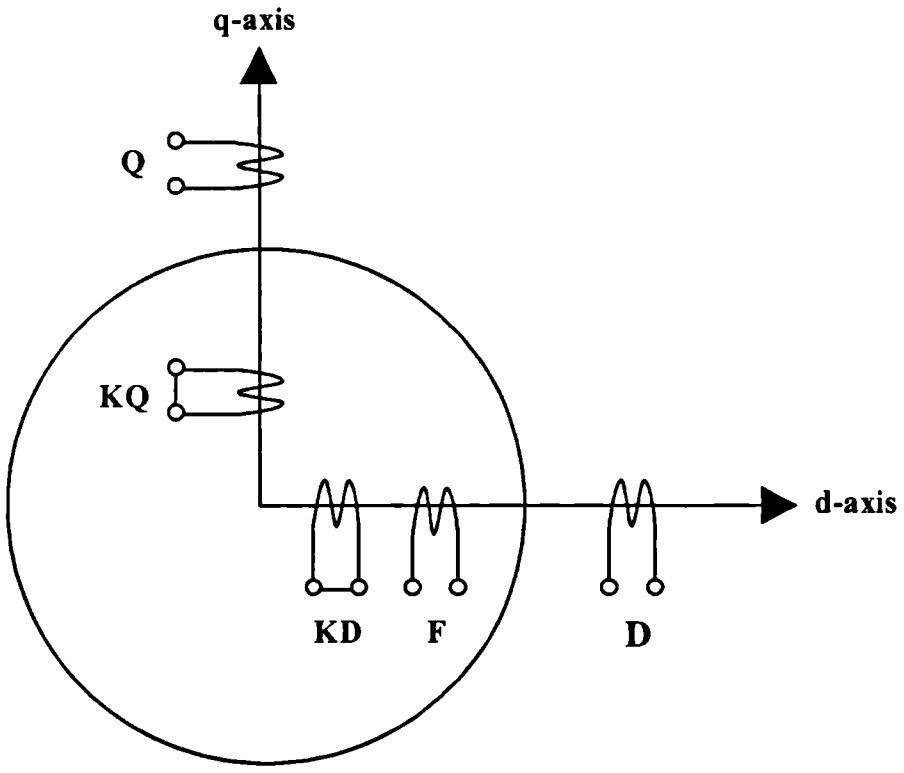


Figure 3.2 d-q axis synchronous machine model

Electrical Equations

To account for changes in rotor flux linkages due to changes in machine or network operation, three rotor differential equations expressed in a d-q reference frame rotating with its own rotor are used [92]:

$$\frac{dE'_q}{dt} = \frac{1}{T'_{do}}(E_{fd} - (X_d - X'_d) I_d - E'_q) \tag{3.15}$$

$$\frac{dE''_q}{dt} = \frac{1}{T''_{do}}(E'_q - (X'_d - X''_d) I_d - E''_q) \tag{3.16}$$

$$\frac{dE''_d}{dt} = \frac{1}{T''_{qo}}((X_q - X''_q) I_q - E''_d) \tag{3.17}$$

Mechanical Equations

To describe the rotational dynamics of the synchronous machine, two first-order differential equations are used [18]:

$$\frac{d\omega}{dt} = \frac{1}{2H}[P_m - P_e - D(\omega - 1)] \tag{3.18}$$

$$\frac{d\delta}{dt} = (\omega - 1)\omega_o \tag{3.19}$$

where

$$P_e = E''_d I_d + E''_q I_q \tag{3.20}$$

In this analysis, the machine damping coefficient D is set to zero. It is always small and setting it to zero gives marginally pessimistic results.

As stator transients are neglected, the synchronous machine is further characterized by two stator algebraic equations which are coupled to the network equations

$$E''_d - V_d = R_a I_d - X''_q I_q \tag{3.21}$$

$$E''_q - V_q = R_a I_q + X''_d I_d \tag{3.22}$$

or in the matrix form

$$\begin{bmatrix} I_d \\ I_q \end{bmatrix} = \frac{1}{R_a^2 + X''_d X''_q} \begin{bmatrix} R_a & X''_q \\ -X''_d & R_a \end{bmatrix} \left\{ \begin{bmatrix} E''_d \\ E''_q \end{bmatrix} - \begin{bmatrix} V_d \\ V_q \end{bmatrix} \right\} \tag{3.23}$$

The network is described by a D-Q reference frame which is assumed to rotate at synchronous speed [18]. In order to couple each synchronous machine to the network, the machine stator currents and voltages (Equation (3.23)) expressed in its own machine (d-q) reference frame must be transformed into the network (D-Q) reference frame. The relationship between the individual machine (d-q) reference frame and the network (D-Q) reference frame, as shown in Figure 3.3, is adopted [93].

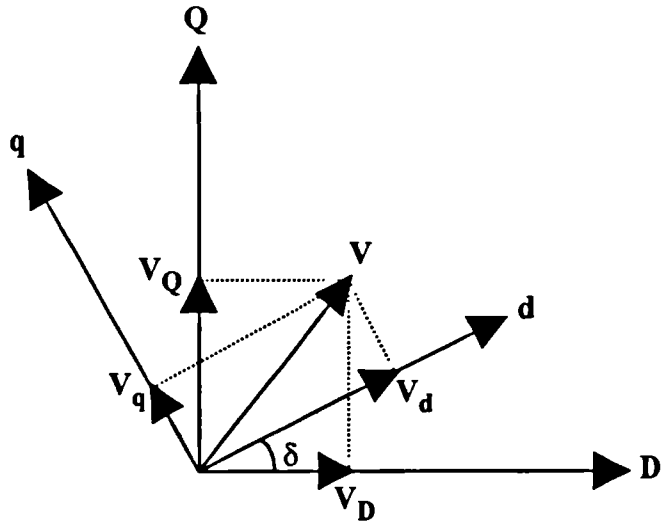


Figure 3.3 Reference frame transformation

From Figure 3.3, the components of voltages and currents of each synchronous machine can be referred to the network reference frame by using the following transformation

$$\begin{bmatrix} V_d \\ V_q \end{bmatrix} = \begin{bmatrix} \cos\delta & \sin\delta \\ -\sin\delta & \cos\delta \end{bmatrix} \begin{bmatrix} V_D \\ V_Q \end{bmatrix} \tag{3.24}$$

and

$$\begin{bmatrix} I_d \\ I_q \end{bmatrix} = \begin{bmatrix} \cos\delta & \sin\delta \\ -\sin\delta & \cos\delta \end{bmatrix} \begin{bmatrix} I_D \\ I_Q \end{bmatrix} \tag{3.25}$$

and the inverse transformation

$$\begin{bmatrix} V_D \\ V_Q \end{bmatrix} = \begin{bmatrix} \cos\delta & -\sin\delta \\ \sin\delta & \cos\delta \end{bmatrix} \begin{bmatrix} V_d \\ V_q \end{bmatrix} \tag{3.26}$$

and

$$\begin{bmatrix} I_D \\ I_Q \end{bmatrix} = \begin{bmatrix} \cos\delta & -\sin\delta \\ \sin\delta & \cos\delta \end{bmatrix} \begin{bmatrix} I_d \\ I_q \end{bmatrix} \tag{3.27}$$

The general structure of the complete power system model is shown in Figure 3.4. The stator equations of each synchronous machine, transformed into the network reference frame, are coupled to the equations of the network, loads and other dynamic devices.

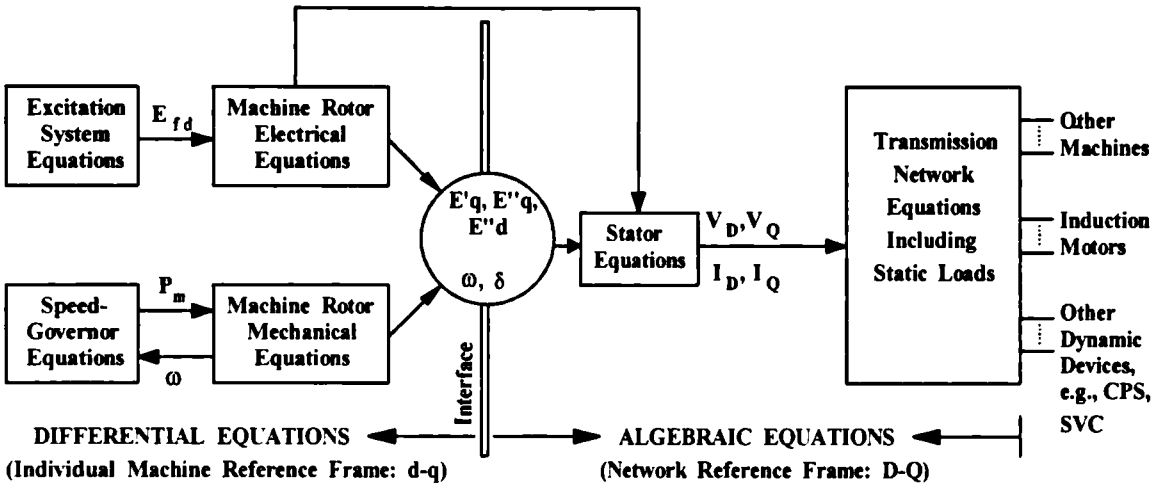


Figure 3.4 Structure of the complete power system model

As the differential equations governing the machine dynamics are non-linear, they are linearized about an operating point for the study of small disturbances. The synchronous machine dynamic behaviour is represented by a hybrid model in which the flux linkage voltages are taken as state variables [94] while the terminal axis voltages representing interaction with the network are taken as algebraic variables. This can be written compactly as [95]

$$\Delta \dot{x}_g = [A_g]\Delta x_g + [C_g]\Delta V_g \tag{3.28}$$

where

Δx_g is the generator state vector

ΔV_g is the vector of terminal voltage deviations in the network D-Q reference frame

Matrices $[A_g]$ and $[C_g]$ are block-diagonal and numerically dependent on the system operating point and on the synchronous machine parameters. Matrix $[A_g]$ also conveys information about the excitation system $[A_{eg}]$ and speed-governing system $[A_{sg}]$ models and settings. In a multimachine system, Δx_g, ΔV_g, $[A_g]$ and $[C_g]$ as defined in equation (3.28) are

$$\Delta x_g = [\Delta x_{g1}^T, \Delta x_{g2}^T, ..., \Delta x_{gi}^T, ..., \Delta x_{gn}^T]^T \tag{3.29}$$

where

$i = (1,2,.....,n)$ represents the i-th generator of a power system having n generators

$$\Delta x_{gi} = \left[\Delta x_{ggi}^T \;\; \Delta x_{egi}^T \;\; \Delta x_{sgi}^T\right]^T$$

with $\Delta x_{ggi} = \left[\Delta E'_{qi} \;\; \Delta E''_{qi} \;\; \Delta E''_{di} \;\; \Delta \omega_i \;\; \Delta \delta_i\right]^T$ = generator states

$$\Delta x_{egi} = \left[\Delta E_{1i} \;\; \Delta E_{2i} .....\Delta E_{fdi}\right]^T = \text{exciter states}$$

$$\Delta x_{sgi} = \left[\Delta S_i \;\; \Delta P_{mi}\right]^T = \text{speed-governor states}$$

$$\Delta V_g = \left[\Delta V_{g1}^T, \Delta V_{g2}^T, ...\Delta V_{gi}^T, ..., \Delta V_{gn}^T\right]^T \tag{3.30}$$

where

$$\Delta V_{gi} = \left[\Delta V_{gDi} \;\; \Delta V_{gQi}\right]^T$$

$$[A_g] = diag\ [A_{g1}\ \ A_{g2}.....A_{gi}.....A_{gn}] \tag{3.31}$$

where

$$A_{gi} = \begin{bmatrix} A_{ggi} & 0 & 0 \\ 0 & A_{egi} & 0 \\ 0 & 0 & A_{sgi} \end{bmatrix}$$

and

$$[C_g] = diag\ [C_{g1}\ \ C_{g2}.....C_{gi}.....C_{gn}] \tag{3.32}$$

where

$$C_{gi} = \begin{bmatrix} C_{gg}i \\ C_{egi} \\ 0 \end{bmatrix}$$

It is seen from equation (3.23) that the generator axis currents can be expressed as a function of generator states and terminal voltages. For a multimachine system the interface generator-network equations in linearized form are

$$\Delta I_g = [W_g]\Delta x_g + [N_g]\Delta V_g \tag{3.33}$$

where $I_g = [I_{g1}^T, I_{g2}^T, ..., I_{gi}^T, ..., I_{gn}^T]^T$ (and $I_{gi} = [I_{gDi}\ \ I_{gQi}]^T$) is the vector of generator current injections into the network. $[W_g]$ and $[N_g]$ are block-diagonal matrices whose structure is dependent on the system operating point and the machine model (see Appendix A.1).

3.4 EXCITATION SYSTEM MODELS

Three types of exciters are considered in order to study their effects on inter-area oscillations:

-Manually controlled exciters
-Fast-acting exciters
-Slow-acting exciters

The block diagrams of the exciter models are shown in Figure 3.5 [79]. Only the effect of varying the voltage regulator gain was investigated. Other special controls, such as power system stabilizers, were not considered.

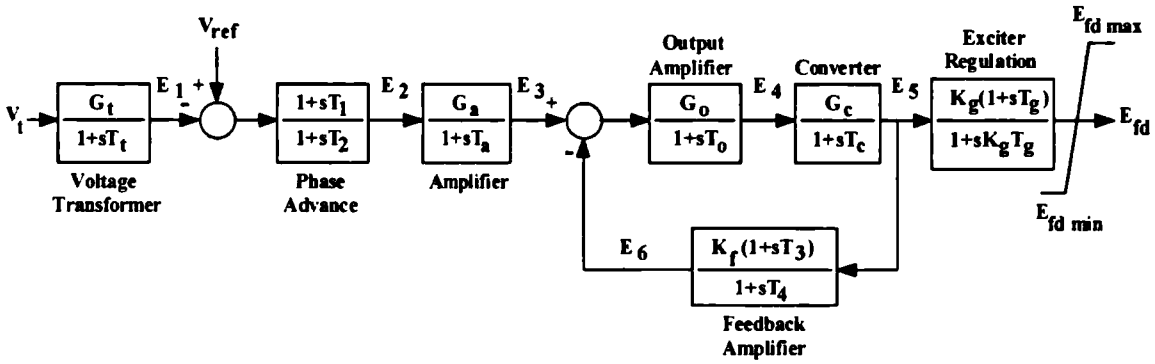


Figure 3.5a Fast-acting exciter model

The differential equations describing the fast-acting exciter dynamics are given by

$$\dot{E}_1 = \frac{G_t}{T_t} V_t - \frac{1}{T_t} E_1 \tag{3.34}$$

$$\dot{E}_2 = \frac{1}{T_2}(1 - \frac{T_1}{T_2}) V_{ref} - \frac{1}{T_2}(1 - \frac{T_1}{T_2}) E_1 - \frac{1}{T_2} E_2 \tag{3.35}$$

$$\dot{E}_3 = \frac{G_a}{T_a}\frac{T_1}{T_2} V_{ref} - \frac{G_a}{T_a}\frac{T_1}{T_2} E_1 + \frac{G_a}{T_a} E_2 - \frac{1}{T_a} E_3 \tag{3.36}$$

BIBL. LONDIN. UNIV

$$\dot{E}_4 = \frac{G_o}{T_o} E_3 - \frac{1}{T_o} E_4 - K_f \frac{G_o}{T_o} \frac{T_3}{T_4} E_5 - \frac{G_o}{T_o} E_6 \tag{3.37}$$

$$\dot{E}_5 = \frac{G_c}{T_c} E_4 - \frac{1}{T_c} E_5 \tag{3.38}$$

$$\dot{E}_6 = \frac{K_f}{T_4}(1 - \frac{T_3}{T_4}) E_5 - \frac{1}{T_4} E_6 \tag{3.39}$$

$$\dot{E}_{fd} = \frac{G_c}{T_c} E_4 + (\frac{1}{T_g} - \frac{1}{T_c}) E_5 - \frac{1}{K_g T_g} E_{fd} \tag{3.40}$$

$$E_{fd\,\max} \geq E_{fd} \geq E_{fd\,\min} \tag{3.41}$$

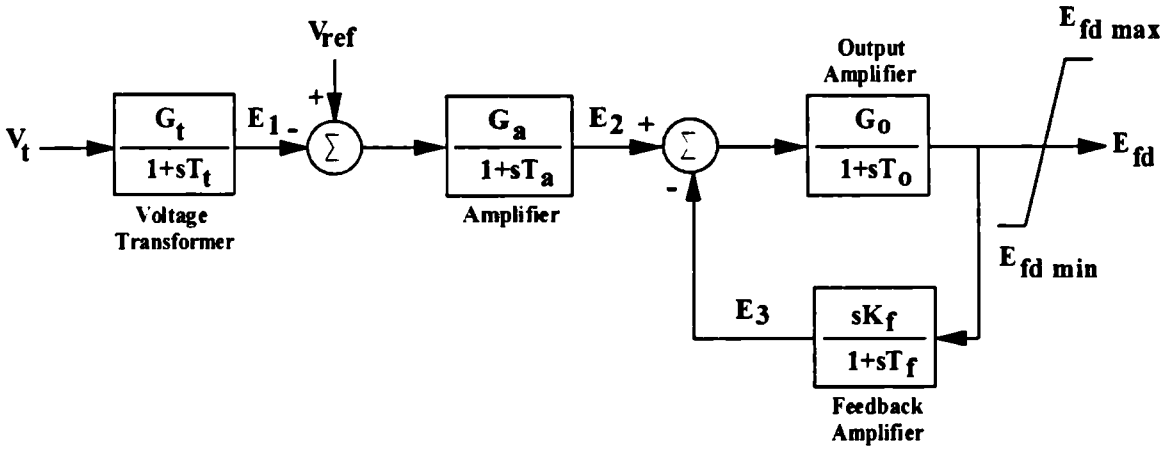


Figure 3.5b Slow-acting exciter model

The differential equations describing the slow-acting exciter dynamics are given by

$$\dot{E}_1 = \frac{G_t}{T_t} V_t - \frac{1}{T_t} E_1 \tag{3.42}$$

$$\dot{E}_2 = \frac{G_a}{T_a} V_{ref} - \frac{G_a}{T_a} E_1 - \frac{1}{T_a} E_2 \tag{3.43}$$

$$\dot{E}_3 = -\frac{1}{T_f} E_3 + \frac{K_f}{T_f^2} E_{fd} \tag{3.44}$$

$$\dot{E}_{fd} = \frac{G_o}{T_o} E_2 + \frac{G_o}{T_o} E_3 - \frac{1}{T_o}(1 + \frac{G_o K_f}{T_f}) E_{fd} \tag{3.45}$$

$$E_{fd\,\max} \geq E_{fd} \geq E_{fd\,\min} \tag{3.46}$$

The linearized state model of the excitation system for the i-th machine can be written as

$$\Delta \dot{x}_{egi} = [A_{egi}] \Delta x_{egi} + [C_{egi}] \Delta V_{gi} \tag{3.47}$$

where

$$\Delta x_{egi} = [\Delta E_{1i}\ \Delta E_{2i}\ \Delta E_{3i}\ \Delta E_{4i}\ \Delta E_{5i}\ \Delta E_{6i}\ \Delta E_{fdi}] = \text{fast-exciter states}$$

$$= [\Delta E_{1i}\ \Delta E_{2i}\ \Delta E_{3i}\ \Delta E_{fdi}] = \text{slow-exciter states}$$

$$\Delta V_{gi} = \left[\Delta V_{gDi}\ \Delta V_{gQi}\right]^T = \text{terminal voltage deviations}$$

Matrix $[A_{egi}]$ is block-diagonal and its order and structure depend on the exciter model and control parameters while matrix $[C_{egi}]$ is a function of the initial terminal voltage. The elements of matrices $[A_{egi}]$ and $[C_{egi}]$ are given in Appendix A.2.

3.5 SPEED-GOVERNING SYSTEM MODEL

Speed-governing systems normally do not have a very significant effect on inter-area oscillations [18]. However, if they are not properly tuned, they may decrease damping of the oscillations. Hence the governor model used in this study is a simplified second order representation as shown in Figure 3.6.

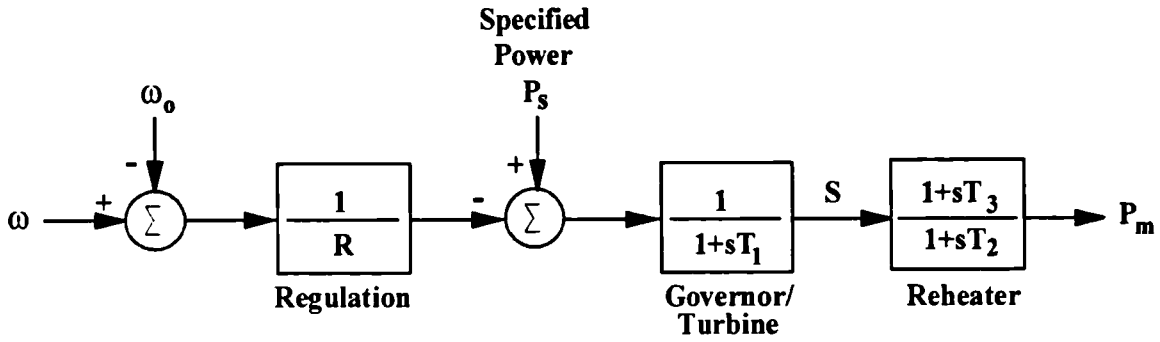


Figure 3.6 Speed-governor model

The differential equations describing the speed-governor dynamics are given by

$$\dot{S} = \frac{1}{T_1} P_s - \frac{1}{T_1 R}\omega + \frac{1}{T_1 R}\omega_o - \frac{1}{T_1} S \tag{3.48}$$

$$\dot{P}_m = \frac{T_3}{T_1 T_2} P_s - \frac{T_3}{T_1 T_2 R}\omega + \frac{T_3}{T_1 T_2 R}\omega_o + \frac{1}{T_2}(1 - \frac{T_3}{T_1}) S - \frac{1}{T_2} P_m \tag{3.49}$$

The linearized state model of the speed-governing system for the i-th machine can be written as

$$\Delta \dot{x}_{sgi} = [A_{sgi}] \Delta x_{sgi} \tag{3.50}$$

where

$$\Delta x_{sgi} = [\Delta S_i \;\; \Delta P_{mi}] = \text{ speed-governor states}$$

Matrix $[A_{sgi}]$ is a block-diagonal and its order and structure depend on the speed-governor model and control parameters. The elements of the matrix $[A_{sgi}]$ are given in Appendix A.3.

3.6 COMPENSATION-BASED CONTROLLABLE PHASE SHIFTER MODEL

A phase shifter changes the bus admittance matrix $[Y_{bus}]$ to an unsymmetrical matrix which is a function of the phase shift angle ϕ (see Equation (2.6)). The asymmetry of the $[Y_{bus}]$ has the disadvantage that a constant factorized $[Y_{bus}]$ cannot be repeatedly used when the phase shift angle is changeable in the process of power flow and transient stability calculations. For this reason, a compensation-based phase shifter model is developed to avoid using the unsymmetrical $[Y_{bus}]$. With the addition of different control systems, the combined model can be used for steady state, eigenvalue and transient stability studies. So far, to the best of author's knowledge, the compensation-based phase shifter model has only been applied to power flow studies by Han [51], Noroozian and Andersson [53], and Taranto, Pinto and Pereira [96]. The compensation-based phase shifter model developed in this research has been extended to the eigenvalue analysis and transient stability computation. The accuracy of the model developed is verified by comparing the results obtained from eigenvalue analysis with those from time domain simulations.

A systematic approach for mathematical modelling of a compensation-based CPS is described below. The structure of the dynamic representation of the CPS follows that of synchronous machines. Each CPS is represented by a set of differential and algebraic equations which are expressed as a function of CPS states and terminal bus voltages. Referring to Figure 2.1, the main assumptions for developing the model are that [57]

(1) the three-phase thyristor circuits work in a balanced condition;

(2) the switching control of the thyristors is continuous;

(3) the harmonics due to the thyristor switching and the filter circuits in the CPS are neglected.

As discussed in Section 2.3, the effect of a phase shifter connected between nodes i and k with a complex tap ratio $1 : t_{ik} e^{j\phi}$ in series with its reactance jx can be represented by an equivalent circuit as shown in Figure 3.7.

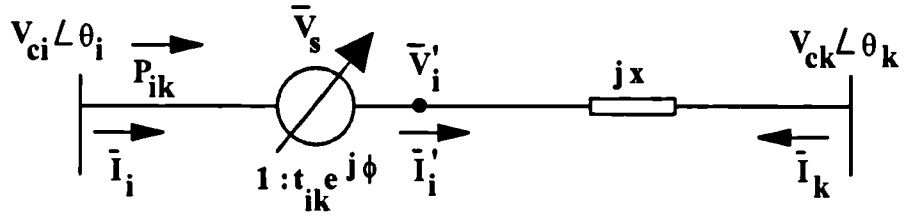


Figure 3.7 Phase shifter equivalent circuit

$\bar{I}_i$ and $\bar{I}_k$ are the complex phase shifter currents at nodes i and k, $\overline{V}_{ci}$ and $\overline{V}_{ck}$ are the complex voltages at nodes i and k, and $\overline{V}_i'$ is the virtual voltage behind the series reactance.

From Figure 3.7, it can be shown that

$$\begin{aligned}\overline{V}_i' &= \overline{V}_{ci} + \overline{V}_s \\ &= t_{ik} e^{j\phi} \overline{V}_{ci} \\ &= (1 + j\alpha_{ik})\overline{V}_{ci}\end{aligned} \tag{3.51}$$

$$\bar{I}_i = \frac{(t_{ik}^2 \overline{V}_{ci} - t_{ik} e^{-j\phi} \overline{V}_{ck})}{jx} \tag{3.52}$$

$$\bar{I}_k = \frac{(\overline{V}_{ck} - t_{ik} e^{j\phi} \overline{V}_{ci})}{jx} \tag{3.53}$$

where $t_{ik} = \sqrt{1+\alpha_{ik}^2}$ is the tap ratio magnitude, $\phi = \tan^{-1}\alpha_{ik}$ is the phase shift angle limited to $\pm 20^o$ and is taken as the control variable.

The phase shifter represented by its reactance jx and the unit giving phase shifting action shown in Figure 3.7 can be reduced to the form shown in Figure 3.8.

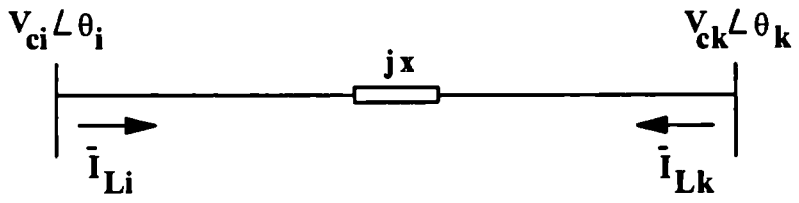


Figure 3.8 Representation of a phase shifter in the transmission network

the nodal currents $\bar{I}_{Li}$ and $\bar{I}_{Lk}$ at nodes i and k are

$$\bar{I}_{Li} = \frac{\overline{V}_{ci} - \overline{V}_{ck}}{jx} \tag{3.54}$$

$$\bar{I}_{Lk} = -\bar{I}_{Li} \tag{3.55}$$

Compensation-Based Phase Shifter Model

As shown in Figure 3.9, the phase shifter is modelled as a fixed reactance jx, that of the phase shifter itself, with additional compensation currents $\bar{I}_{ci}$ and $\bar{I}_{ck}$ injected at nodes i and k to ensure the equivalent condition. Thus the symmetry property of the $[Y_{bus}]$ is maintained.

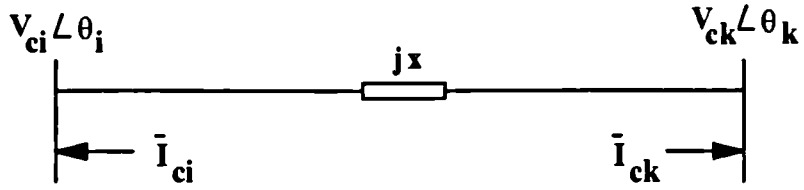


Figure 3.9 Equivalent circuit of a compensation-based phase shifter model

The compensation currents $\bar{I}_{ci}$ and $\bar{I}_{ck}$ are given by

$$\bar{I}_{ci} = \bar{I}_{Li} - \bar{I}_i \tag{3.56}$$

$$= \frac{\overline{V}_{ci} - \overline{V}_{ck}}{jx} - \frac{(t_{ik}^2 \overline{V}_{ci} - t_{ik} e^{-j\phi} \overline{V}_{ck})}{jx}$$

$$\bar{I}_{ck} = \bar{I}_{Lk} - \bar{I}_k \tag{3.57}$$

$$= \frac{\overline{V}_{ck} - \overline{V}_{ci}}{jx} - \frac{(\overline{V}_{ck} - t_{ik} e^{j\phi} \overline{V}_{ci})}{jx}$$

3.6.1 STEADY-STATE POWER FLOW STUDIES

For steady-state power flow studies, the effect of a phase shifter is equivalent to the injection of complex powers $\overline{S}_{ci}$ and $\overline{S}_{ck}$ at nodes i and k

$$\overline{S}_{ci} = \overline{V}_{ci} \bar{I}_{ci}^* \tag{3.58}$$
$$= P_{ci} + jQ_{ci}$$

$$\overline{S}_{ck} = \overline{V}_{ck} \bar{I}_{ck}^* \tag{3.59}$$
$$= P_{ck} + jQ_{ck}$$

Since

$$t_{ik} = \sqrt{1+\alpha_{ik}^2}$$

and

$$\alpha_{ik} = \tan\phi$$

then

$$t_{ik}^2 = 1+\tan^2\phi \tag{3.60}$$

Putting $t_{ik} = 1/\cos\phi$ from equation (3.60), the real and reactive injected powers at nodes i and k are derived as

$$P_{ci} = -\frac{V_{ci}V_{ck}}{x}\tan\phi\cos\theta_{ik} \tag{3.61}$$

$$Q_{ci} = -\frac{V_{ci}V_{ck}}{x}\tan\phi\sin\theta_{ik} - \frac{V_{ci}^2}{x}\tan^2\phi \tag{3.62}$$

$$P_{ck} = \frac{V_{ci}V_{ck}}{x}\tan\phi\cos\theta_{ik} \tag{3.63}$$

$$Q_{ck} = -\frac{V_{ci}V_{ck}}{x}\tan\phi\sin\theta_{ik} \tag{3.64}$$

where $\theta_{ik} = \theta_i - \theta_k$. The phase shifter power injection model shown in Figure 3.10 can be incorporated in a load flow program. See [51, 53] for further details.

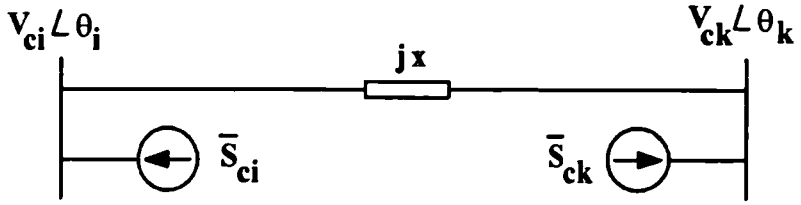


Figure 3.10 Phase shifter power injection model

3.6.2 DYNAMIC STABILITY STUDIES

For dynamic stability studies, the compensation currents $\bar{I}_{ci}$ and $\bar{I}_{ck}$, and the nodal voltages $\overline{V}_{ci}$ and $\overline{V}_{ck}$ corresponding to the phase shifter are expressed in the network D-Q reference frame to couple with other components through the network as

$$\bar{I}_{ci} = I_{cDi} + jI_{cQi} \tag{3.65}$$

$$\bar{I}_{ck} = I_{cDk} + jI_{cQk} \tag{3.66}$$

$$\overline{V}_{ci} = V_{cDi} + jV_{cQi} \tag{3.67}$$

$$\overline{V}_{ck} = V_{cDk} + jV_{cQk} \tag{3.68}$$

Substituting equations (3.65), (3.66), (3.67), (3.68) and (3.60) into equations (3.56) and (3.57), the algebraic equations (3.69) through (3.72) of the compensation-based phase shifter model are obtained as

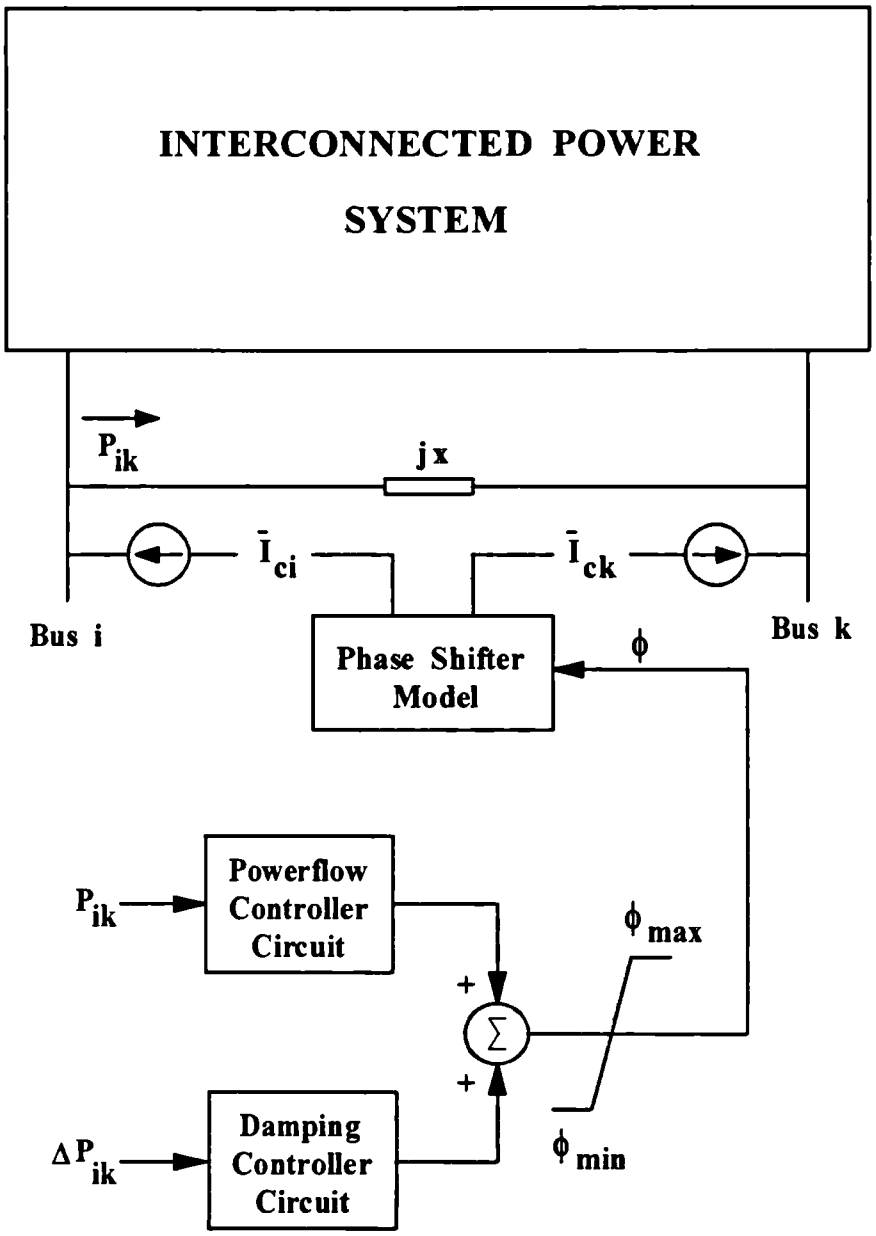
$$I_{cDi} = -\frac{\tan^2\phi}{x}V_{cQi} - \frac{\tan\phi}{x}V_{cDk} \tag{3.69}$$

$$I_{cQi} = \frac{\tan^2\phi}{x}V_{cDi} - \frac{\tan\phi}{x}V_{cQk} \tag{2.70}$$

$$I_{cDk} = \frac{\tan\phi}{x}V_{cDi} \tag{2.71}$$

$$I_{cQk} = \frac{\tan\phi}{x}V_{cQi} \tag{3.72}$$

The compensation-based CPS model for power flow, small signal and large signal studies is formed by adding different control systems to the basic phase shifter model as shown in Figure 3.11.



P_{ik} = tie-line active power

Figure 3.11 Functional block diagram of the CPS with tie-line power feedback

Figure 3.12 shows a block representation of the transfer function of the controllers used for the CPS. During steady-state conditions (the damping controller is inactive), a PI controller is used to regulate the power flow through the tie line containing the CPS. The magnitude of the phase shift ϕ is

determined by an error signal Δe which compares the measured power signal P_{ik} with the reference transfer power signal P_{ref}.

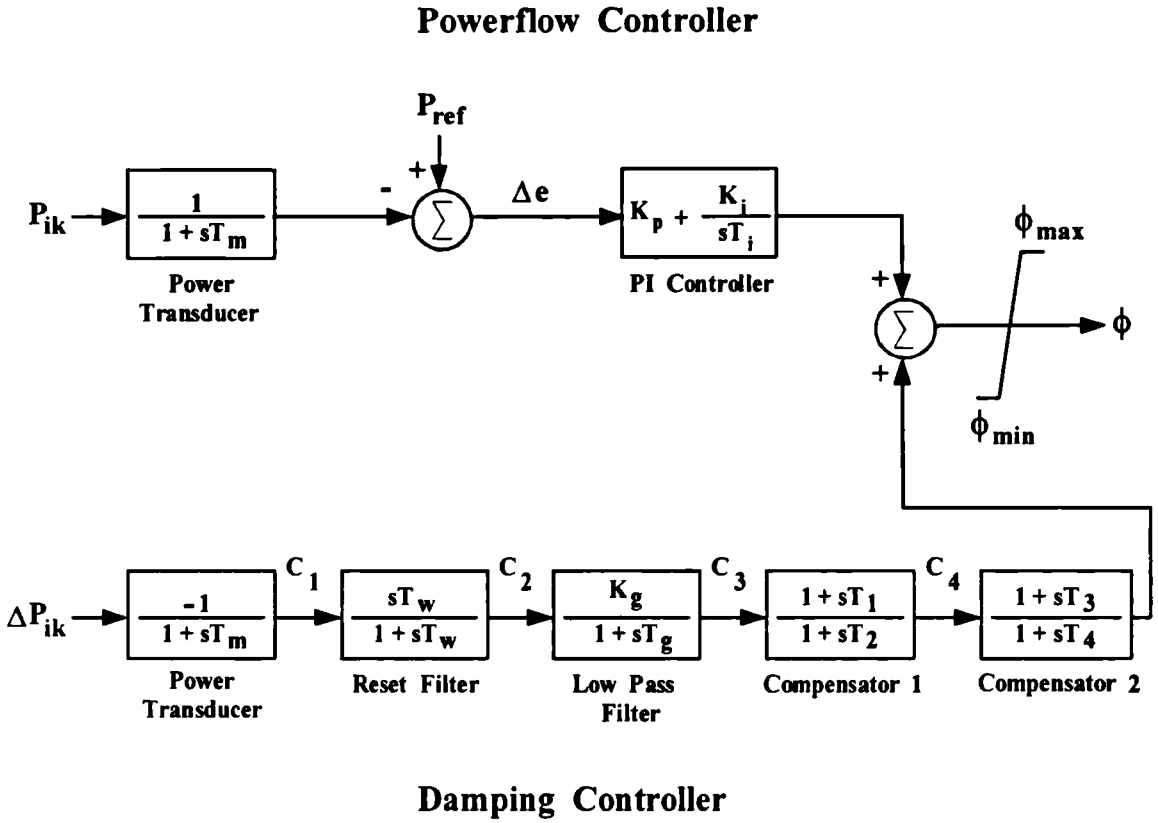


Figure 3.12 Control system diagram of the CPS

However, under dynamic or transient disturbance conditions, the steady-state powerflow controller is inhibited. The damping controller utilizes tie-line power deviation ΔP_{ik} as the feedback control signal. The signal is passed through a power transducer, a reset filter, a low pass filter, and then its required phase shift is provided by two lead-lag stages of phase compensation. The function of the reset filter is to ensure that the CPS controller will not respond to any DC offset or very low frequencies below 0.2 Hz and an appropriate setting of 10 seconds is chosen for Tw. The response of the CPS to a phase angle modulation command is represented by a first order system (low pass filter) characterized by a gain K_g and a time constant T_g. The amount of phase shift

ϕ required for modulating tie-line power flow to provide inter-area oscillation damping is dynamically controlled by the feedback control signal ΔP_{ik}.

The CPS damping controller is represented by five state variables: C_1, C_2, C_3, C_4 and ϕ. The differential equations describing the CPS dynamics, after some manipulations, are given by

$$\dot{C}_1 = -\frac{1}{T_m} P_{ik} - \frac{1}{T_m} C_1 \tag{3.73}$$

$$\dot{C}_2 = \frac{1}{T_w} C_1 - \frac{1}{T_w} C_2 \tag{3.74}$$

$$\dot{C}_3 = \frac{K_g}{T_g} C_1 - \frac{K_g}{T_g} C_2 - \frac{1}{T_g} C_3 \tag{3.75}$$

$$\dot{C}_4 = \frac{1}{T_2}(1 - \frac{T_1}{T_2}) C_3 - \frac{1}{T_2} C_4 \tag{3.76}$$

$$\dot{\phi} = \frac{K_g}{T_g}\frac{T_1}{T_2}\frac{T_3}{T_4} C_1 - \frac{K_g}{T_g}\frac{T_1}{T_2}\frac{T_3}{T_4} C_2$$

$$+ [\frac{T_1}{T_2}\frac{1}{T_4}(1 - \frac{T_3}{T_g}) + \frac{1}{T_2}\frac{T_3}{T_4}(1 - \frac{T_1}{T_2})] C_3 + \frac{1}{T_4}(1 - \frac{T_3}{T_2}) C_4 - \frac{1}{T_4}\phi \tag{3.77}$$

The dynamic behaviour of the CPS subsystem is obtained from the dynamic model described by equations (3.73) through (3.77) and expressed as (see Appendix B)

$$\Delta \dot{x}_c = [A_c]\Delta x_c + [C_c]\Delta V_c + [B_1]\Delta u_c \tag{3.78}$$

where

$\Delta x_c = [\Delta x_{c1}^T, \Delta x_{c2}^T, ..., \Delta x_{ci}^T ...., \Delta x_{cp}^T]^T$ is the CPS state vector

with $\Delta x_{ci} = [\Delta C_{1i}\ \Delta C_{2i}\ \Delta C_{3i}\ \Delta C_{4i}\ \Delta \phi_i]^T$ = the i-th CPS states

$\Delta V_c = \left[\Delta V_{c1}^T, \Delta V_{c2}^T, ... \Delta V_{ci}^T, ..., \Delta V_{cp}^T\right]^T$ is the vector of CPS terminal bus voltage deviations

with $\Delta V_{ci} = \left[\Delta V_{ciDi}\ \Delta V_{ciQi}\ \Delta V_{ciDk}\ \Delta V_{ciQk}\right]^T$ = the i-th CPS terminal bus voltage deviations

$\Delta u_c = [\Delta \phi_1, \Delta \phi_2, ..., \Delta \phi_i, ... \Delta \phi_{ip}]^T$ is the CPS control input vector

with $\Delta \phi_i$ = the i-th CPS control input variable

$[A_c] = diag\ [A_{c1}\ \ A_{c2} ..... A_{ci} ..... A_{cp}]$

$[C_c] = diag\ [C_{c1}\ \ C_{c2} ..... C_{ci} ..... C_{cp}]$

Matrix $[A_c]$ is a function of the control parameters of the CPS stabilizing control loop representation, while matrix $[C_c]$ is mainly dependent on the initial terminal bus voltages. They are block-diagonal matrices and their order and structure depend on the control strategy and the details of the modelling. Matrix $[B_1]$ establishes the appropriate connection with the control input vector u_c.

Interaction with the network is a second aspect to be addressed in modelling CPS. A CPS is seen from the network as a continuously variable phase shift angle. The varying phase shifting action can be represented by the differential equation (3.77) and transferred to the network through the algebraic equations (3.69) through (3.72) (see Figure 3.11).

For low frequency oscillation studies the transient representation of the CPS is normally neglected, thus matching with the steady-state network representation. As a consequence, the steady-state interface CPS-network equations in linearized form are represented as

$$\Delta I_c = [W_c] \Delta x_c + [N_c] \Delta V_c + [B_2] \Delta u_c \qquad (3.79)$$

where

$I_c = [I_{c1}^T, I_{c2}^T, ..., I_{ci}^T, ..., I_{cp}^T]^T$ is the vector of CPS compensation current injections into the network

with $I_{ci} = [I_{ciDi}\ \ I_{ciQi}\ \ I_{ciDk}\ \ I_{ciQk}]^T$ = the i-th CPS compensation injected currents at terminal buses i and k.

$[W_c]$ and $[N_c]$ are block-diagonal matrices whose structure depends mainly on the system operating point. Matrix $[B_2]$ is an appropriate connection matrix with the control input vector u_c (see Appendix B).

3.6.3 TRANSIENT STABILITY STUDIES

The compensation based CPS model can easily be included in a time simulation program. Since the behaviour of the interconnected network is described by

$$\begin{bmatrix} I_g \\ I_c \\ 0 \end{bmatrix} = \begin{bmatrix} Y_{gg} & Y_{gc} & Y_{gl} \\ Y_{cg} & Y_{cc} & Y_{cl} \\ Y_{lg} & Y_{lc} & Y_{ll} \end{bmatrix} \begin{bmatrix} V_g \\ V_c \\ V_l \end{bmatrix} \tag{3.80}$$

or

$$[I] = [Y_{bus}][V] \tag{3.81}$$

where

I_g, I_c = are the vectors of injected currents into the network due to generators and CPS. Since loads are represented by constant impedances, the injected currents due to these loads are set to zero

$[Y_{bus}]$ = is the bus admittance matrix which denotes interaction between generators and CPS through the interconnected network

V_g, V_c, V_l = are the vectors of nodal voltages at generator, CPS and load buses

then the impact of the phase shifting action on the generators can be simulated by the injection of compensation currents into the network with no modification of the $[Y_{bus}]$ required at each iteration.

3.7 LOAD MODELS

It is well accepted that load characteristics have a significant effect on system stability. Load dynamics are of growing importance to the studies of small-disturbed oscillations in power systems [97, 98]. If the load representation is not of sufficient accuracy, the study results will not correspond to the actual response of the load. This will affect the assessment of system stability [99].

The load models are classified into two categories: static models and dynamic models.

3.7.1 STATIC LOAD MODELS

Since bus voltage and frequency are not constant during system disturbances and oscillations, the method in which bus loads are modelled can affect the study results. In stability studies, the change in load due to frequency is generally negligible compared to the effects due to voltage. Neglecting frequency, the active and reactive bus load can be represented by the exponential model [18, 80]:

$$P_L = P_L^o \left(\frac{V_L}{V_L^o} \right)^{K_p} \tag{3.82}$$

$$Q_L = Q_L^o \left(\frac{V_L}{V_L^o} \right)^{K_q} \tag{3.83}$$

where P_L and Q_L are the active and reactive powers supplied to the static load when the bus voltage magnitude is V_L, P_L^o, Q_L^o and V_L^o are the values at the initial operating condition, and the exponents K_p and K_q are constants whose values depend on the nature of the load.

In this study, three types of static load models are considered:

(1) Constant impedance $(K_p, K_q = 2)$
(2) Constant current $(K_p, K_q = 1)$
(3) Constant power $(K_p, K_q = 0)$

In terms of the network admittance model, loads are modelled as current sources (or sinks):

$$\begin{aligned} \bar{I}_L = I_{LD} + jI_{LQ} &= \frac{\bar{S}_L^*}{\bar{V}_L^*} \\ &= \frac{P_L - jQ_L}{V_{LD} - jV_{LQ}} \\ &= \frac{P_L - jQ_L}{V_{LD} - jV_{LQ}} \left\{ \frac{V_{LD} + jV_{LQ}}{V_{LD} + jV_{LQ}} \right\} \end{aligned} \tag{3.84}$$

where $\bar{S}_L = P_L + jQ_L$ is the complex power and $\bar{V}_L = V_{LD} + jV_{LQ}$ is the complex voltage with its magnitude $V_L = \sqrt{V_{LD}^2 + V_{LQ}^2}$ at the load bus.

The components of the currents $\bar{I}_L$ in equation (3.84) can be expressed as

$$\begin{bmatrix} I_{LD} \\ I_{LQ} \end{bmatrix} = \frac{1}{V_L^2} \begin{bmatrix} P_L & Q_L \\ -Q_L & P_L \end{bmatrix} \begin{bmatrix} V_{LD} \\ V_{LQ} \end{bmatrix} \tag{3.85}$$

By linearizing equation (3.85) and taking into account equations (3.82) and (3.83), it can be shown that each bus load can be represented, in the network D-Q reference frame, as follows:

$$\begin{bmatrix} \Delta I_{LD} \\ \\ \Delta I_{LQ} \end{bmatrix} = \begin{bmatrix} \dfrac{\partial I_{LD}}{\partial V_{LD}} & \dfrac{\partial I_{LD}}{\partial V_{LQ}} \\ \\ \dfrac{\partial I_{LQ}}{\partial V_{LD}} & \dfrac{\partial I_{LQ}}{\partial V_{LQ}} \end{bmatrix} \begin{bmatrix} \Delta V_{LD} \\ \Delta V_{LQ} \end{bmatrix} \tag{3.86}$$

$$= \begin{bmatrix} N_L 11 & N_L 12 \\ N_L 21 & N_L 22 \end{bmatrix} \begin{bmatrix} \Delta V_{LD} \\ \Delta V_{LQ} \end{bmatrix}$$

where the admittance coefficients of the matrix $[N_L]$ are well documented in literature [80] and can be found in Appendix C.1.

3.7.2 DYNAMIC LOAD MODEL

A third-order model is used to represent each dynamic induction motor load. In this representation stator flux dynamics are normally neglected due to the small time constants. In inter-area oscillation studies, it is necessary to include rotor flux dynamics in order to account for any magnetizing effects in the motor as the terminal voltage changes. Therefore, the induction motor model used is as follows [100]:

Electrical Equations

To account for changes in rotor flux dynamics, two rotor differential equations expressed in the network D-Q reference frame are used:

$$\frac{dE'_{mD}}{dt} = \omega_o S E'_{mQ} - \frac{(E'_{mD} + (X_o - X') I_{mQ})}{T'_o} \tag{3.87}$$

$$\frac{dE'_{mQ}}{dt} = -\omega_o S E'_{mD} - \frac{(E'_{mQ} - (X_o - X')I_{mD})}{T'_o} \tag{3.88}$$

where

$$X_o = X_1 + X_m \tag{3.89}$$

$$X' = X_1 + \frac{X_2 X_m}{X_2 + X_m} \tag{3.90}$$

$$T'_o = \frac{X_2 + X_m}{\omega_o R_2} \tag{3.91}$$

Mechanical Equation

Assuming negligible windage and friction losses and smooth mechanical shaft power, the equation of motion is:

$$\frac{dS}{dt} = \frac{T_m - T_e}{2H} \tag{3.92}$$

where

$$T_m = T_m^o(1 + bS + cS^2) \tag{3.93}$$

$$T_e = \frac{E'_{mD} I_{mD} + E'_{mQ} I_{mQ}}{\omega_o} \tag{3.94}$$

As stator transients are neglected, the induction motor is further characterized by two stator algebraic equations which are coupled to the network equations

$$V_{mD} - E'_{mD} = R_1 I_{mD} - X' I_{mQ} \tag{3.95}$$

$$V_{mQ} - E'_{mQ} = R_1 I_{mQ} + X' I_{mD} \tag{3.96}$$

or in the matrix form

$$\begin{bmatrix} I_{mD} \\ I_{mQ} \end{bmatrix} = \frac{1}{R_1^2 + X'^2} \begin{bmatrix} R_1 & X' \\ -X' & R_1 \end{bmatrix} \left\{ \begin{bmatrix} V_{mD} \\ V_{mQ} \end{bmatrix} - \begin{bmatrix} E'_{mD} \\ E'_{mQ} \end{bmatrix} \right\} \tag{3.97}$$

By linearizing equations (3.87), (3.88) and (3.92) and taking into account equations (3.97), (3.93) and (3.94), the following state model is obtained:

$$\Delta \dot{x}_m = [A_m] \Delta x_m + [C_m] \Delta V_m \tag{3.98}$$

where

$\Delta x_m = [\Delta x_{m1}^T, \Delta x_{m2}^T, ..., \Delta x_{mi}^T, ..., \Delta x_{mq}^T]^T$ is the induction motor state vector

with $\Delta x_{mi} = [\Delta E'_{mDi} \;\; \Delta E'_{mQi} \;\; \Delta S_i]^T$ = the i-th induction motor states

$\Delta V_m = \left[\Delta V_{m1}^T, \Delta V_{m2}^T, ... \Delta V_{mi}^T, ..., \Delta V_{mq}^T\right]^T$ is the vector of induction motor terminal voltage deviations

with $\Delta V_{mi} = \left[\Delta V_{mDi} \;\; \Delta V_{mQi}\right]^T$ = the i-th induction motor terminal voltage deviations

$[A_m] = diag\,[A_{m1} \;\; A_{m2} ..... A_{mi} ..... A_{mq}]$

$[C_m] = diag\,[C_{m1} \;\; C_{m2} ..... C_{mi} ..... C_{mq}]$

Matrices $[A_m]$ and $[C_m]$ are block-diagonal and numerically dependent on the system operating point and on the induction motor parameters (see Appendix C.2).

Upon linearization of equations (3.97), the interface between motor and network equations are represented by

$$\Delta I_m = [W_m]\Delta x_m + [N_m]\Delta V_m \tag{3.99}$$

where $I_m = [I_{m1}^T, I_{m2}^T, ..., I_{mi}^T, ..., I_{mq}^T]^T$ (and $I_{mi} = [I_{mDi}\ I_{mQi}]^T$) is the vector of induction motor current injections into the network. $[W_m]$ and $[N_m]$ are block-diagonal matrices whose structure is dependent on the system operating point and the induction motor model (see Appendix C.2).

The final load model considered for inter-area oscillations is a combination of static and dynamic models.

3.8 NETWORK REPRESENTATION

Static equipment is represented by lumped equivalent π parameters independent of changes in the generation/demand balance and frequency. Transmission lines and transformers are usually in this category. Even if a line is considered as short, its π equivalent is used. This is done so that it can consume or generate reactive power [101].

An appropriate network representation is necessary for the precise evaluation of the system dynamic performance and the tuning of damping controllers. According to the aim of the study and the accuracy requirement, two modelling practices are in common use in simulation programs [95]:

(1) Instantaneous formulation

(2) Phasor formulation

In instantaneous formulation balanced three-phase quantities are transformed to an arbitrary D-Q reference frame by application of Park's transformation [20]. This approach allows for each electrical energy-storage element to be initially represented in network coordinates by its corresponding differential equation from

where circuit theory considerations applied to the network model determine the necessary number of state variables for the overall system state representation. Such a procedure can be applied to each network element including loads and series and shunt compensation. Loads present a particular problem as the instantaneous formulation does not match with the usual representation of voltage and frequency dependency characteristics.

Practical considerations concerning the dimension of the model have often limited the use of the instantaneous formulation in large systems. Because network transients decay rapidly and do not affect the damping of electromechanical oscillation modes they are not usually considered when evaluating inter-area oscillation studies.

In phasor formulation the network is described here by lumped-parameter π-equivalent circuits in which synchronous machines, controllable phase shifters and dynamic loads are seen as two-axis current sources (or sinks) expressed in the network D-Q reference frame. Thus the nodal balance equations, after linearization, can be expressed in terms of the bus admittance matrix as

$$\begin{bmatrix} \Delta I_g \\ \Delta I_c \\ \Delta I_m \end{bmatrix} = \begin{bmatrix} Y_{gg} & Y_{gc} & Y_{gm} \\ Y_{cg} & Y_{cc} & Y_{cm} \\ Y_{mg} & Y_{mc} & Y_{mm} \end{bmatrix} \begin{bmatrix} \Delta V_g \\ \Delta V_c \\ \Delta V_m \end{bmatrix} \tag{3.100}$$

or

$$[\Delta I] = [Y_{bus}]\,[\Delta V] \tag{3.101}$$

where

I_g, I_c, I_m = are the vectors of injected currents into the network due to generators, CPS and induction motor loads

$[Y_{bus}]$ = is the network bus admittance matrix

V_g, V_c, V_m = are the vectors of nodal voltages at generator, CPS and induction motor load buses

Here the submatrices of the $[Y_{bus}]$ in equation (3.100) denote interaction among the different dynamic components (generators, CPS and induction motor loads) through the network. Matrix $[Y_{bus}]$ is symmetric and is composed of 2 X 2 sub-blocks given by [102]

$$[Y_{ij}] = \begin{bmatrix} G_{ij} & -B_{ij} \\ B_{ij} & G_{ij} \end{bmatrix} \tag{3.102}$$

where G_{ij} and B_{ij} are, respectively, the conductance and susceptance linking busbars i and j.

3.9 COMPLETE MODEL OF THE INTERCONNECTED SYSTEM

A system of linearized state equations characterized by a network interconnecting n generating units, p controllable phase shifters and q induction motor loads can be obtained by combining equations (3.28), (3.78) and (3.98)

$$\begin{bmatrix} \Delta \dot{x}_g \\ \Delta \dot{x}_c \\ \Delta \dot{x}_m \end{bmatrix} = \begin{bmatrix} A_g & 0 & 0 \\ 0 & A_c & 0 \\ 0 & 0 & A_m \end{bmatrix} \begin{bmatrix} \Delta x_g \\ \Delta x_c \\ \Delta x_m \end{bmatrix} + \begin{bmatrix} C_g & 0 & 0 \\ 0 & C_c & 0 \\ 0 & 0 & C_m \end{bmatrix} \begin{bmatrix} \Delta V_g \\ \Delta V_c \\ \Delta V_m \end{bmatrix} + \begin{bmatrix} 0 \\ B_1 \\ 0 \end{bmatrix} [\Delta u] \tag{3.103}$$

or

$$\Delta \dot{x} = [J_1] \Delta x + [J_2] \Delta V + [B_1] \Delta u \tag{3.104}$$

Analogously, the interface subsystem-network equations, obtained by combining equations (3.33), (3.79) and (3.99), can be arranged as follows

$$\begin{bmatrix}\Delta I_g\\ \Delta I_c\\ \Delta I_m\end{bmatrix}=\begin{bmatrix}W_g & 0 & 0\\ 0 & W_c & 0\\ 0 & 0 & W_m\end{bmatrix}\begin{bmatrix}\Delta x_g\\ \Delta x_c\\ \Delta x_m\end{bmatrix}+\begin{bmatrix}N_g & 0 & 0\\ 0 & N_c & 0\\ 0 & 0 & N_m\end{bmatrix}\begin{bmatrix}\Delta V_g\\ \Delta V_c\\ \Delta V_m\end{bmatrix}+\begin{bmatrix}0\\ B_2\\ 0\end{bmatrix}\begin{bmatrix}\Delta u\end{bmatrix} \quad (3.105)$$

By substituting equation (3.100) into equation (3.105), the following relationship can be obtained

$$\begin{bmatrix}0\\ 0\\ 0\end{bmatrix}=\begin{bmatrix}-W_g & 0 & 0\\ 0 & -W_c & 0\\ 0 & 0 & -W_m\end{bmatrix}\begin{bmatrix}\Delta x_g\\ \Delta x_c\\ \Delta x_m\end{bmatrix}+\begin{bmatrix}Y_{gg}-N_g & Y_{gc} & Y_{gm}\\ Y_{cg} & Y_{cc}-N_c & Y_{cm}\\ Y_{mg} & Y_{mc} & Y_{mm}-N_m\end{bmatrix}\begin{bmatrix}\Delta V_g\\ \Delta V_c\\ \Delta V_m\end{bmatrix}+\begin{bmatrix}0\\ -B_2\\ 0\end{bmatrix}\begin{bmatrix}\Delta u\end{bmatrix} \quad (3.106)$$

or

$$0=\begin{bmatrix}J_3\end{bmatrix}\Delta x+\begin{bmatrix}J_4\end{bmatrix}\Delta V+\begin{bmatrix}-B_2\end{bmatrix}\Delta u \quad (3.107)$$

The linearized state-space model of the entire interconnected system can be derived by eliminating the vector of algebraic variables ΔV in equations (3.104) and (3.107)

$$\Delta\dot{x}=\left[J_1-J_2J_4^{-1}J_3\right]\Delta x+\left[B_1-J_2J_4^{-1}(-B_2)\right]\Delta u \quad (3.108)$$

or

$$\Delta\dot{x}=A\Delta x+B\Delta u \quad (3.109)$$

This linearized state model is used to analyse the dynamic interaction between generator and CPS subsystems or between generator and dynamic load subsystems, and in particular the effect of this interaction on system damping enhancement.

CHAPTER FOUR

ANALYSIS OF INTER-AREA OSCILLATIONS

4.1 INTRODUCTION

Inter-area post-fault and spontaneous oscillations of electromechanical nature have been observed in large interconnected systems involving areas or groups of generators swinging against each other. Analysis of inter-area modes of oscillation is often difficult because such modes involve many generators in a complex interconnected system.

In this chapter an analytical study for examining various factors affecting the damping characteristics of low frequency inter-area oscillations in an interconnected system is presented. The effects of system running arrangements, operating conditions, excitation systems and load characteristics on the damping of inter-area oscillations are discussed. Based on this understanding, alternative practical remedies are investigated in order to improve the inter-area oscillation damping. Both eigenvalue analysis and time domain simulations are used to diagnose the dynamic stability problem. By using mode shape analysis, the machines causing instability are identified. To determine the machines participating in the interaction, the participation factor approach is used.

4.2 INTERCONNECTED 8-MACHINE SYSTEM

A 2-area interconnected 8-machine 112-bus system shown in Figure 4.1 is considered in this study. Inter-area oscillations with poor damping or even with increasing amplitude have been observed in such an interconnected system in 1984 [103]. The machines within each power station are assumed identical and therefore each power station is represented by a composite machine model. The power flow through the two interconnectors is about 110 MW. A particular operating condition of the machines is given in Table 4.1 where the machines are listed in merit order. As seen from Table 4.1, the machines of Area 1 are more economic than those of Area 2, and therefore the power flow is always from Area 1 to Area 2. Fast exciters (Figure 3.5a) are installed in Area 1 and

slow exciters (Figure 3.5b) in Area 2. The governors used for all machines are shown in Figure 3.6. Complete system data is subject to commercial confidentiality.

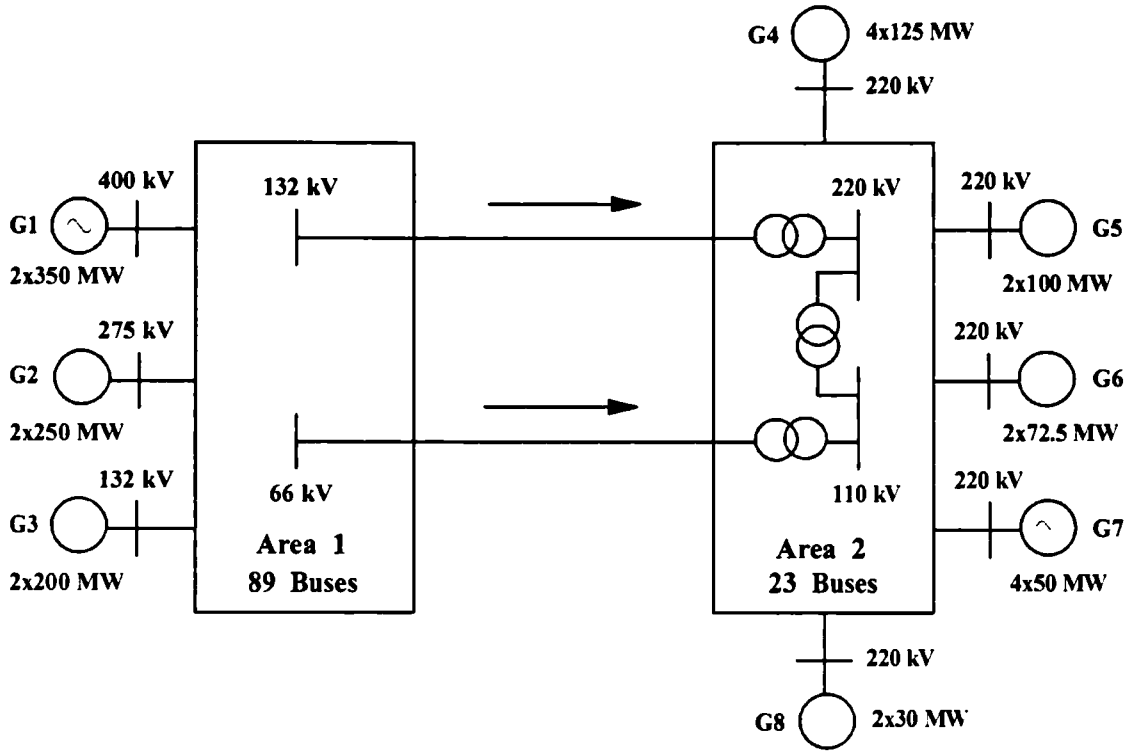


Figure 4.1 Interconnected 8-machine 112-bus system under study

Table 4.1 Operating condition of the machines

Machine	Rating (MW)	Loading (MW)	(MVAr)	Power Factor
G1	2x350	723	69	0.9955
G2	2x250	401	18	0.9990
G3	2x200	231	-22	-0.9955
G4	4x125	363	154	0.9206
G5	2x100	201	71	0.9429
G6	2x72.5	81	51	0.8462
G7	4x50	222	91	0.9253
G8	2x30	61	28	0.9088

4.3 IDENTIFICATION OF MACHINES CAUSING INSTABILITY

Based on this system condition, the linearized state model of the interconnected system was formed and the eigenvalues of the open-loop system using constant impedance loads were computed. Since there are 8 groups of machines, there are $8-1=7$ electromechanical modes of oscillation which are listed in Table 4.2.

Table 4.2 System eigenvalues of the 8-machine system

Mode Description	Eigenvalue	Participating Machines	Freq. (Hz)	Damping Ratio
Inter-area Mode 1	0.0570±4.7860	G1+G2+G3 ↔G4+G5+G6+G7+G8	0.7617	-0.0119
Local Mode 2	-0.3659±7.6632	G3+G4+G6+G7 ↔G2+G5+G8	1.2196	0.0477
Local Mode 3	-0.6151±7.8302	G3+G5+G8 ↔G1+G2+G4+G6+G7	1.2462	0.0783
Local Mode 4	-0.4943±8.3108	G1+G7 ↔G2+G3+G4+G5+G6+G8	1.3227	0.0594
Local Mode 5	-0.9113±8.5127	G4+G6 ↔G2+G3+G5+G7+G8	1.3548	0.1064
Local Mode 6	-1.1384±10.2466	G3+G5 ↔G1+G2+G4+G5+G7+G8	1.6308	0.1104
Local Mode 7	-1.1000±10.8201	G4+G8 ↔G3+G5+G6+G7	1.7221	0.1011

Of these oscillatory modes, mode 1 is inter-area having a frequency lower than the other modes, with a frequency of 4.79 rad/s (0.76 Hz) and a damping ratio of -0.012, which is unstable. Modes 2 through 7 are considered as local modes, with frequencies ranging from 1.22 to 1.72 Hz, in which the machines in each area oscillate against each other. The damping ratios are positive indicating that these modes are stable. As already discussed in Section 1.3, only the unstable inter-area mode 1 will be considered.

The rotor speed mode shape and participation factors corresponding to the dominant 0.76 Hz inter-area mode were calculated and are listed in Table 4.3.

Table 4.3 Mode shape and participation factors of the inter-area mode

Machine	Mode Shape		Participation Factors
	Amplitude	Angle (deg)	
G1	0.01	146.44	0.34
G2	0.01	132.49	0.31
G3	0.01	125.29	0.07
G4	0.04	-17.95	0.66
G5	0.04	-20.52	0.56
G6	0.04	-22.42	0.58
G7	0.04	-20.20	1.00
G8	0.04	-22.24	0.39

The mode shape plotted in Figure 4.2 indicates that the machines G4, G5, G6, G7 and G8 at the receiving end (Area 2) swing with a higher amplitude against the machines G1, G2 and G3 at the sending end (Area 1), while the participation factors indicate that the machine G1 in Area 1 and the machine G7 in Area 2 participate most (Figure 4.3).

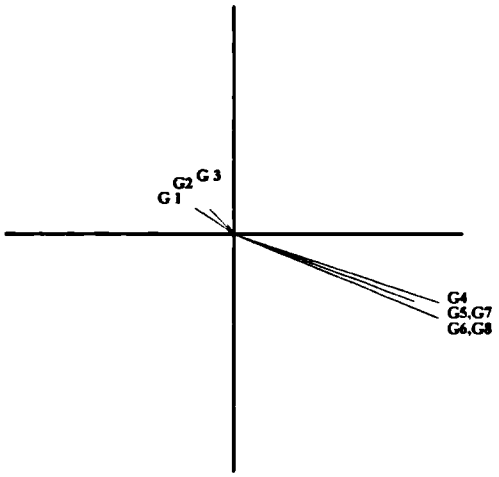


Figure 4.2 Inter-area mode shape with respect to rotor speed

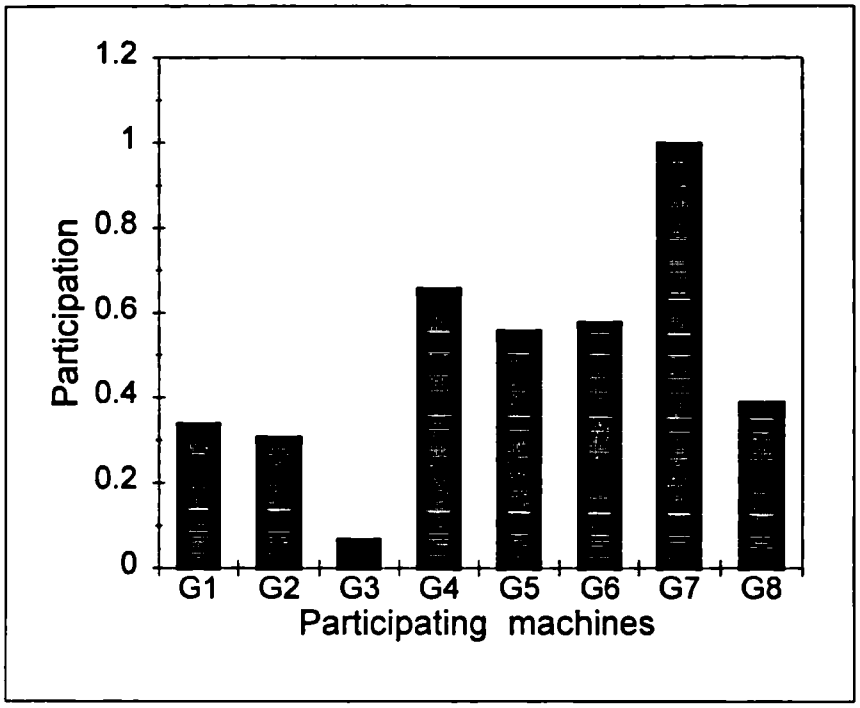


Figure 4.3 Speed participation factors of the inter-area mode

4.4 ANALYSIS OF FACTORS AFFECTING THE DAMPING OF THE INTER-AREA MODE

The factors influencing the damping characteristics of the inter-area mode and some possible remedial actions taken are analysed in this section.

4.4.1 EFFECT OF TIE-LINE FLOW

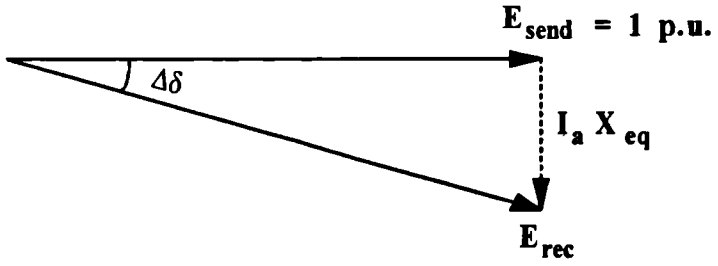
The problem of dynamic stability in the interconnected system was examined by reducing the tie-line transfer. Tie-line transfers were created by adjusting the system loads. The eigenvalues of the inter-area mode calculated under four different values of the tie-line flow are shown in Table 4.4. It is observed that, when the tie-line flow is reduced from 110 MW to 80 MW, the system would become dynamically stable. Thus, one of the possible remedial measures is to reduce the tie-line flow when the oscillations have occurred.

Table 4.4 Effect of tie-line flow on the inter-area mode

Power Flow Area 1 To 2 (MW)	Eigenvalue	Frequency (Hz)	Damping Ratio
110*	0.0570±4.7860	0.7617	-0.0119
100	0.0301±4.8109	0.7657	-0.0063
90	0.0039±4.8347	0.7695	-0.0008
80	-0.0213±4.8575	0.7731	0.0044

* Base operating condition

The cause of instability with high tie-line flow is presumably due to the large angle difference $\Delta\delta$ between the two groups of machines. Referring to Figure 4.4 [104], since $\Delta\delta \approx I_a X_{eq}$ ($\approx \Sigma I_a X$ for multi-buses), where I_a is the active current (representing power flow) and X_{eq} is the equivalent reactance between machines, the system is prone to oscillate with heavy power transfer (large I_a), and if there is a weak tie (high X_{eq}). Thus, it would suggest that the unstable system of Figure 4.1 might be made more stable by reducing the tie-line transfer in order to reduce $\Delta\delta$ between the two groups of machines.



E_{send} = Sending end voltage
E_{rec} = Receiving end voltage

Figure 4.4 Angle difference for a 2-bus system

4.4.2 EFFECT OF TIE-LINE IMPEDANCE

Dynamic instability is known to arise when the equivalent reactance X_{eq} between the two areas is large (areas connected by weak ties). It is possible to reduce X_{eq} by reinforcing the interconnection, that is, by installing additional parallel ties. In these tests, the tie-line impedance was varied by changing the number of tie-line circuits in service. The results of eigenvalue analysis on the inter-area mode are given in Table 4.5.

Table 4.5 Effect of tie-line impedance on the inter-area mode

Power Flow Area 1 To 2 (MW)	Ties in Service	Eigenvalue	Frequency (Hz)	Damping Ratio
110	2*	0.0570±4.7860	0.7617	-0.0119
110	3	-0.0100±5.2255	0.8317	0.0019
130	3**	-0.0042±5.1749	0.8236	0.0008
110	4	-0.0399±5.4426	0.8662	0.0073
110	5	-0.0566±5.5705	0.8866	0.0102

* Base operating case

As seen from Table 4.5, the frequency and damping ratio of the inter-area mode increase as the tie-line strength is reinforced. However, when only one tie line ** is added, the frequency and damping ratio of the inter-area mode drop when the tie-line flow is increased to 130 MW.

4.4.3 EFFECT OF EXCITATION SYSTEMS

Several reports [16] indicate that high gain excitation systems in general tend to reduce damping. The effect of excitation systems on the damping of the inter-area mode is summarised in Table 4.6.

Table 4.6 Effect of excitation systems on the inter-area mode

	Test	Eigenvalue	Frequency	Damping Ratio
	No action	0.0570±4.7860	0.7617	-0.0119
1	Reduce G1 exciter gain by 33 %	-0.0151±4.7504	0.7560	0.0032
2	Switch G1 exciter to manual	-0.1319±4.8000	0.7639	0.0275
3	Replace slow exciters of Area 2 machines by fast exciters of Area 1 machines	-0.3487±4.7707	0.7593	0.0729

The study of the system revealed that reduction of gain on the excitation system of the machine G1 (which has high participation in the inter-area mode) by 33% would increase damping (Test 1). In an emergency, a fast and effective way to damp out tie-line oscillations is to put the excitation system of the machine G1 to manual operation (i.e. exciter gain = 0), as shown in Test 2. Test 3 indicates that by replacing the slow exciters of the Area 2 machines with the fast exciters of the Area 1 machines, the system would become more stable by better matching of excitation system responses between the two areas.

4.4.4 EFFECT OF LOAD CHARACTERISTICS

In order to examine the impact of load characteristics on the inter-area mode, the following four types of load models were used:

-Constant impedance
-Constant current
-Constant power
-Induction motor

The non-linear loads were assumed to constitute 30% of the total load at each bus, while the remaining load was modelled as constant impedance. The computed eigenvalues for these tests are given in Table 4.7. It can be seen from Table 4.7 that load characteristics have a significant effect on the stability of the inter-area mode. Non-linear loads, such as constant current and constant power, have an adverse effect on the damping of the inter-area mode. On the other hand, induction motor loads improve the inter-area mode damping but lower the inter-area mode frequency because of the higher combined inertia of generators and induction motors on both areas.

Table 4.7 Effect of load characteristics on the inter-area mode

Load Model	Eigenvalue	Frequency	Damping Ratio
100 % Constant impedance	0.0570±4.7860	0.7617	-0.0119
30 % Constant current + 70 % Constant impedance	0.0843±4.7600	0.7576	-0.0177
30 % Constant power + 70 % Constant impedance	0.1169±4.7364	0.7538	-0.0247
30 % Induction motor + 70 % Constant impedance	-0.0664±4.3822	0.6974	0.0152

4.4.5 EFFECT OF MACHINE LOADINGS

In this set of tests the effect of machine loadings on the inter-area mode was investigated. To achieve these tests, four different operating conditions of the machine G1 were considered, provided the operating conditions of other machines and tie-line flow remained unchanged. The results, summarised in Table 4.8, show that the damping of the inter-area mode is significantly affected by the operating conditions of the machines themselves. The damping ratio of

the inter-area mode drops as the machine G1 is operated from 0.85 power factor lagging to 0.95 power factor leading. It can be concluded that the machines operating at leading power factor will have a detrimental effect on damping. Thus, during light load periods, the machines should run at lagging power factor in order to increase inter-area mode damping.

Table 4.8 Effect of machine G1 loadings on the inter-area mode

Active Power Output (MW)	Power Factor	Eigenvalue	Frequency	Damping Ratio
723	0.85	-0.0237±4.8119	0.7658	0.0049
723	0.95	0.0126±4.7965	0.7634	-0.0026
723	1.00	0.0570±4.7860	0.7617	-0.0119
723	-0.95	0.3559±4.6466	0.7395	-0.0764

4.4.6 EFFECT OF GENERATION RESCHEDULING

In the following two tests relocation part of generation from the high participation of the machine G1 to the other machine in the same area or in the other area were analyzed. The results of these tests are summarized in Table 4.9. These results show that the improvement in the damping of the inter-area mode is corroborated by

- the shift of 2 x 50 MW loading from the machine G1 to the machine G3 in Area 1 (Test 1).

- the increase of G4 loading by 4 x 10 MW in Area 2, i.e. the shift of 40 MW loading from the machine G1 in Area 1 to the machine G4 in Area 2 (Test 2).

Rescheduling of generation was implemented by some utilities as a remedial measure to damp out inter-area oscillations [105]. However, shifting the

generation from the more efficient machines to the less efficient machines is economically undesirable.

Table 4.9 Effect of generation rescheduling on the inter-area mode

	Test	Eigenvalue	Frequency	Damping Ratio
	No action	0.0570±4.7860	0.7617	-0.0119
1	Shift 2 x 50 MW loading from G1 to G3	-0.0158±4.8346	0.7694	0.0033
2	Increase G4 loading by 4 x 10 MW	-0.0443±4.8768	0.7762	0.0091

4.5 TIME SIMULATION RESULTS

To verify the results of eigenvalue analysis, time domain simulations of the open-loop system using constant impedance loads were performed for two types of disturbance:

(i) Large disturbance - a three-phase fault was applied to an EHV transmission line in Area 1 for 100 ms and the fault was cleared by tripping the line, with the objective of exciting all the system modes.

(ii) Small disturbance -

(a) a 1% step was applied to the reference voltage input of the machine G1 for 200 ms.

(b) switching off an EHV transmission line in Area 1.

Figures 4.5a-d show the system responses when a large disturbance as mentioned above is applied to the system. The relative rotor angle swings following this contingency are represented in Figure 4.5a. Figure 4.5b shows the responses of tie-line active power, voltage and current to the large disturbance. The responses

of generators' active power output and generators' terminal voltage to the large disturbance are depicted in Figures 4.5c and 4.5d respectively. The simulation results indicate that the system exhibits poorly damped inter-area oscillations following a three-phase fault. The inter-area mode is seen to dominate the time response.

Figures 4.6a-d show the dynamic responses when a 1% step small disturbance is applied to the reference voltage input of the machine G1 for 200 ms. The dynamic responses of the relative rotor angle swings following this contingency are represented in Figure 4.6a. Figure 4.6b shows the dynamic responses of tie-line active power, voltage and current to the 1% step small disturbance. The dynamic responses of generators' active power output and generators' terminal voltage to the 1% step small disturbance are depicted in Figures 4.6c and 4.6d respectively. Similarly, Figures 4.7a-d show the dynamic responses when a small disturbance of switching off an EHV transmission line in Area 1 is simulated. The dynamic responses of the relative rotor angle swings following this contingency are represented in Figure 4.7a. Figure 4.7b shows the dynamic responses of tie-line active power, voltage and current to the small disturbance of line switching. The dynamic responses of generators' active power output and generators' terminal voltage to the small disturbance of line switching are depicted in Figures 4.7c and 4.7d respectively. It can be concluded from the time responses in Figures 4.6a-d and Figures 4.7a-d that the inter-area mode is unstable following a small disturbance, with a low frequency of oscillation at 0.76 Hz. The results of the time domain simulations are fully consistent with those of the eigenvalue analysis, as far as the damping and frequency of the inter-area mode are concerned (see Table 4.2)

The time simulations, when the system is subject to the same disturbances as mentioned above, are also run with reduction of gain on the excitation system of the machine G1 by 33%. The simulation results for the system without and with reduction of gain are given in Figures 4.8a-d, 4.9a-d and 4.10a-d as a dotted-line curve and a full-line curve, respectively. It can be observed from the time responses in these Figures that the damping of the inter-area mode is improved. This finding again corresponds well with the eigenanalysis result in Test 1 of Table 4.6 (Section 4.4.3).

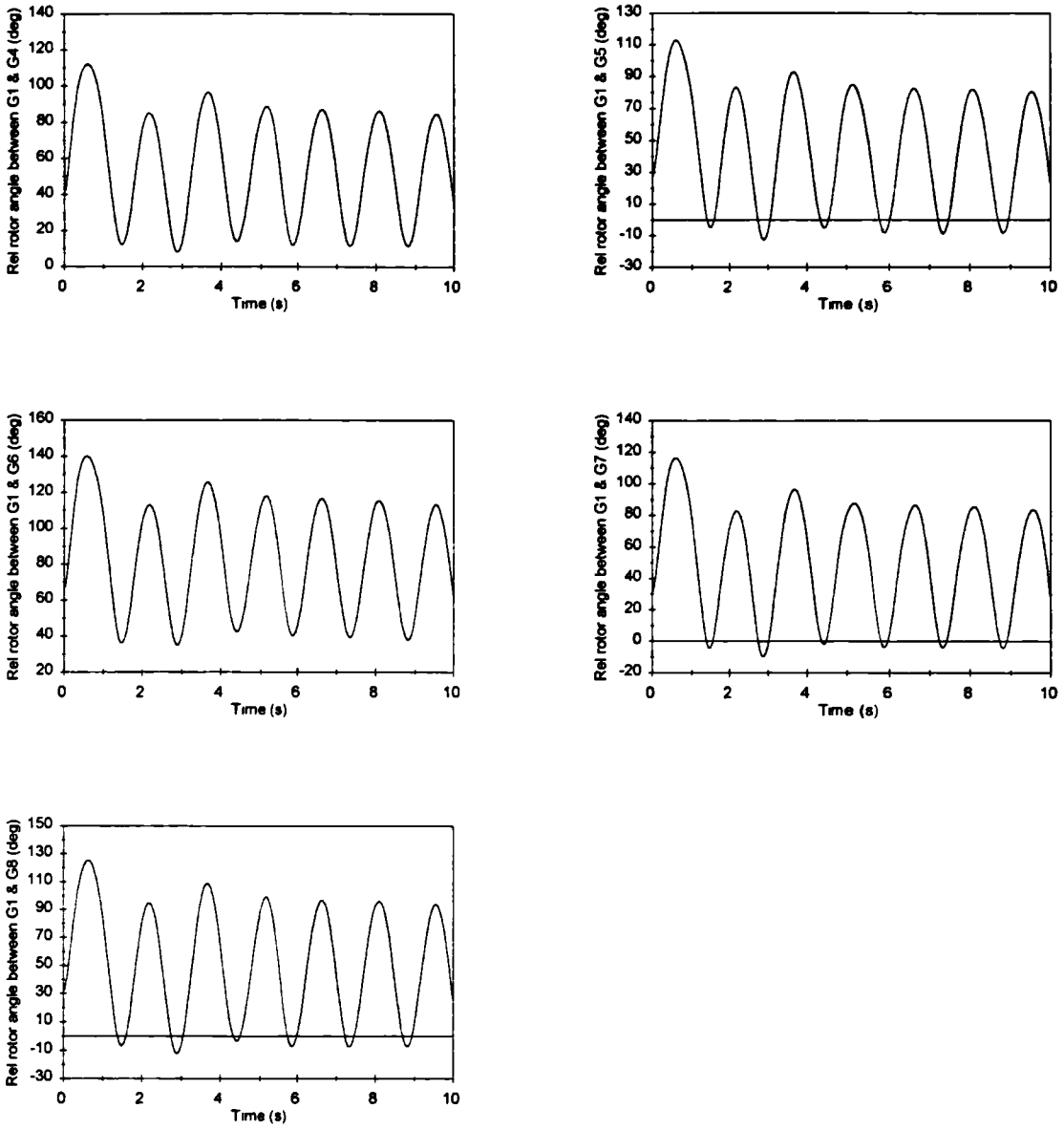


Figure 4.5a Rotor angle swings following a large disturbance

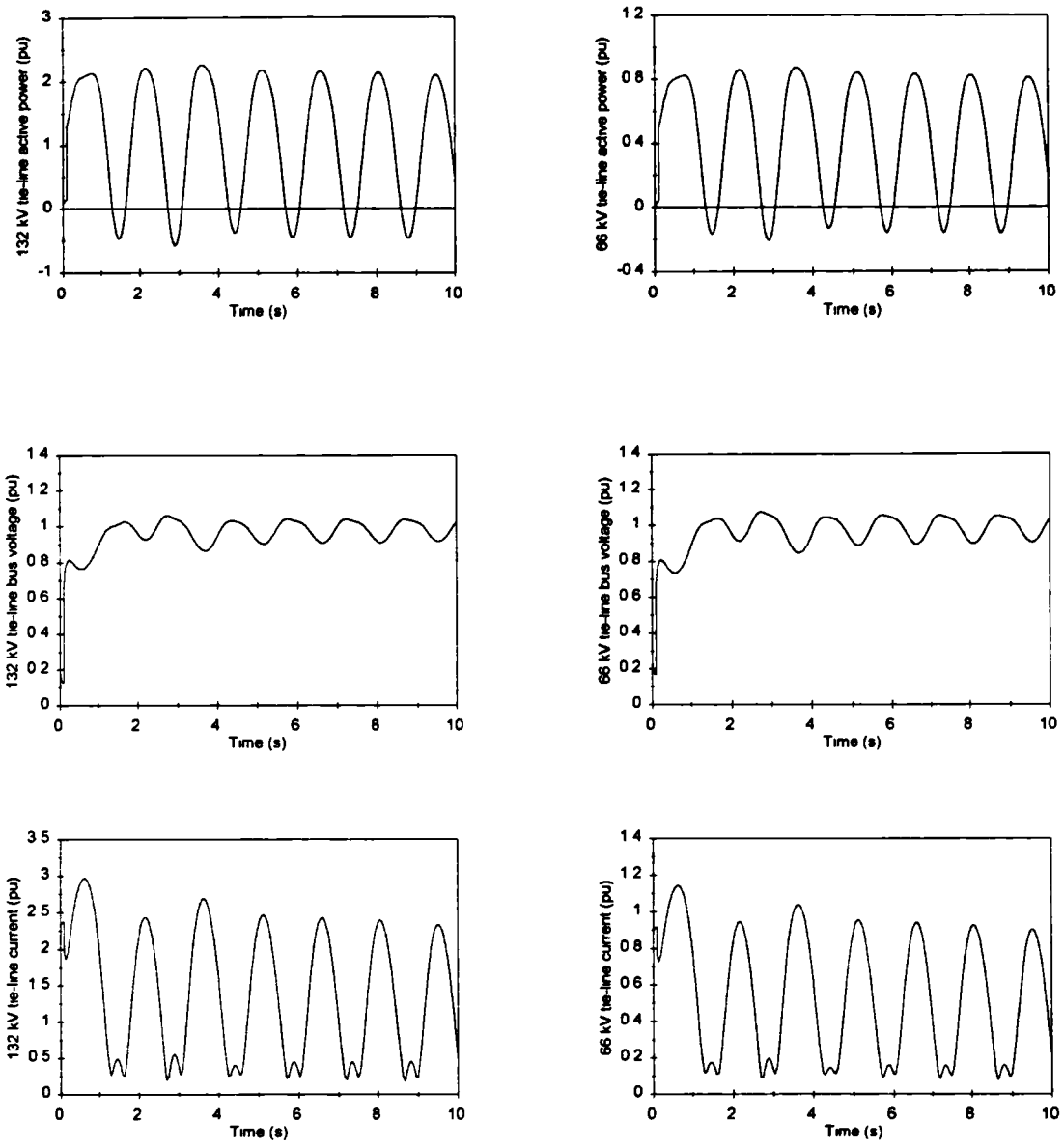


Figure 4.5b Tie-line active power, voltage and current responses to a large disturbance

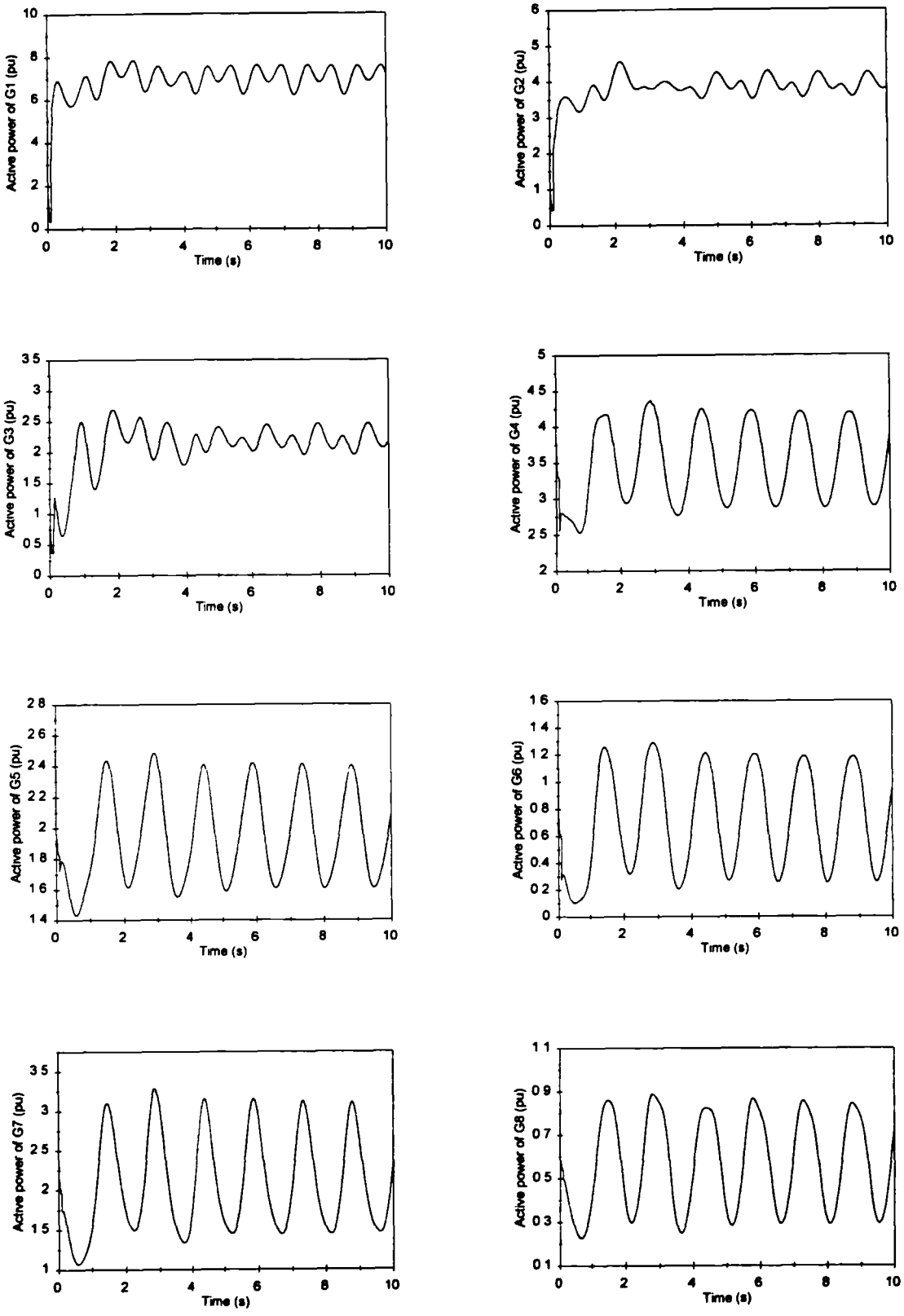


Figure 4.5c Generators' active power output responses to a large disturbance

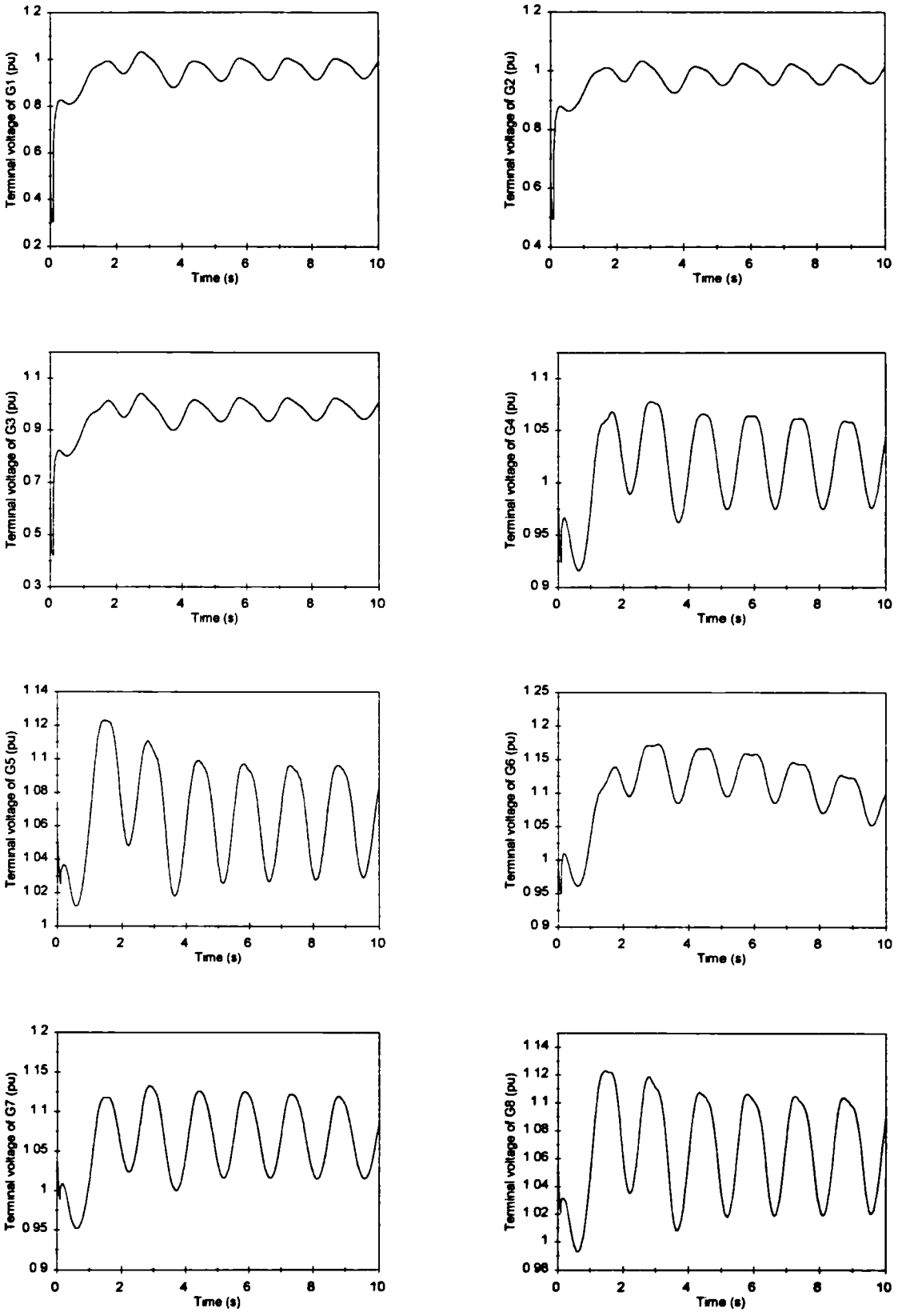


Figure 4.5d Generators' terminal voltage responses to a large disturbance

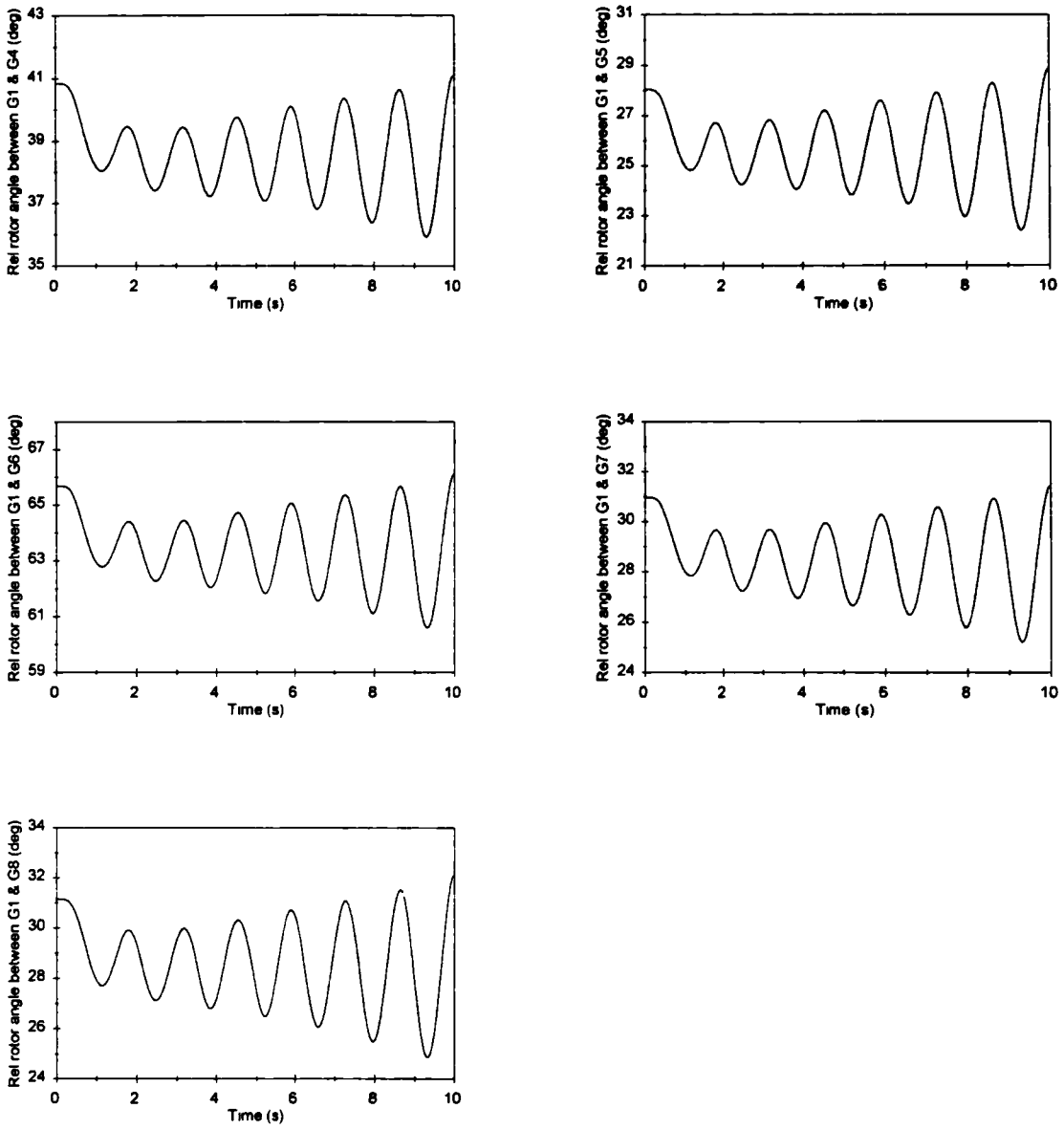


Figure 4.6a Dynamic responses of rotor angle swings following a 1% step small disturbance

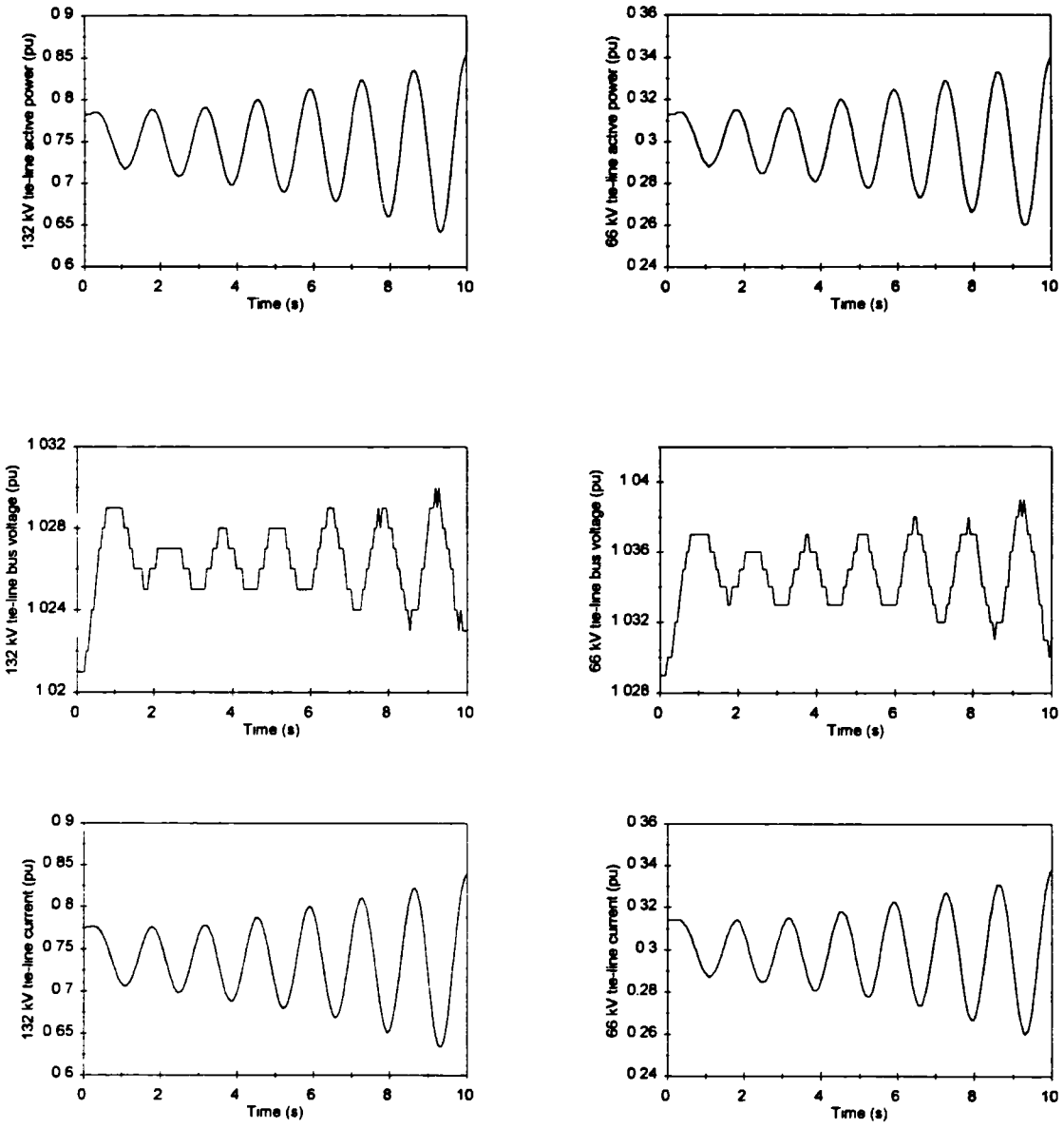


Figure 4.6b Dynamic responses of tie-line active power, voltage and current following a 1% step small disturbance

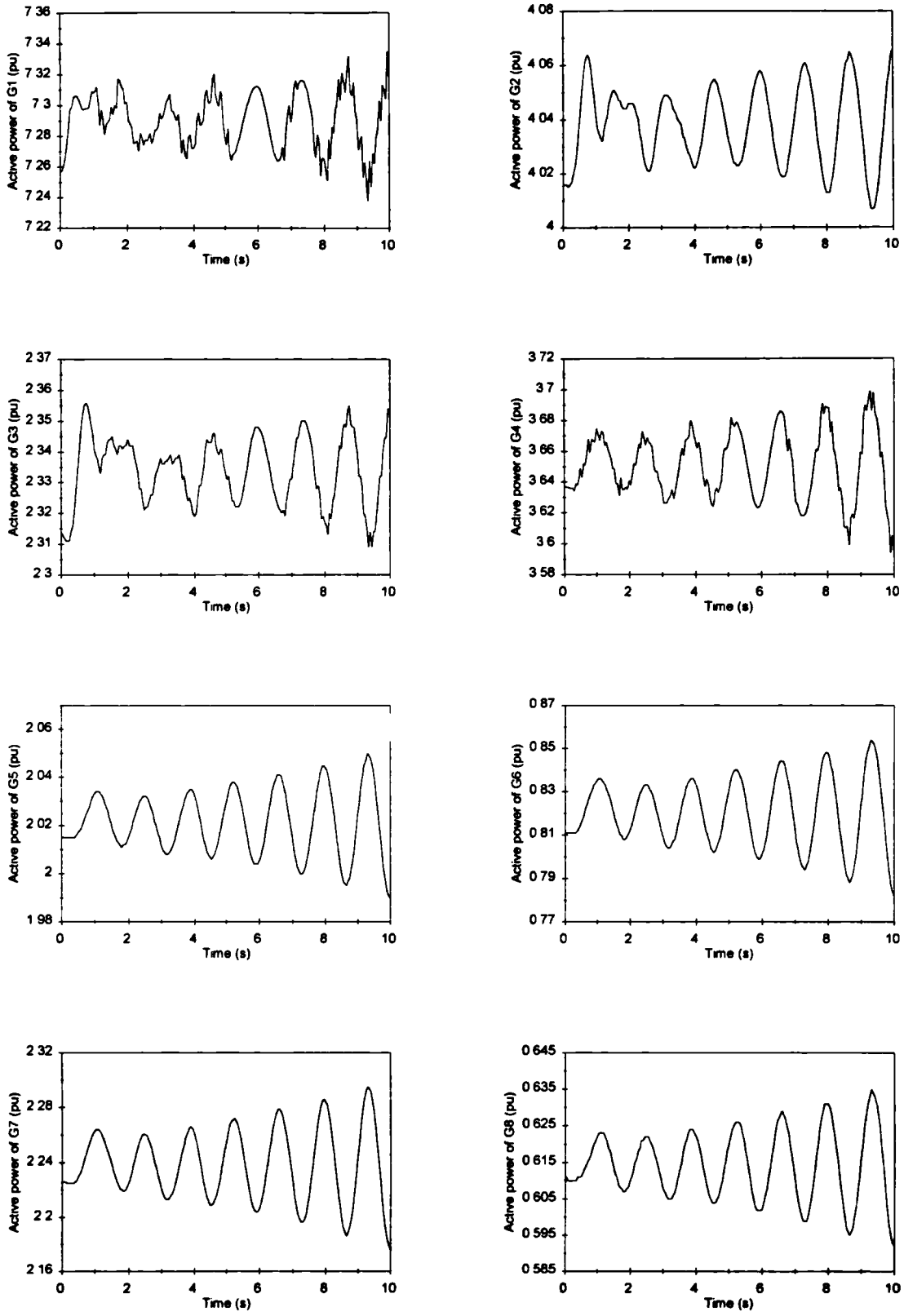


Figure 4.6c Dynamic responses of generators' active power output following a 1% step small disturbance

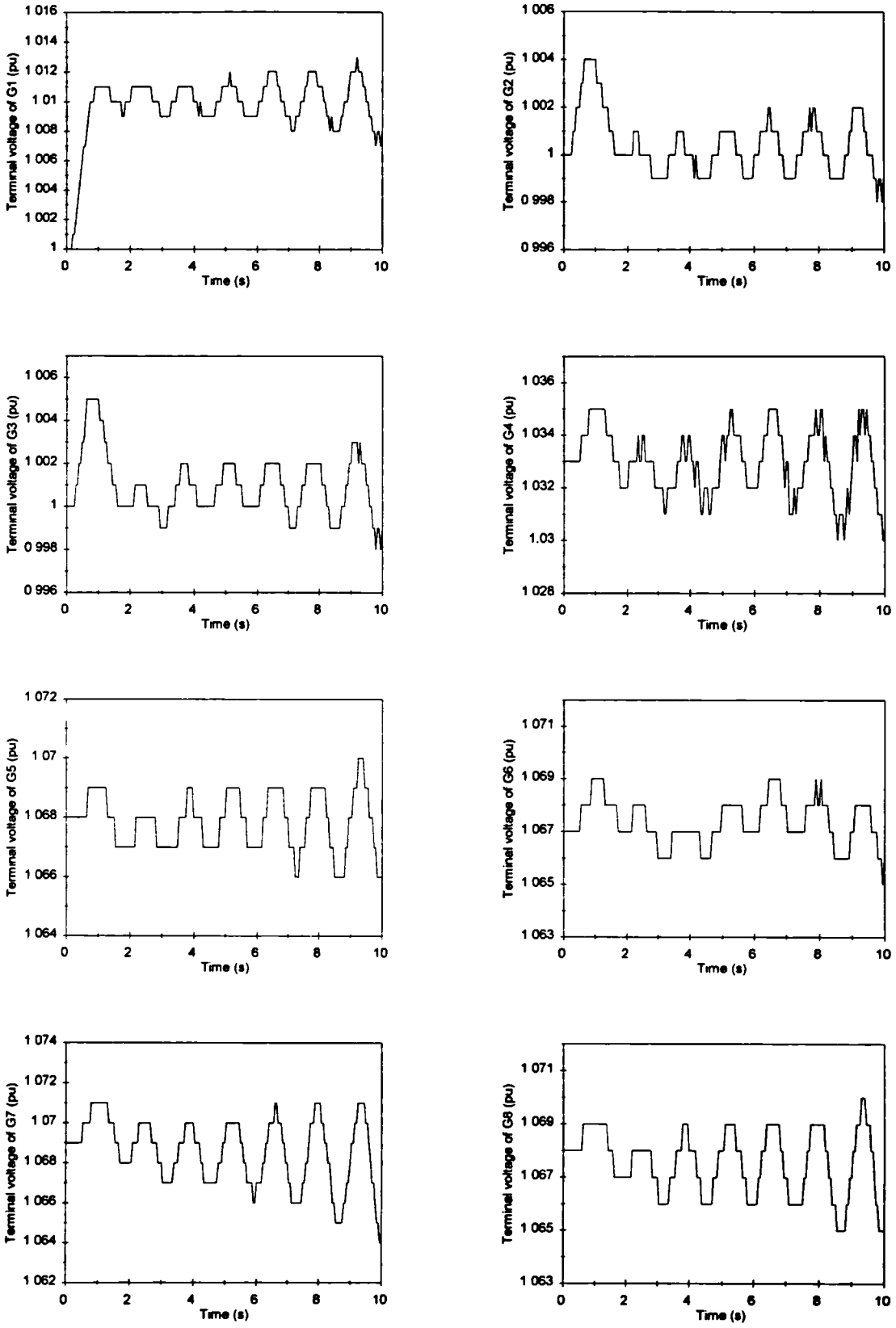


Figure 4.6d Dynamic responses of generators' terminal voltage following a 1% step small disturbance

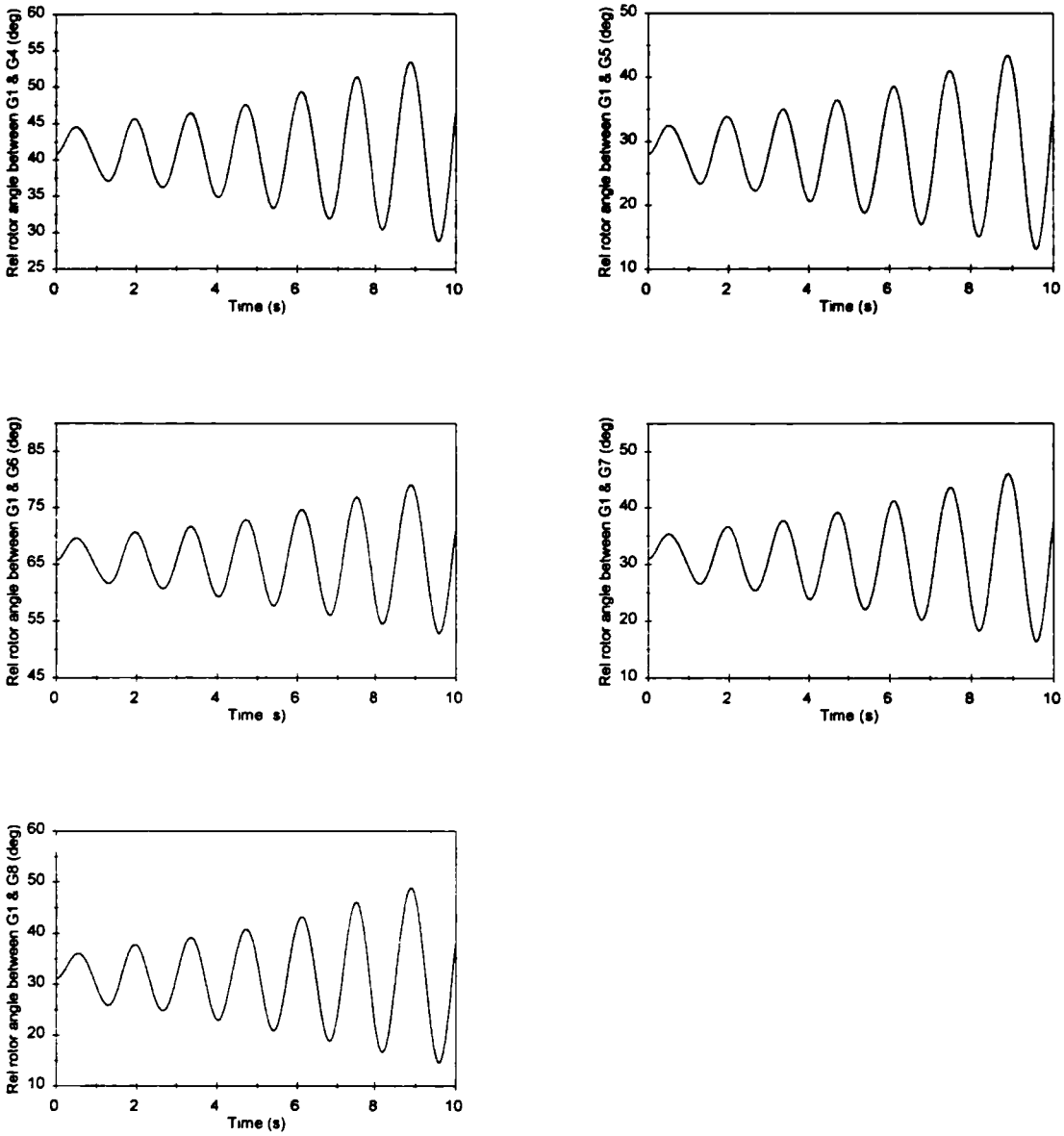


Figure 4.7a Dynamic responses of rotor angle swings following a small disturbance of line switching

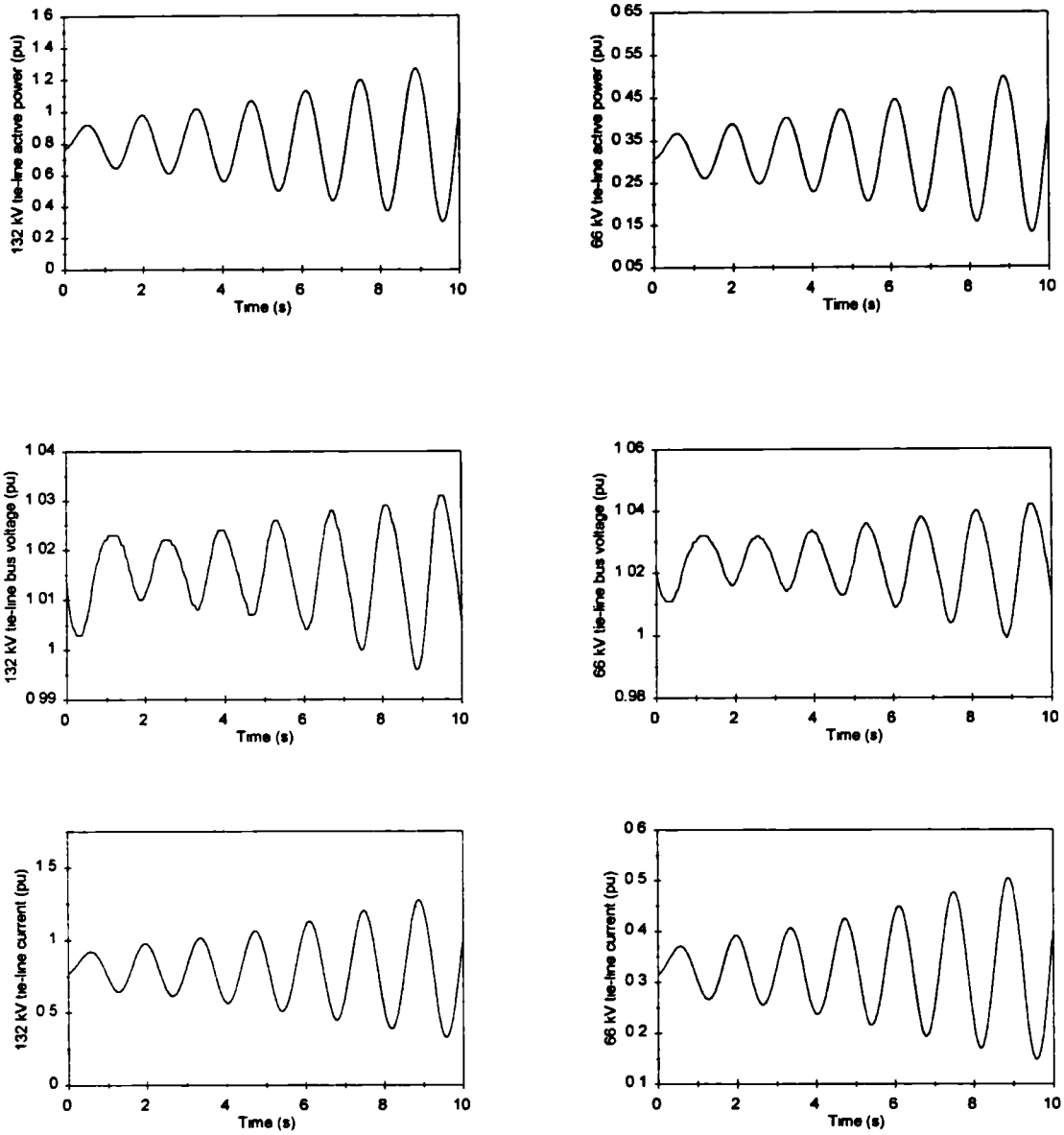


Figure 4.7b Dynamic responses of tie-line active power, voltage and current following a small disturbance of line switching

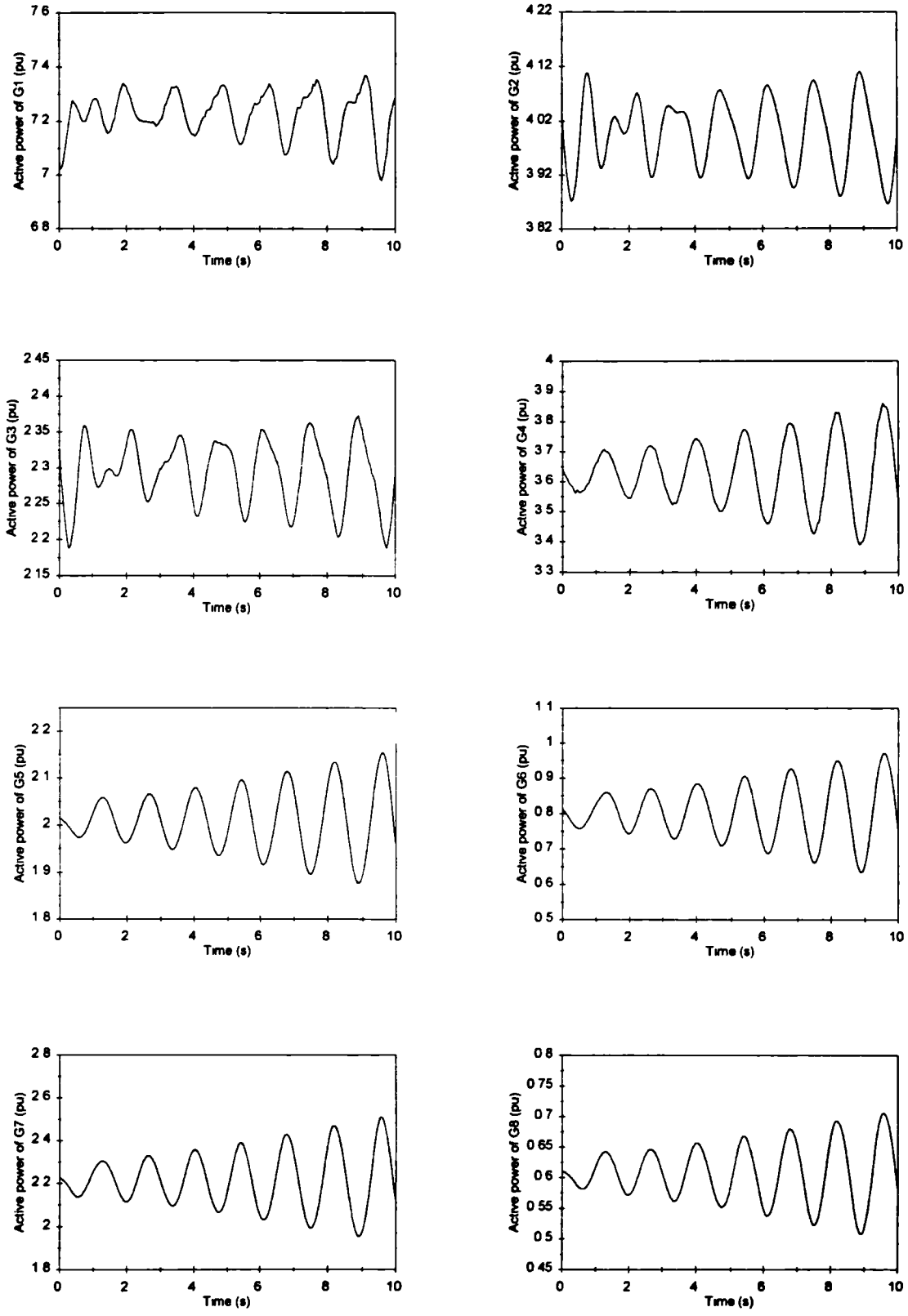


Figure 4.7c Dynamic responses of generators' active power output following a small disturbance of line switching

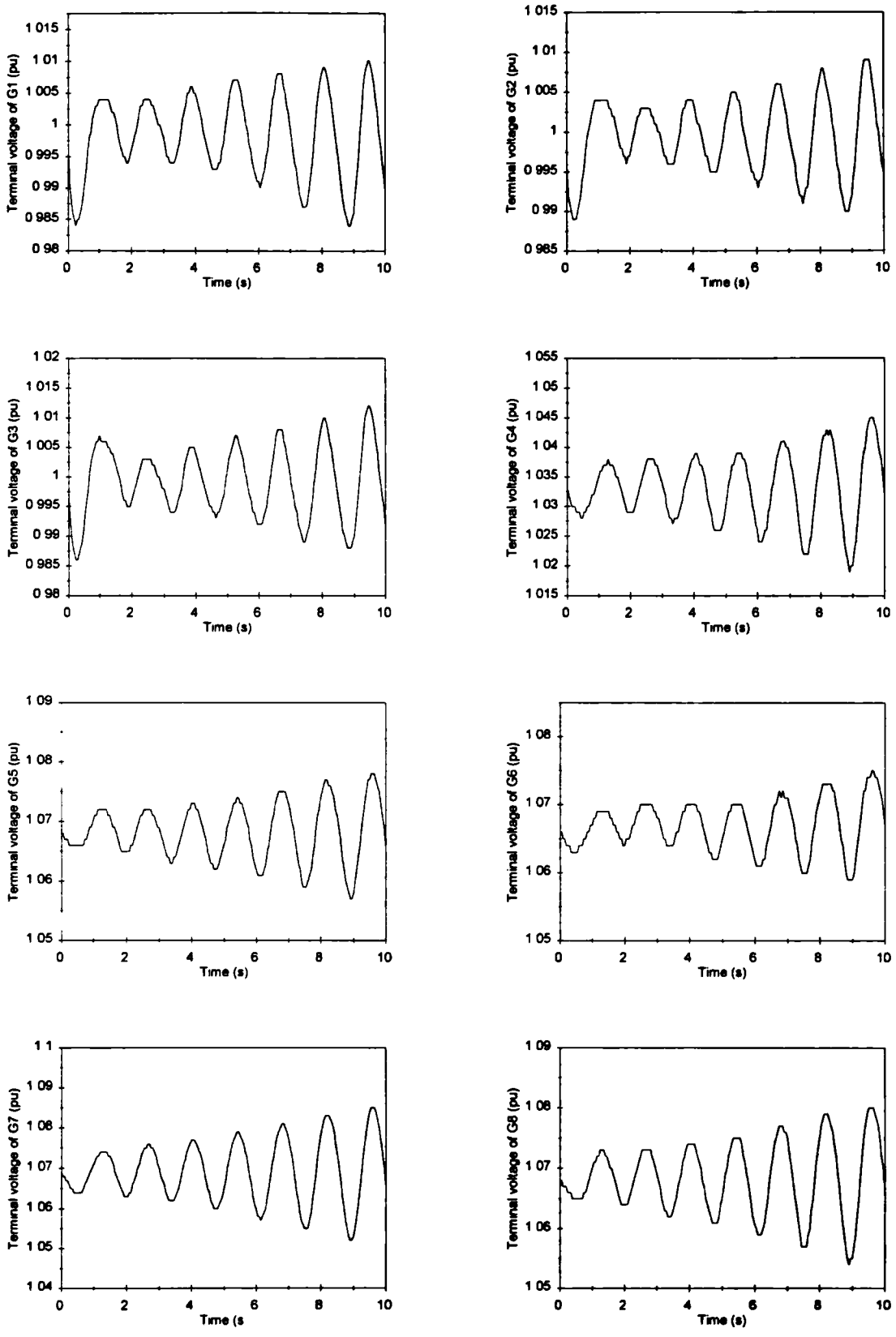


Figure 4.7d Dynamic responses of generators' terminal voltage following a small disturbance of line switching

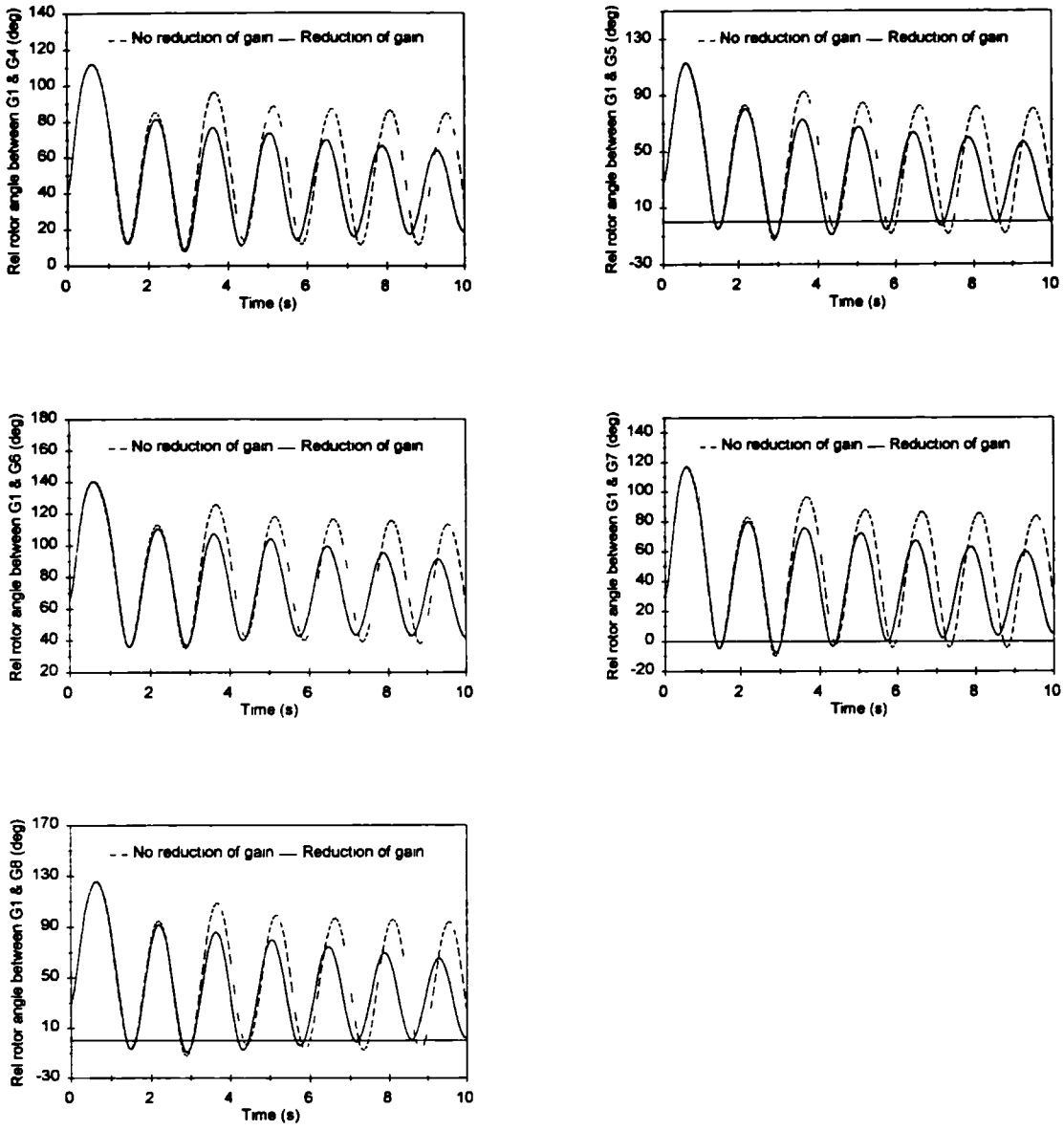


Figure 4.8a Rotor angle swings following a large disturbance with reduction of G1 exciter gain by 33%

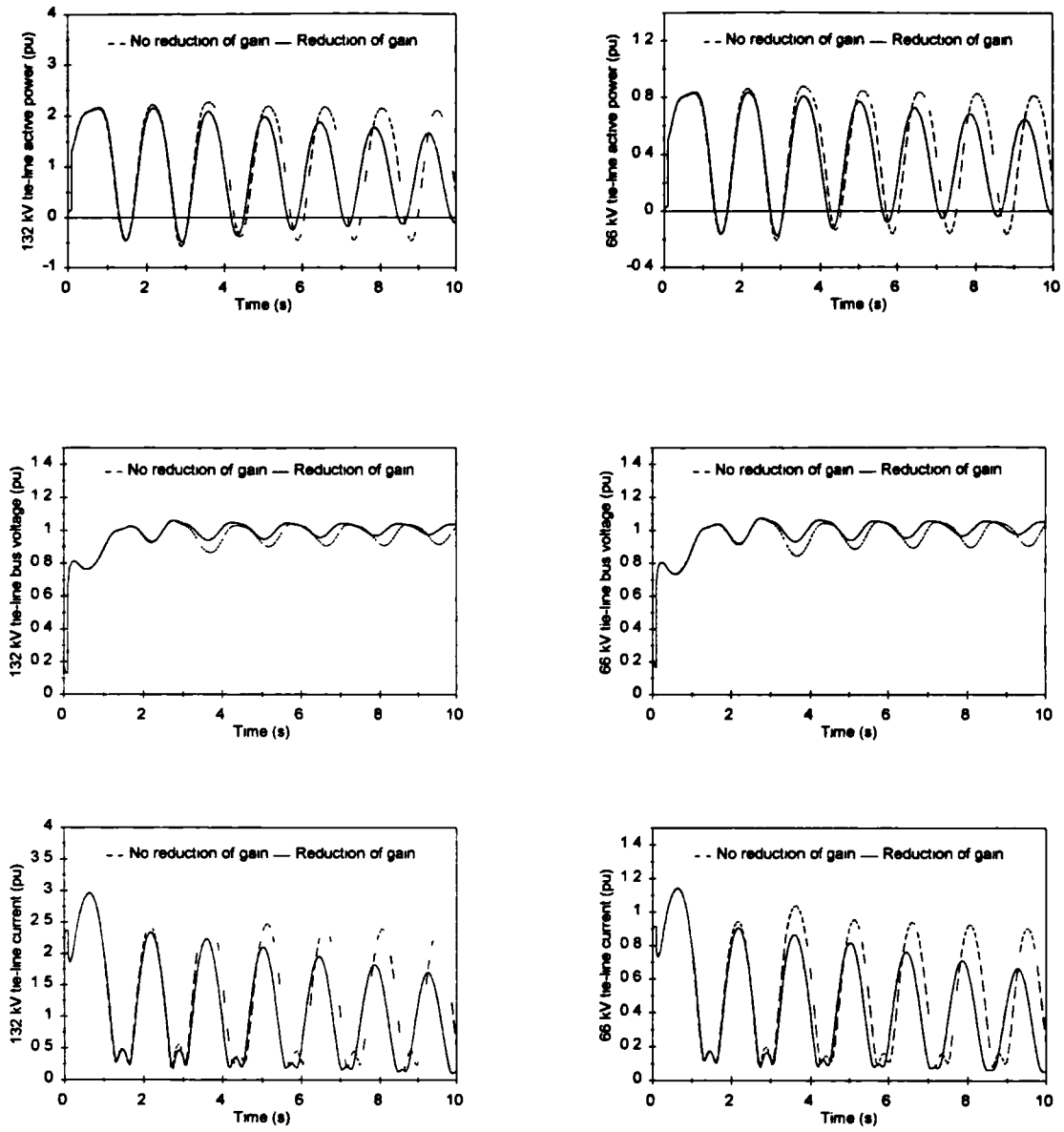


Figure 4.8b Tie-line active power, voltage and current responses to a large disturbance with reduction of G1 exciter gain by 33%

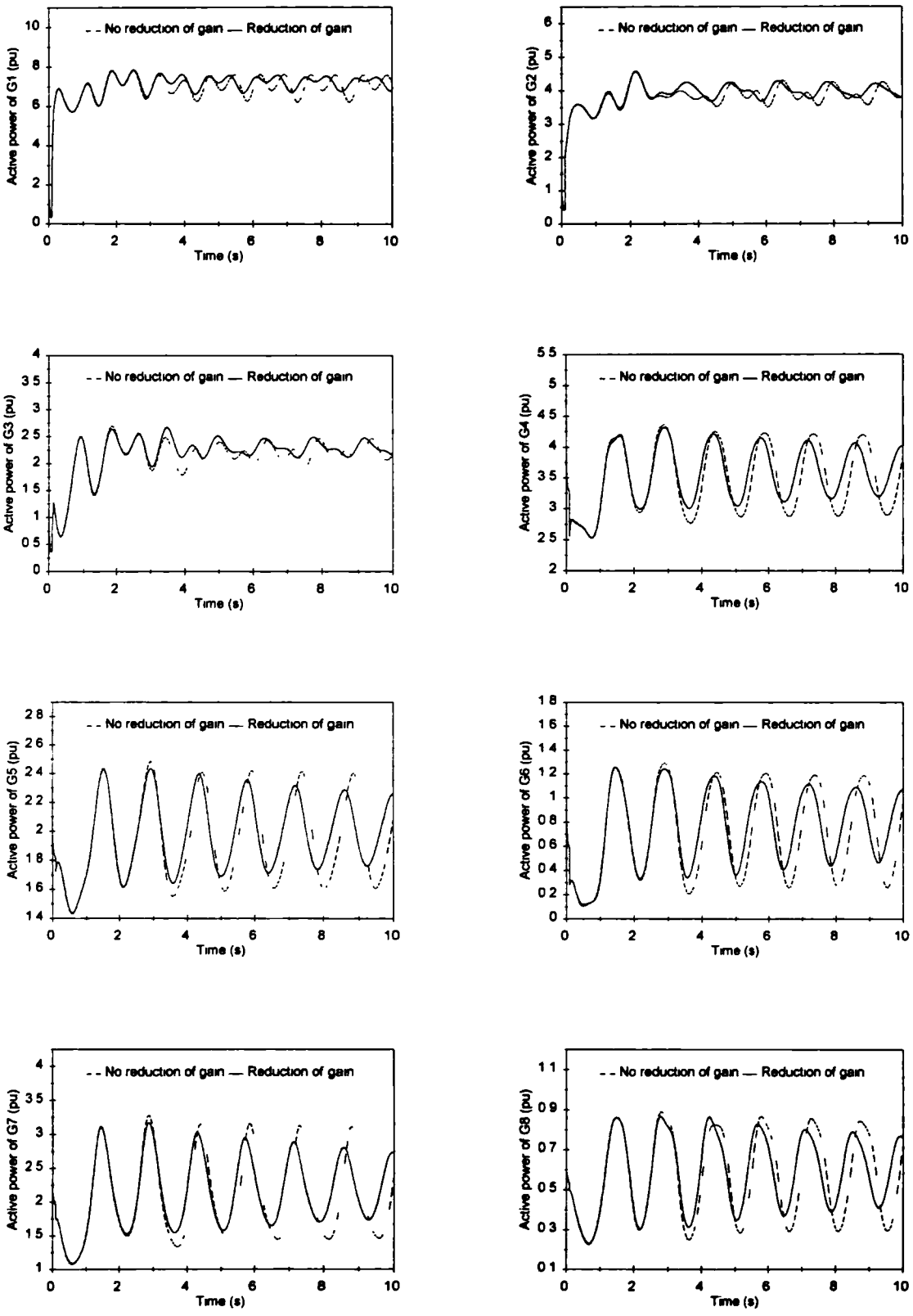


Figure 4.8c Generators' active power output responses to a large disturbance with reduction of G1 exciter gain by 33%

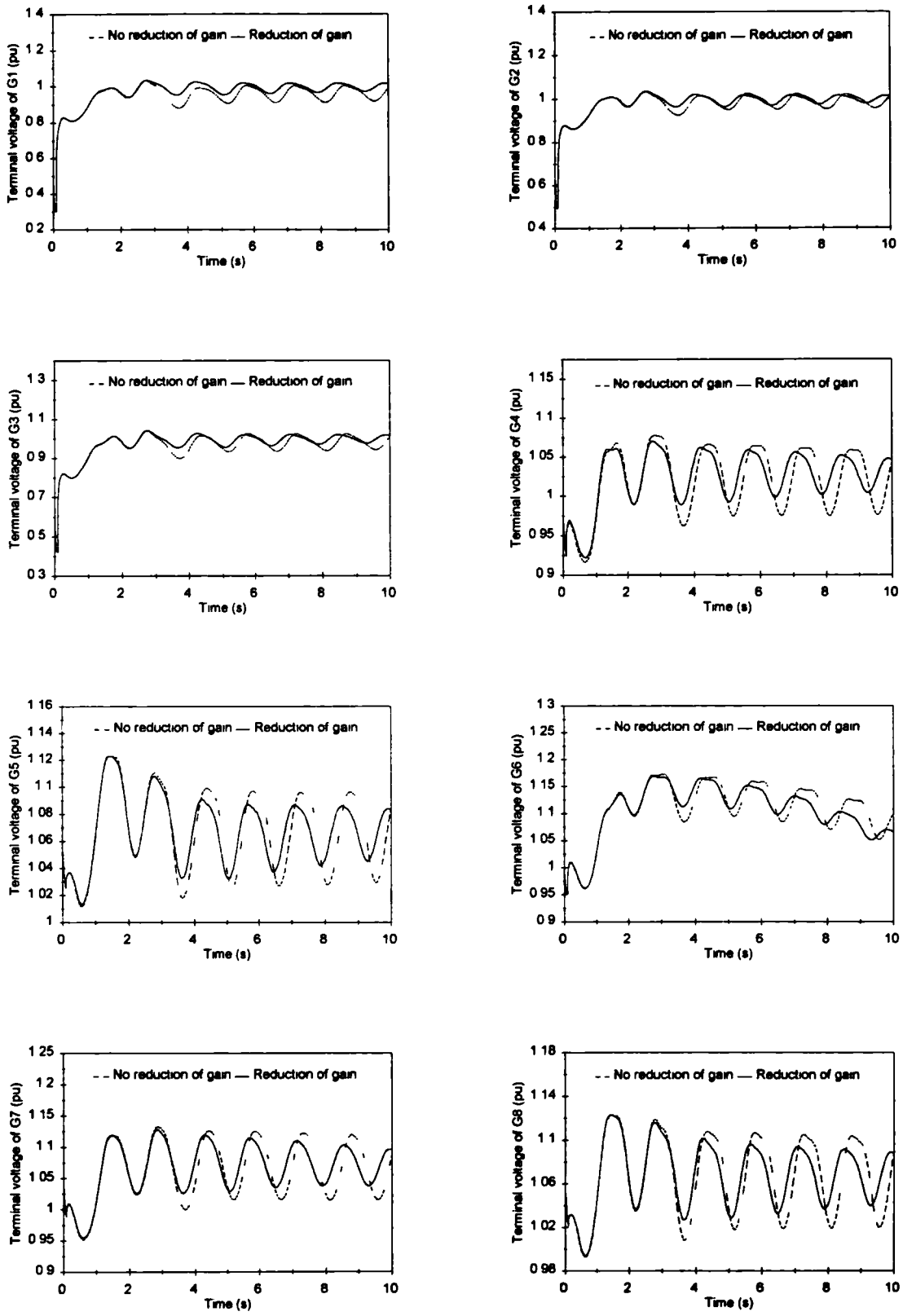


Figure 4.8d Generators' terminal voltage responses to a large disturbance with reduction of G1 exciter gain by 33%

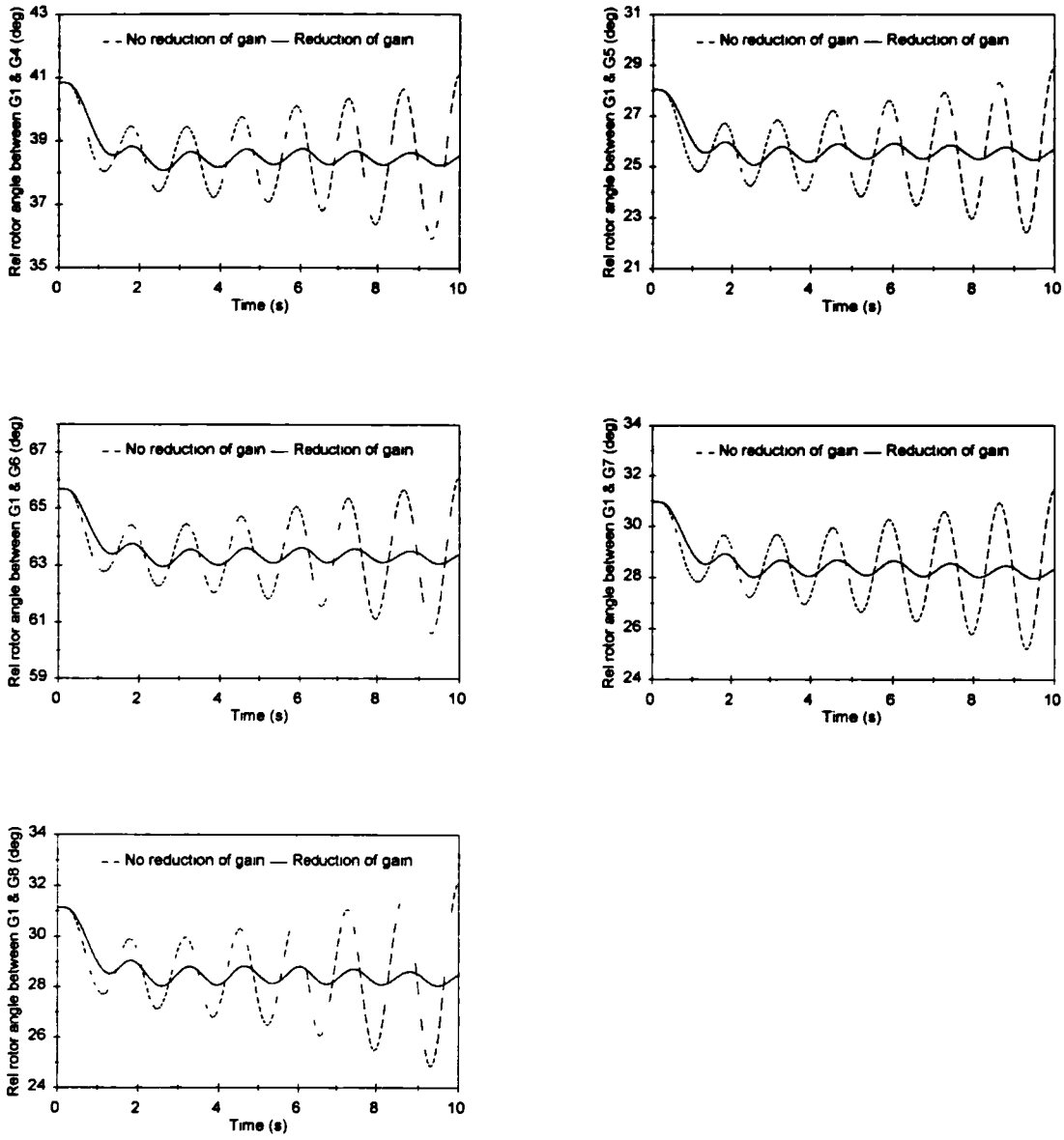


Figure 4.9a Dynamic responses of rotor angle swings following a 1% step small disturbance with reduction of G1 exciter gain by 33%

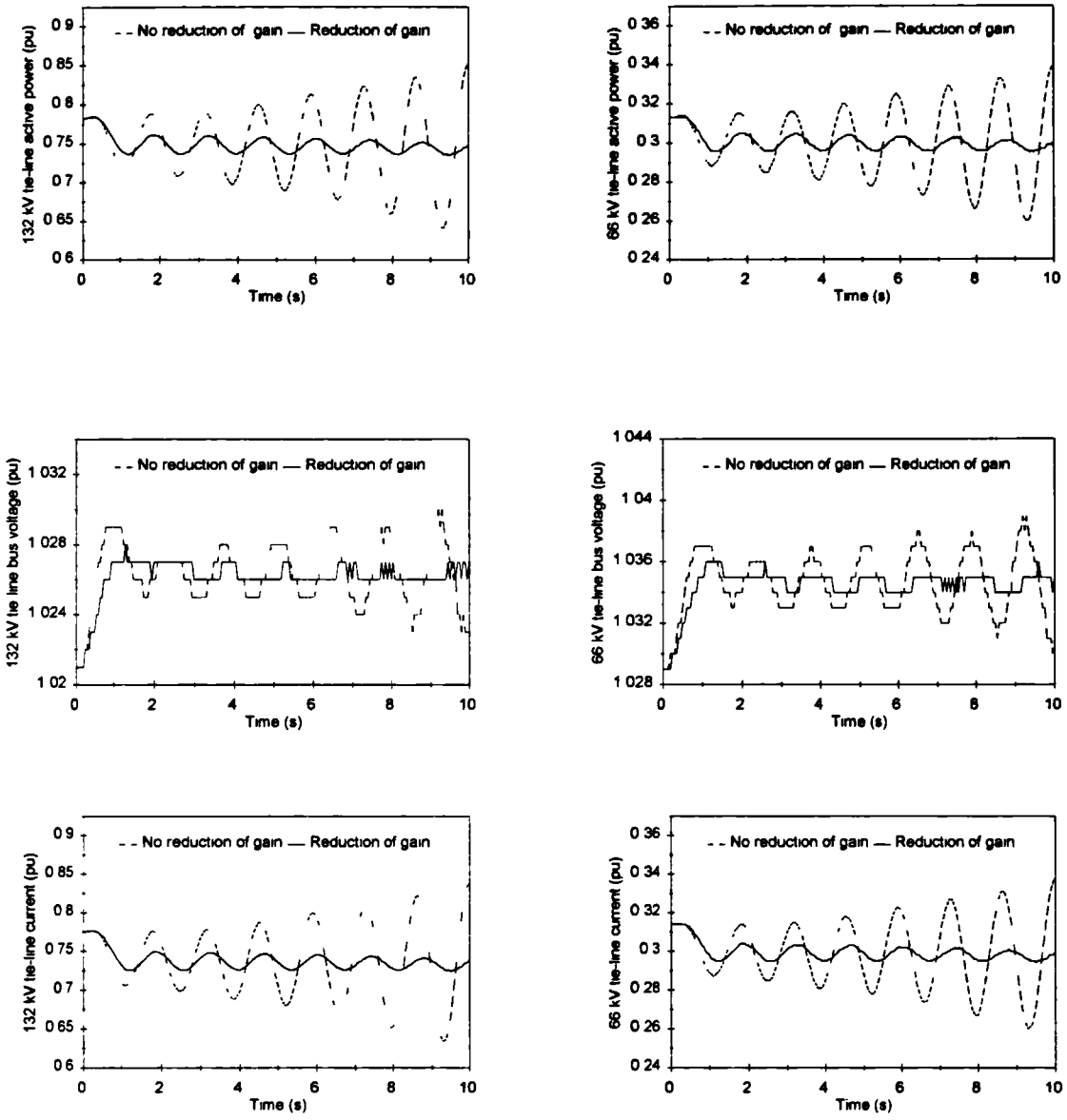


Figure 4.9b Dynamic responses of tie-line active power, voltage and current following a 1% step small disturbance with reduction of G1 exciter gain by 33%

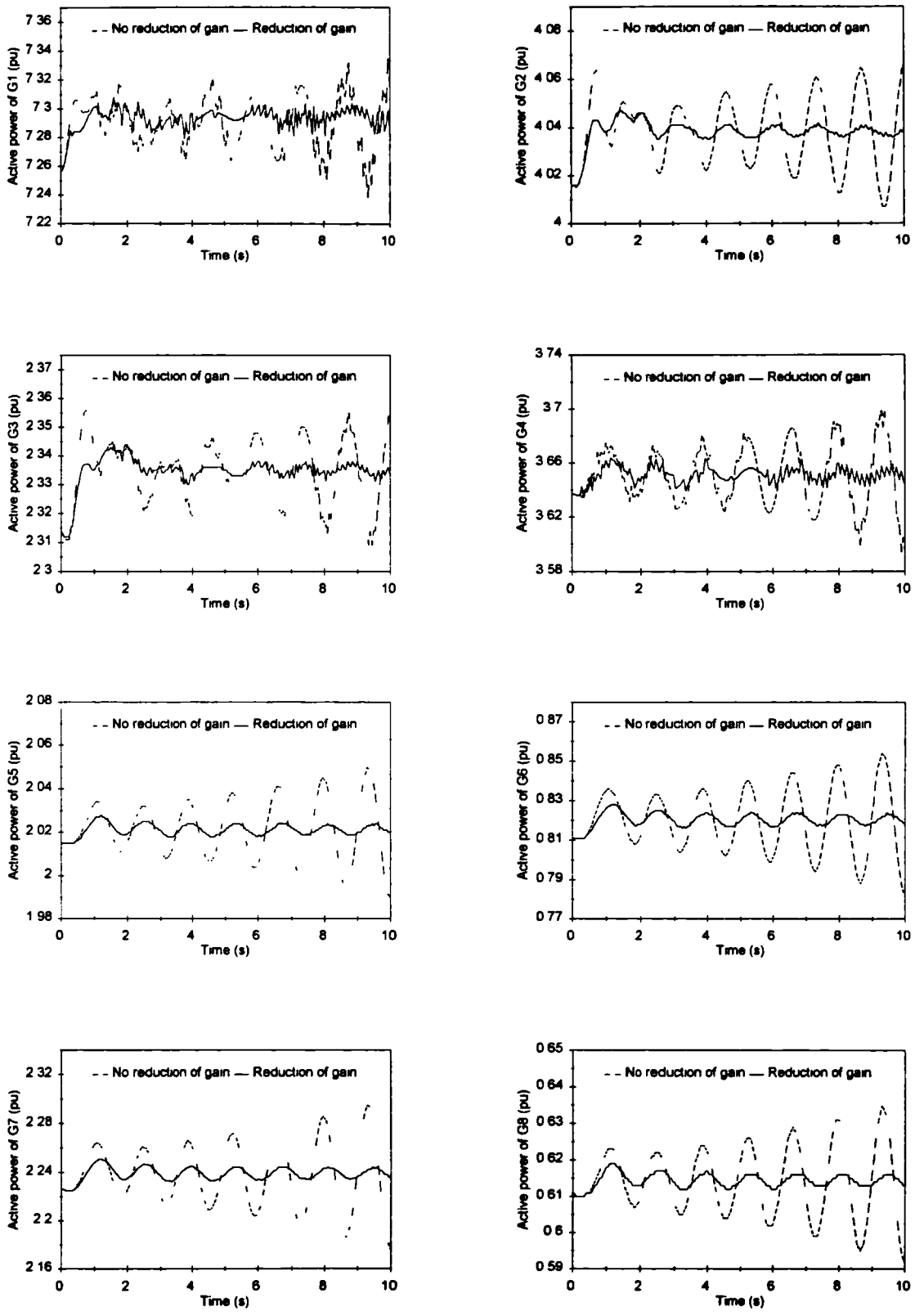


Figure 4.9c Dynamic responses of generators' active power output following a 1% step small disturbance with reduction of G1 exciter gain by 33%

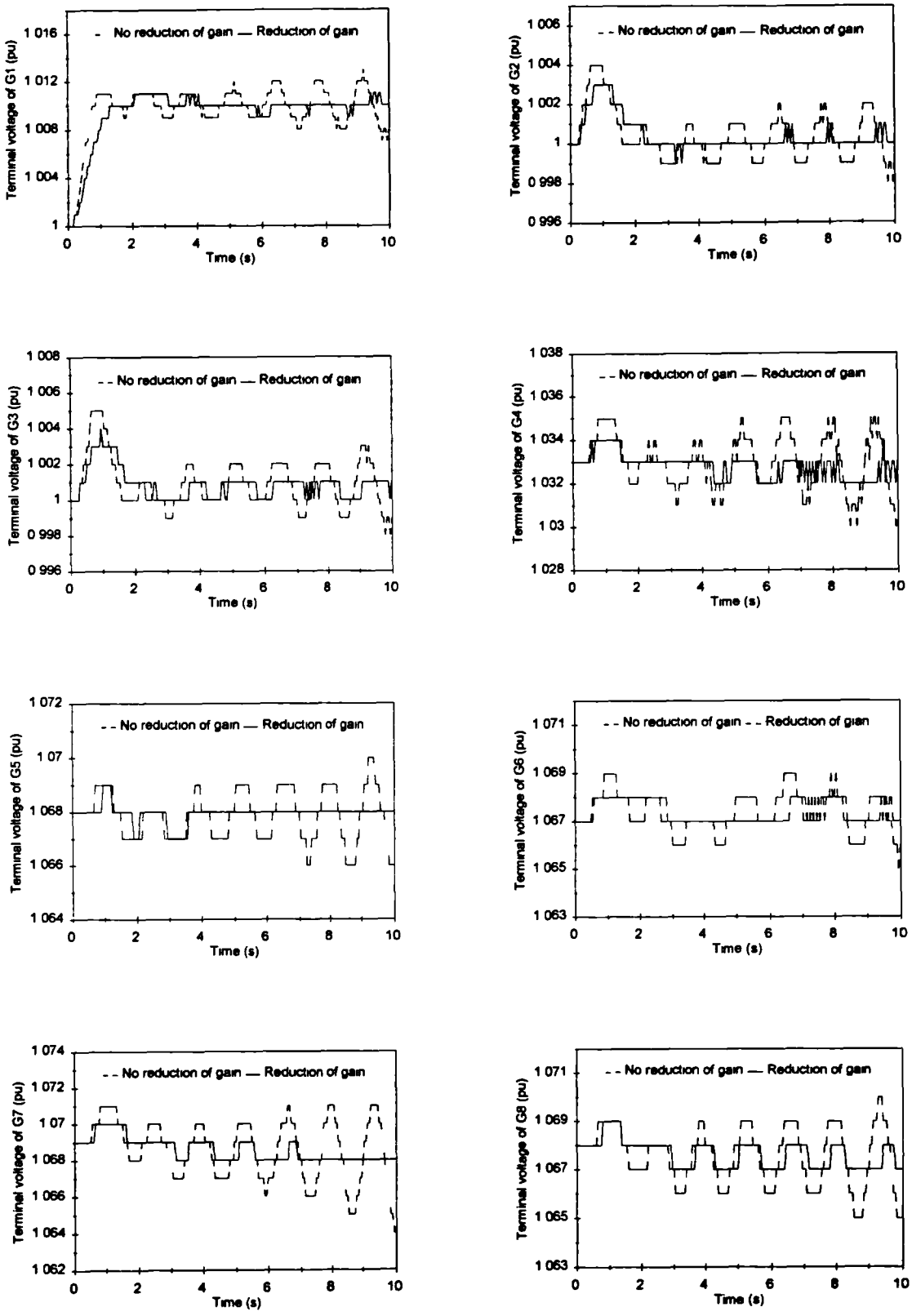


Figure 4.9d Dynamic responses of generators' terminal voltage following a 1% step small disturbance with reduction of G1 exciter gain by 33%

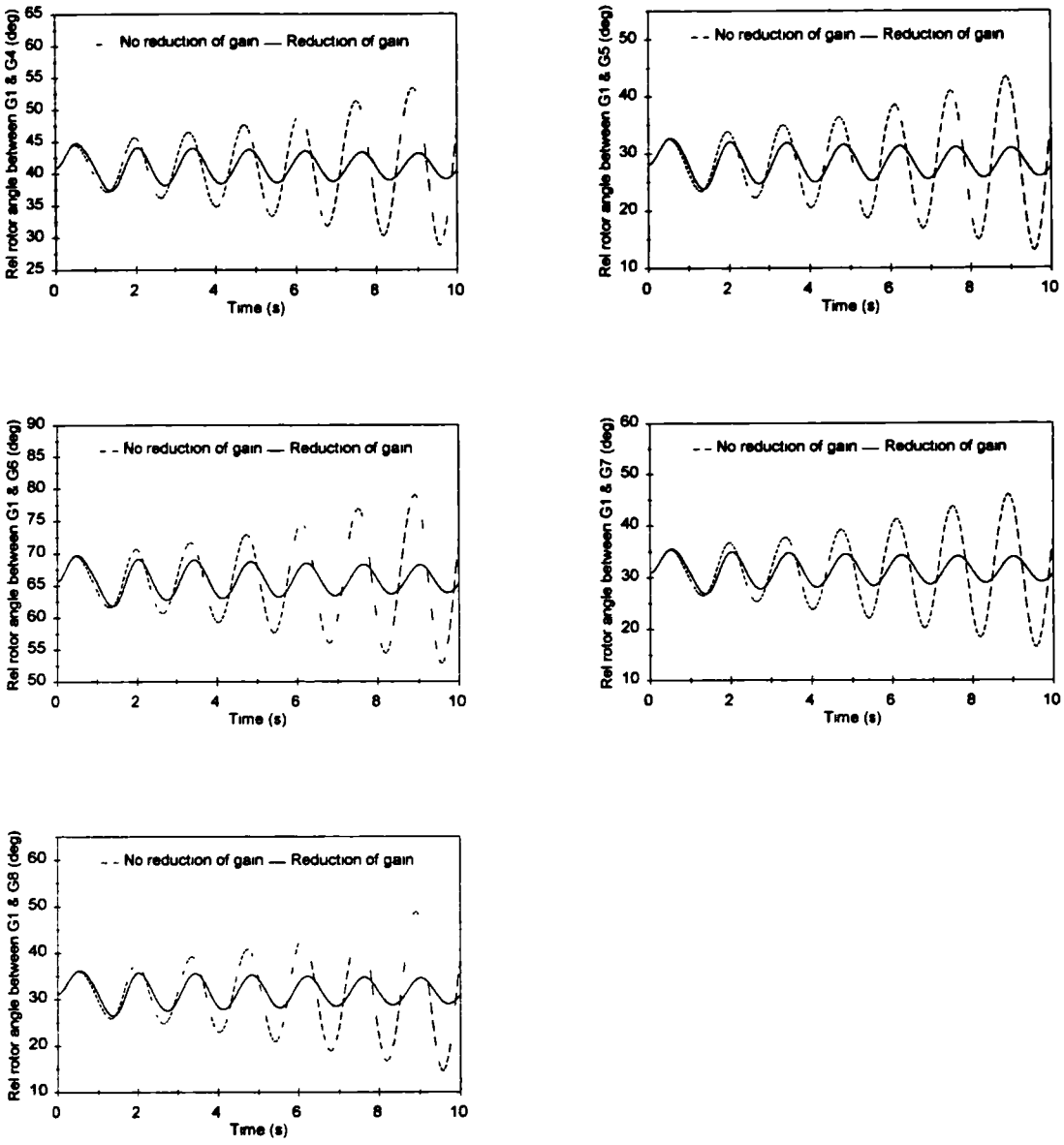


Figure 4.10a Dynamic responses of rotor angle swings following a small disturbance of line switching with reduction of G1 exciter gain by 33%

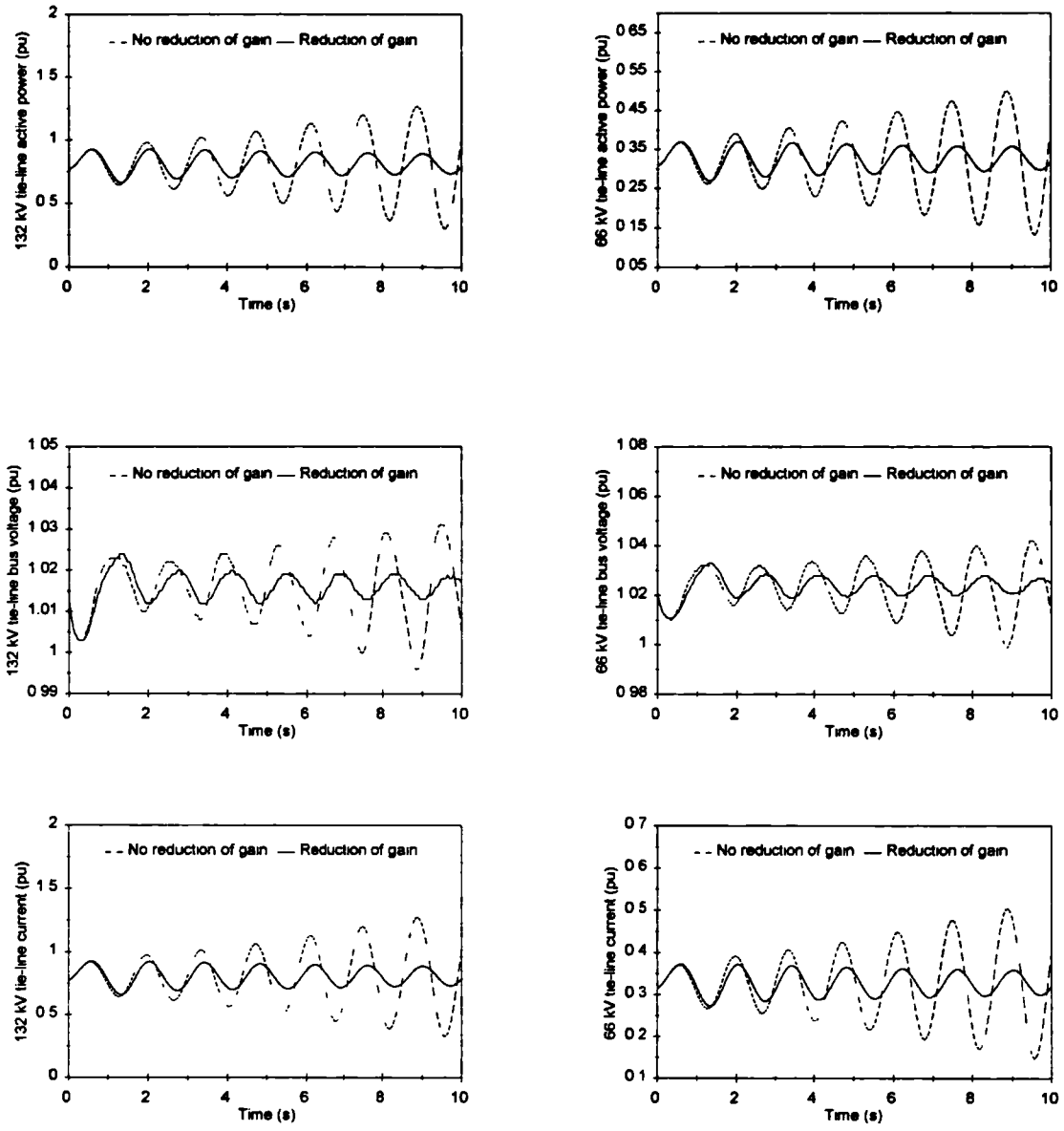


Figure 4.10b Dynamic responses of tie-line active power, voltage and current following a small disturbance of line switching with reduction of G1 exciter gain by 33%

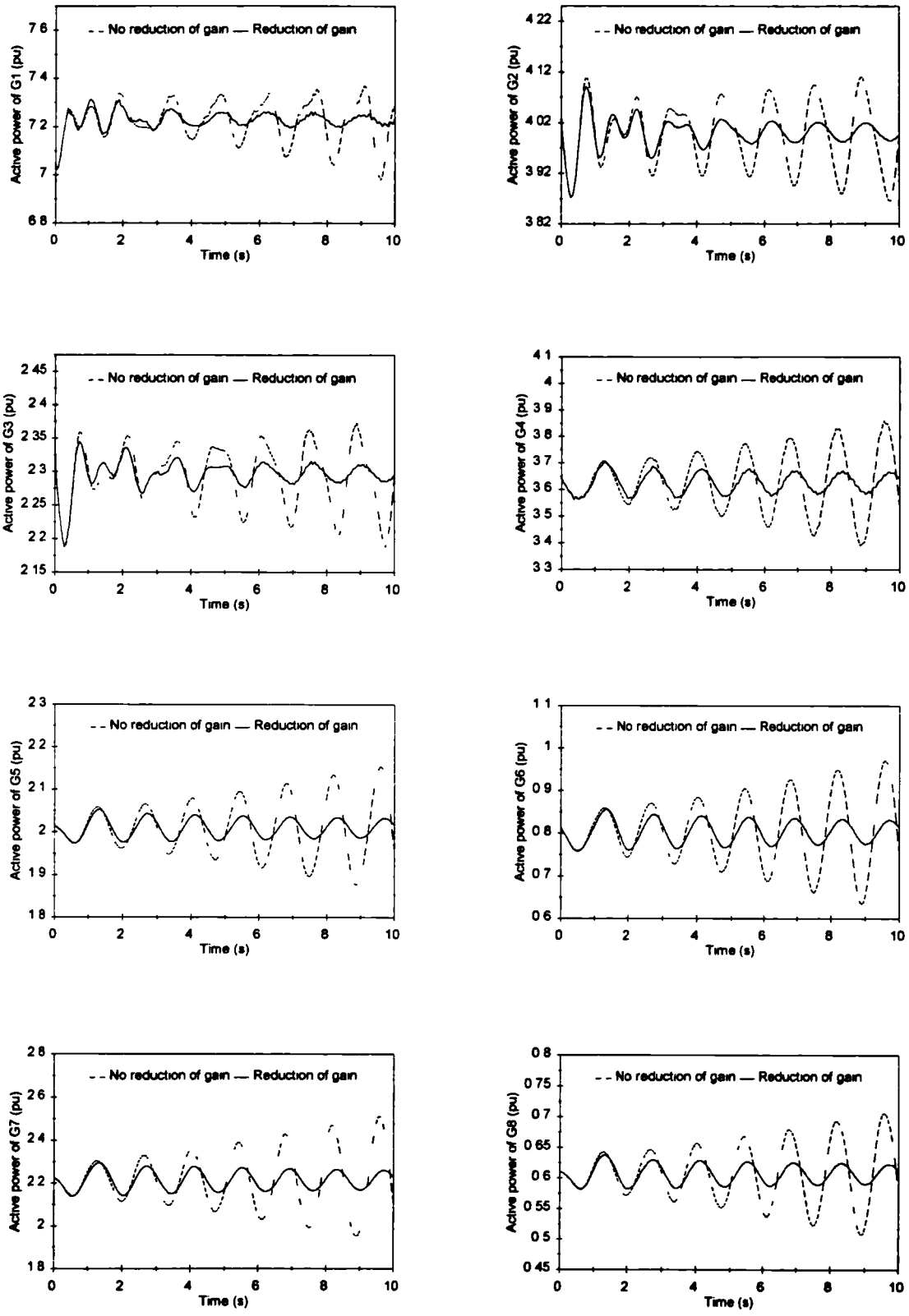


Figure 4.10c Dynamic responses of generators' active power output following a small disturbance of line switching with reduction of G1 exciter gain by 33%

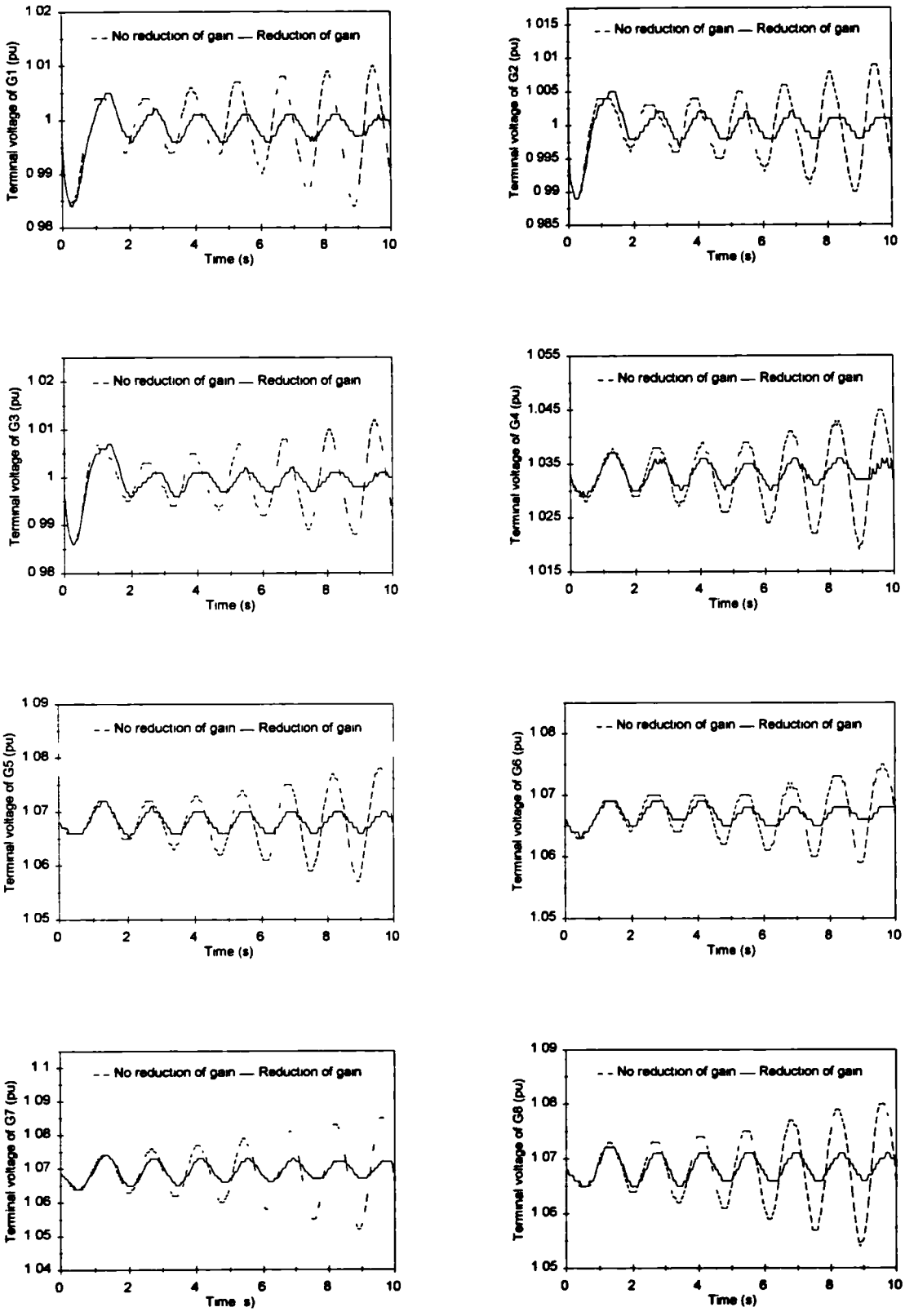


Figure 4.10d Dynamic responses of generators' terminal voltage following a small disturbance of line switching with reduction of G1 exciter gain by 33%

CHAPTER FIVE

DAMPING INTER-AREA OSCILLATIONS USING A CONTROLLABLE PHASE SHIFTER

5.1 INTRODUCTION

In view of the instability for the inter-area mode, it was considered desirable to see how a FACTS controller might damp out inter-area oscillations. The advantages of using FACTS controllers to add damping to inter-area modes of oscillation have been discussed in Section 1.4. This chapter outlines a procedure used to design a FACTS controller for stabilizing an unstable inter-area oscillatory mode in an interconnected system. Two problems are discussed: location and controller design. The location problem involves siting a FACTS controller where its modulation control can be most effective in damping out the inter-area mode of concern. The participation factor approach [106] and mode controllability matrix approach as suggested by Lal and Fleming [107] have been applied for identifying the optimum location of a FACTS controller in the interconnected system. The controller design requires the design of the phase compensation network and the calculation of the controller gain. The small signal model of the interconnected system developed in Chapter 3 and the corresponding closed-loop eigenvalue sensitivities have been used to determine the controller parameters [108]. The selection of a FACTS device and the selection of a feedback signal to a FACTS controller are also discussed in this chapter.

5.2 SELECTION OF A FACTS DEVICE

The selection of a FACTS device for modulation is based on the participation of the device in the oscillation. In other words, the search is for a device by which the inter-area mode is controllable. As far as the 2-area interconnected 8-machine system is concerned, series and shunt devices have been considered. Several authors [38, 42, 69] have demonstrated that series devices such as TCSC and CPS can exhibit more effective damping than shunt devices like SVC for inter-area modes. Therefore, a feasibility study of using series devices in

the study system was conducted. Because of the short transmission lines in the study system, a TCSC cannot be applied effectively. For this reason, a CPS was employed in this context to enhance the damping of the inter-area mode. The CPS is one of the potential options in the context of FACTS. Promising results have been obtained for enhancing the small signal stability of interconnected systems [38-40, 54-59].

5.3 SELECTION OF A FEEDBACK SIGNAL

Once the CPS has been chosen, the feedback, input or control signal needs to be selected. The signal should be sensitive to the inter-area mode of concern, while insensitive to the local modes. In addition, the use of the signal should not cause any adverse interactions between the controllers [37].

A FACTS device can be installed at any place in a power system according to the system requirements. However, it is impractical for a FACTS controller to feedback a state variable or an output variable that is not locally available at the controller location due to economy as well as reliability reasons. For these reasons, a decentralized control scheme is adopted here, by which only locally measurable quantities (frequency, active power, current, voltage, etc.) are used as the feedback signal for the CPS controller.

In Section 2.4 the variation of the system frequency or the transmitted active power was shown to be an effective feedback signal for damping action. In the case of damping inter-area oscillations, the area frequency difference has been recommended by Larsen and Chow [37] as a suitable feedback signal for a series device installed in the tie line. Here the active power flow through the tie line containing the CPS (the selection of the CPS installation location will be discussed in the next section) is selected as the feedback signal because

(i) it is easy to measure,

(ii) it is observable in the inter-area mode of interest,

(iii) it is sensitive to inter-area mode oscillations on the machines and tie lines of interest, while it has little sensitivity to local mode oscillations, and

(iv) several authors [55, 58, 59] have shown that a CPS equipped with a feedback controller utilizing tie-line power deviation can effectively damp the inter-area mode.

In general, the current, voltage or other signal synthesised from locally measurable information is also a possible feedback signal.

5.4 SELECTION OF CPS LOCATION

For a multimachine system, the selection of a transmission line on which the CPS is to be installed is very important because the effectiveness of the phase shifting action varies with its location. In this research, the most effective location for installing a CPS is determined by analyzing the participation factors and mode controllability of the system. The participation factor computation identifies the phase shifting action (state variable ϕ as defined in Equation (3.77)) involved in damping the inter-area mode at different CPS locations.

In Section 3.9 the system response in the presence of input was given as equation (3.109) and is repeated here for reference.

$$\Delta \dot{x} = A\Delta x + B\Delta u \tag{5.1}$$

To obtain a quantitative measure of the controllability of the system, the linearized dynamic system in equation (5.1) is transformed into another dynamic system using the transformation

$$\Delta x = T z \tag{5.2}$$

Then

$$\dot{z} = T^{-1}AT\,z + T^{-1}B\Delta u \tag{5.3}$$

where T is the modal matrix consisting of the right eigenvectors of A and $\Lambda = T^{-1}AT$ is a diagonal matrix with the eigenvalues of A as its elements [18]. The matrix $T^{-1}B$ is called the mode controllability matrix as the entry of $T^{-1}B$ indicates to what extent the inter-area mode can be controlled using the CPS control input u. Therefore, by analyzing the magnitudes of the entries of $T^{-1}B$ for different CPS locations, the best location for installing the CPS can be identified. The best location is chosen where the magnitude of the entry is highest, corresponding to the inter-area mode to be controlled.

Due to a highly meshed network in the study system, it is anticipated that if the CPS is located at a point other than an interconnecting point, the impact of the CPS controller on the damping of the inter-area mode might not be significant. To effectively stabilize the inter-area oscillatory mode, it was decided to place the CPS on the tie line, where the change of phase shifting action can effectively modulate the power swing mode [59, 109].

The dynamic model of the CPS given in Figure 3.12 is shown here in Figure 5.1.

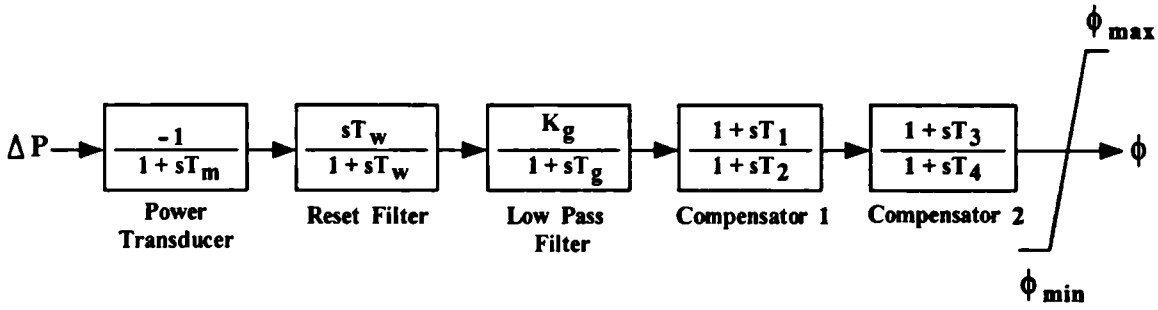


Figure 5.1 CPS damping controller circuit

With the base CPS control setting provided in Table 5.1, the results of participation factor and mode controllability analyses with a CPS installed in the 132 kV or 66 kV tie line (Figure 4.1) are given in Table 5.2.

Table 5.1 Base CPS control setting

T_m (s)	T_w (s)	K_g	T_g (s)	T_1 (s)	T_2 (s)	T_3 (s)	T_4 (s)
0.03	10.0	0.5	0.1	0.1	0.2	0.1	0.2

Table 5.2 Participation factors and controllability of CPS to the inter-area mode

CPS Location	Participation Factors	Controllability	Closed-Loop Eigenvalue	Damping Ratio
132 kV Tie	0.437	0.7171	-0.3150±4.2858	0.0733
66 kV Tie	0.232	0.3820	-0.0095±4.7087	0.0020

Since the control objective is to provide additional damping to the inter-area mode, only the participation factors and controllability of this oscillatory mode need be considered. From Table 5.2, it can be seen that when a CPS is installed in the 132 kV tie line, the participation factor, controllability and damping ratio for the inter-area mode are much higher than those with the CPS installed in the 66 kV tie line. Therefore, the 132 kV tie line is the best location for installing a CPS damping controller for this study system (Figure 5.2).

The damping effects of the CPS on the inter-area mode for these two locations were investigated for two disturbances. One is a large disturbance which was simulated by a 100 ms three-phase fault in an EHV transmission line followed by permanent tripping of the line. The other is a small disturbance which was simulated by opening an EHV transmission line.

The relative rotor angle swings, tie-line power oscillations, tie-line voltage oscillations and the action of the CPS controller following a large disturbance for the CPS installed in the 132 kV tie line and 66 kV tie line are shown in Figures 5.3a-d and 5.4a-d respectively. Figures 5.5a-d and 5.6a-d show the dynamic responses of the relative rotor angle swings, tie-line power, tie-line voltage and the action of the CPS controller under a small disturbance for the CPS installed in the 132 kV tie line and 66 kV tie line, respectively. For comparison the system responses with no CPS control are also given. In this analysis, the CPS has a regulating angle limited to $\pm 20^{o}$.

Figures 5.3a-c and 5.5a-c show that the CPS installed in the 132 kV tie line can significantly increase the damping of the inter-area mode, whereas Figures 5.4a-c and 5.6a-c indicate that the CPS damping effect on the inter-area mode is noticeably reduced when it is installed in the 66 kV tie line. Comparison of Figures 5.3d and 5.4d (or comparison of Figures 5.5d and 5.6d) reveals that the CPS control action is much stronger in the 132 kV tie line than that in the 66 kV tie line. This means that the phase shifting action of the CPS controller has a greater effect in the 132 kV tie line which results in the inter-area mode being controlled. Because the 132 kV tie line is transferring most of the inter-area power, the power modulation due to the CPS located at this strategic point is very effective in damping out the tie-line oscillations. These simulation results agree with those of the eigenvalue analysis given in Table 5.2.

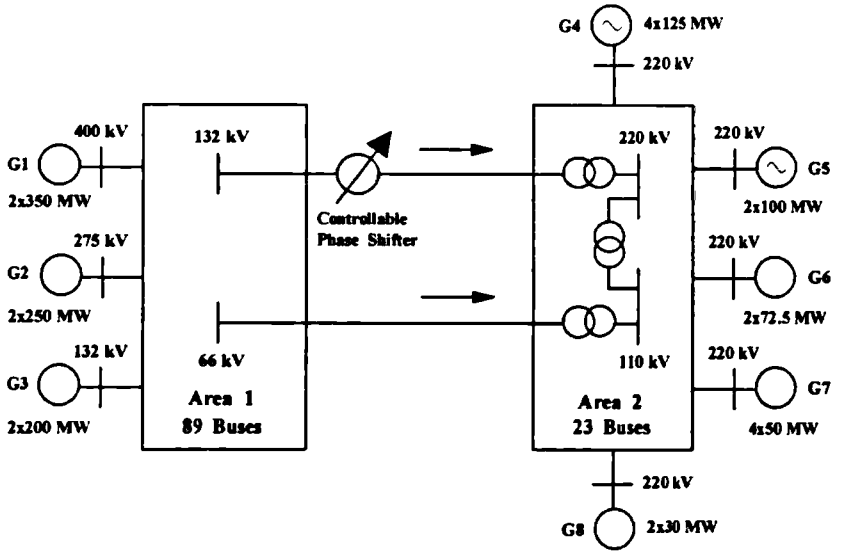
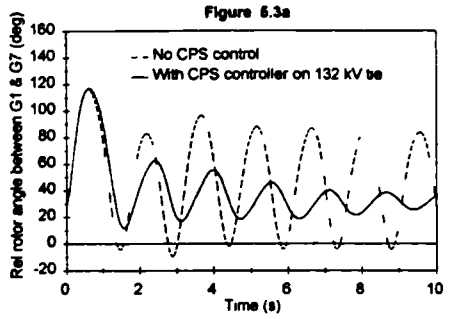
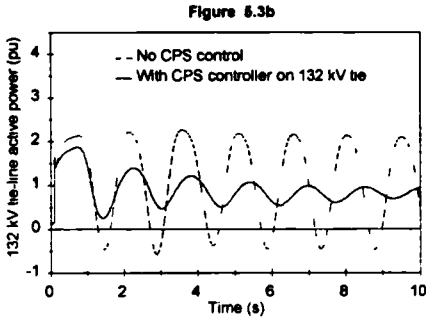
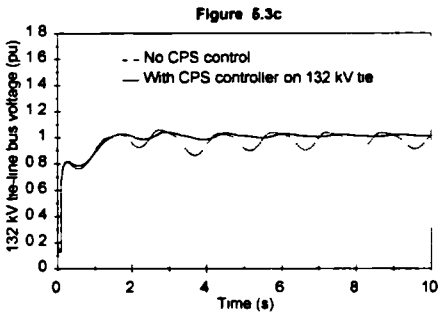


Figure 5.2 Interconnected 8-machine 112-bus system with CPS







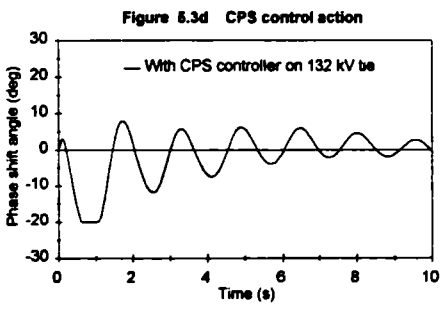
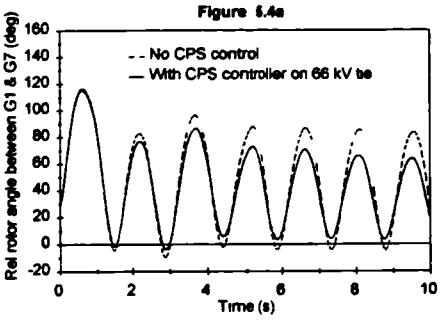
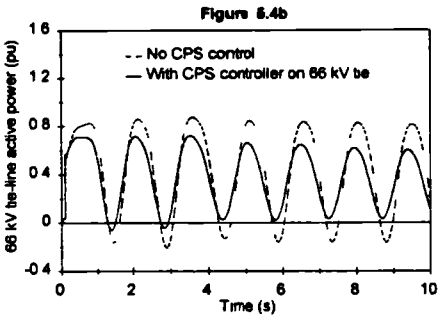
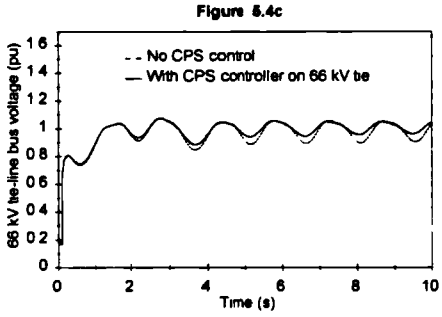


Figure 5.3 Performance of the CPS on the 132 kV tie line following a large disturbance







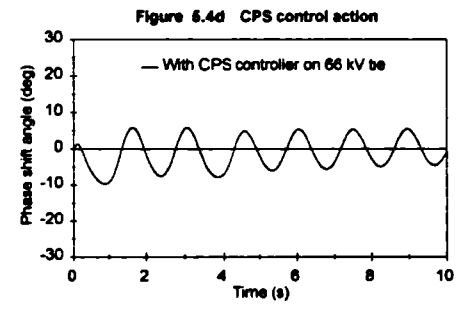
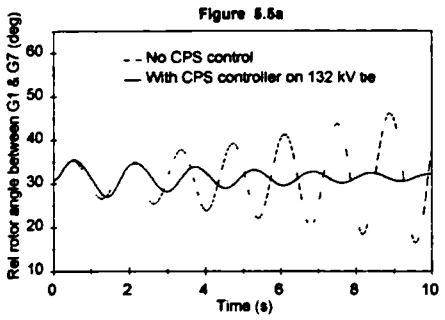
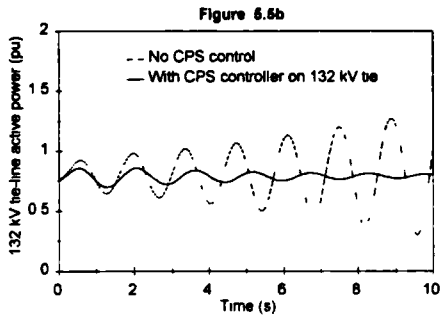
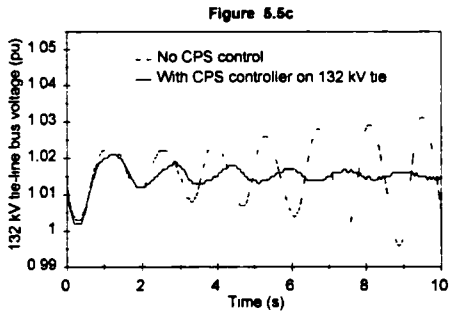


Figure 5.4 Performance of the CPS on the 66 kV tie line following a large disturbance







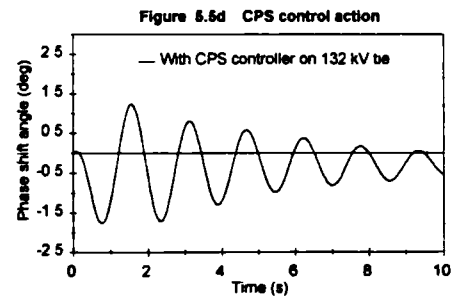
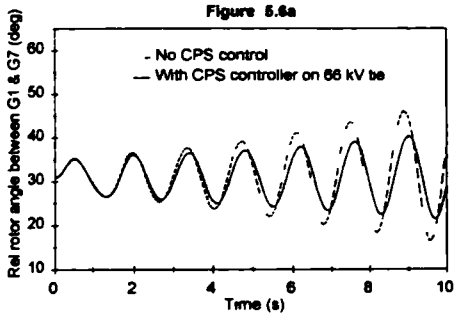
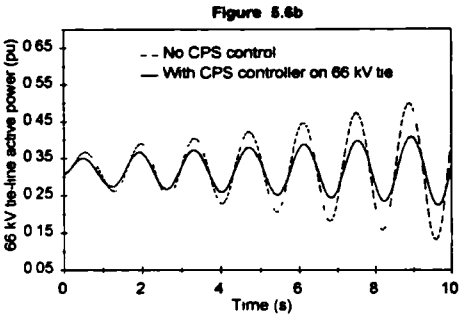
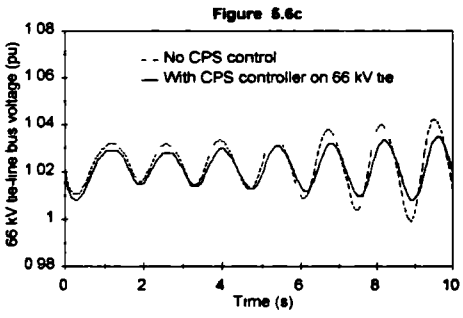


Figure 5.5 Performance of the CPS on the 132 kV tie line following a small disturbance of line switching







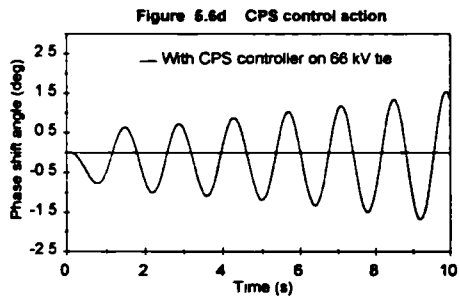


Figure 5.6 Performance of the CPS on the 66 kV tie line following a small disturbance of line switching

5.5 DESIGN OF CPS CONTROLLER

Once the location of a CPS in the system has been decided, the design of its controller can be done using eigenvalue sensitivity analysis which is utilized to tune the CPS control parameters. Whenever there is a change in a CPS parameter x, the closed-loop system matrix A and the eigenvalues vary accordingly. Hence the sensitivity coefficient is given by [110]

$$\frac{\partial \lambda_i}{\partial x} = \frac{w_i \dfrac{\partial A}{\partial x} v_i}{w_i v_i} \tag{5.4}$$

where v_i (w_i) is the eigenvector of A (A^T) with respect to the inter-area mode λ_i. Since the CPS parameter x may range from very large to very small values, it is more meaningful to determine the effect of the fractional variation of the CPS parameter x on the inter-area mode λ_i, and the relative sensitivity coefficient [111] is considered, defined by

$$\frac{\partial \lambda_i}{\partial x} x \cong \frac{\Delta \lambda_i}{\Delta x \; x} \tag{5.5}$$

For a complex eigenvalue $\lambda_i = \alpha_i + j\omega_i$, which is of interest for oscillation studies, the real part of the relative sensitivity coefficient S_{ix} is defined by

$$S_{ix} = \mathrm{Re}\left\{\frac{\partial \lambda_i}{\partial x}\right\} x \cong \frac{\Delta \alpha_i}{\Delta x \; x} \tag{5.6}$$

The aim of eigenvalue sensitivity analysis is to make the real part α_i as negative as possible in order to increase inter-area mode damping. Since $\Delta \alpha_i = S_{ix} \Delta x / x$, whenever S_{ix} is positive (negative), Δx should be made negative (positive) or x should be decreased (increased) by suitable adjustment to achieve the objective. Thus, by investigating the sign of S_{ix}, the correct direction for a desired change of x can be inferred. Finally, x is tuned to its

optimum value when S_{ix} approaches zero. Table 5.3 shows the real parts of the relative sensitivity coefficients of the inter-area mode with respect to a CPS installed in the 132 kV tie line using the base CPS control setting given in Table 5.1.

Table 5.3 Sensitivity coefficients of the inter-area mode

CPS Parameter	Real Parts of Relative Sensitivity Coefficients
K_g	-0.0083
T_g	-0.0149
T_1	0.0149
T_2	-0.0188
T_3	0.0149
T_4	-0.0188

Inspection of these sensitivity coefficients indicates that the unstable inter-area mode can be shifted towards the left hand complex plane by changing the CPS parameters as below

Increase gain K_g
Increase time constant T_g
Decrease lead/lag time constants T_1 and T_3
Increase lead/lag time constants T_2 and T_4

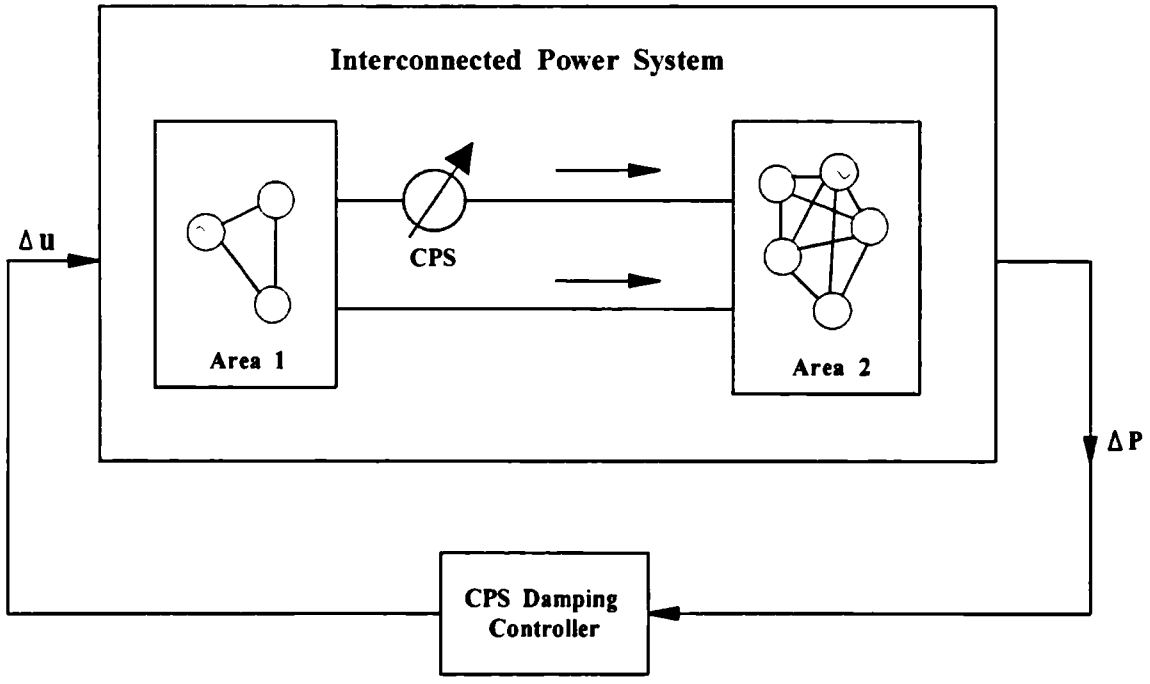
In the course of optimizing the CPS parameters, it was found that increasing T_g would have a small detrimental effect on the damping of the other modes. It is therefore desirable to keep T_g unchanged. Eventually, the optimized new setting having the greatest damping ratio of the inter-area mode is obtained and summarized in Table 5.4. The corresponding computed eigenvalues are given in Table 5.5. It can be seen from Table 5.5 that with a CPS installed in the 132 kV tie line, the damping of the inter-area mode is greatly improved without reducing the damping of other modes, while the frequency is found to be unchanged. The schematic diagram of the decentralized controller for the CPS using 132 kV tie-line active power feedback is shown in Figure 5.7.

Table 5.4 Summary of CPS control settings

CPS Parameter	K_g	T_g (s)	T_1 (s)	T_2 (s)	T_3 (s)	T_4 (s)
Base Setting	0.5	0.1	0.10	0.20	0.10	0.20
New Setting	0.6	0.1	0.05	0.30	0.05	0.30

Table 5.5 Effect of CPS on the inter-area mode

	Eigenvalue	Frequency (Hz)	Damping Ratio
No CPS	0.0570±4.7860	0.7617	-0.0119
With CPS	-0.5844±4.8337	0.7693	0.1200



P = CPS feedback signal using 132 kV tie-line active power

u = CPS control input

Figure 5.7 Decentralized output feedback CPS controller

The rotor speed mode shape for this inter-area mode was calculated and is given in Table 5.6. By examining the mode shape shown in Figure 5.8, no oscillations between the two areas of generators are observed. Since the damping enhancement using a CPS is found adequate, the other lines equipped with CPS are not considered necessary in this case.

Table 5.6 Rotor speed mode shape of the inter-area mode with CPS

Machine	Mode Shape	
	Amplitude	Angle (deg)
G1	0.02	97.13
G2	0.02	96.20
G3	0.02	87.39
G4	0.04	61.04
G5	0.04	53.95
G6	0.04	62.94
G7	0.04	56.22
G8	0.04	50.82

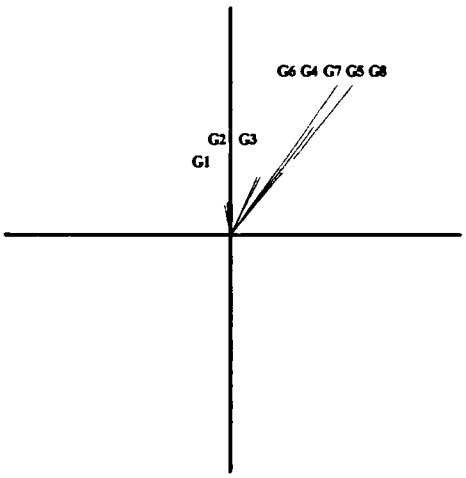


Figure 5.8 Rotor speed mode shape of the inter-area mode with CPS

To ensure that the controller designed is robust over a wide range of power transfers across the tie lines, the eigenvalues of the inter-area mode with a CPS installed in the 132 kV tie line were computed for five different values of tie-line power flow and they are listed in Table 5.7.

Table 5.7 Effect of tie-line flow on the inter-area mode with CPS

Power Flow Area 1 To 2 (MW)	Eigenvalue	Frequency (Hz)	Damping Ratio
110	-0.5844±4.8337	0.7693	0.1200
130	-0.4730±4.7611	0.7577	0.0989
150	-0.3588±4.6951	0.7472	0.0762
170	-0.2438±4.6359	0.7378	0.0525
190	-0.1297±4.5731	0.7278	0.0284

As can be observed from Table 5.7, the frequency and damping ratio of the inter-area mode drop as the tie-line power flow is increased (Figure 5.9). However, the system is still dynamically stable when the tie-line power flow is increased from 110 MW to 190 MW. It can be concluded that a CPS located in the 132 kV tie line can not only enhance the dynamic stability of the interconnected system but can also increase the tie-line power transfer capacity.

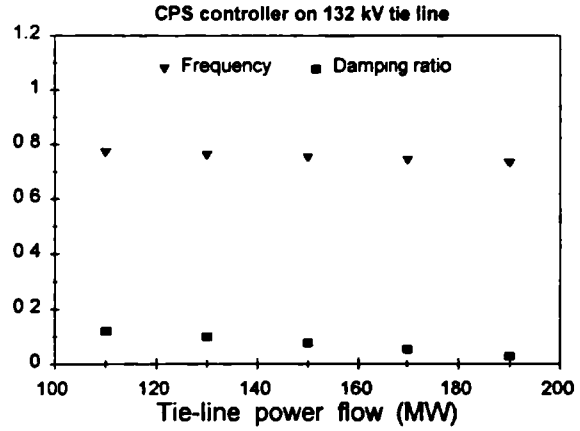
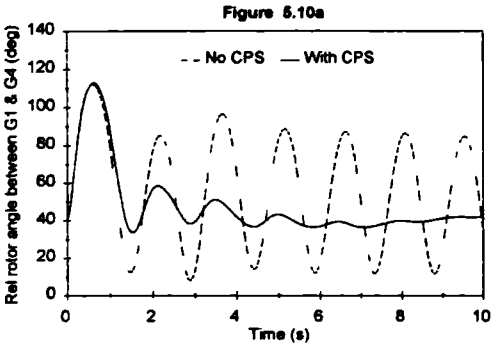


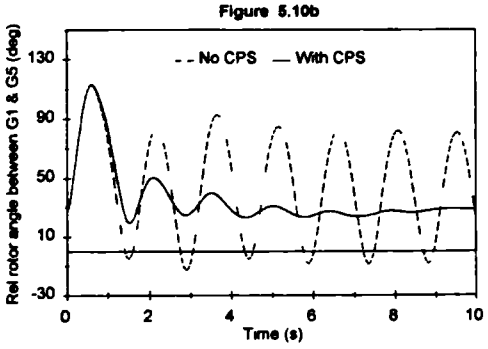
Figure 5.9 Variation of frequency and damping ratio when tie-line power transfer is increased from 110 MW to 190 MW

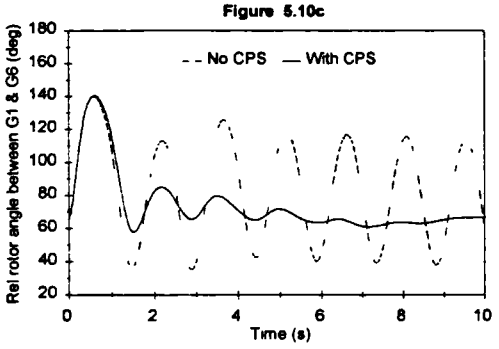
5.6 PERFORMANCE EVALUATION

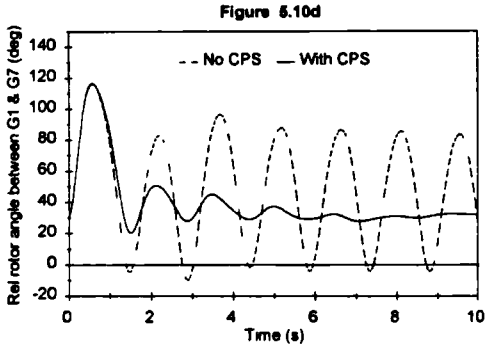
In order to validate the effectiveness of the designed controller in controlling the inter-area mode, non-linear time domain simulations were carried out using a program developed for this work, in which modelling of a compensation-based CPS and its controller are included so that the dynamic performance of the interconnected system under large or small disturbances with and without a CPS can be evaluated. The large and small disturbances described in Section 5.4 are also adopted here for simulation studies.

The relative rotor angle swings, tie-line active power oscillations, tie-line voltage oscillations, CPS input signal and output action, generators' active power oscillations and generators' terminal voltage oscillations following these two contingencies are plotted in Figures 5.10 - 5.13 and Figures 5.14 - 5.17 respectively. For comparison the system performance with no CPS control are also plotted for each contingency. As shown in Figures 5.10 - 5.13, without a CPS in the system, inter-area oscillations with poor damping following a three-phase fault are observed. When a CPS with the optimized new setting given in Table 5.4 is applied to the system, the inter-area mode is damped. As can be observed from the dynamic responses following a small disturbance of line switching (Figures 5.14 - 5.17), the system is unstable with no CPS present in the system. The dynamic oscillations are well damped by the installation of a CPS in the system, and these results correlate well with those of the previous eigenvalue analysis shown in Table 5.5. It is also observed from Figures 5.14 - 5.17 that the settling time for the response is about 4 seconds.









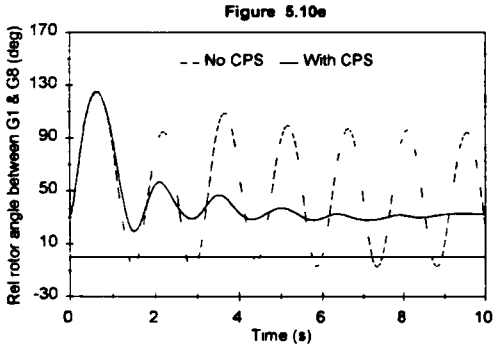


Figure 5.10 Rotor angle swings following a large disturbance with CPS

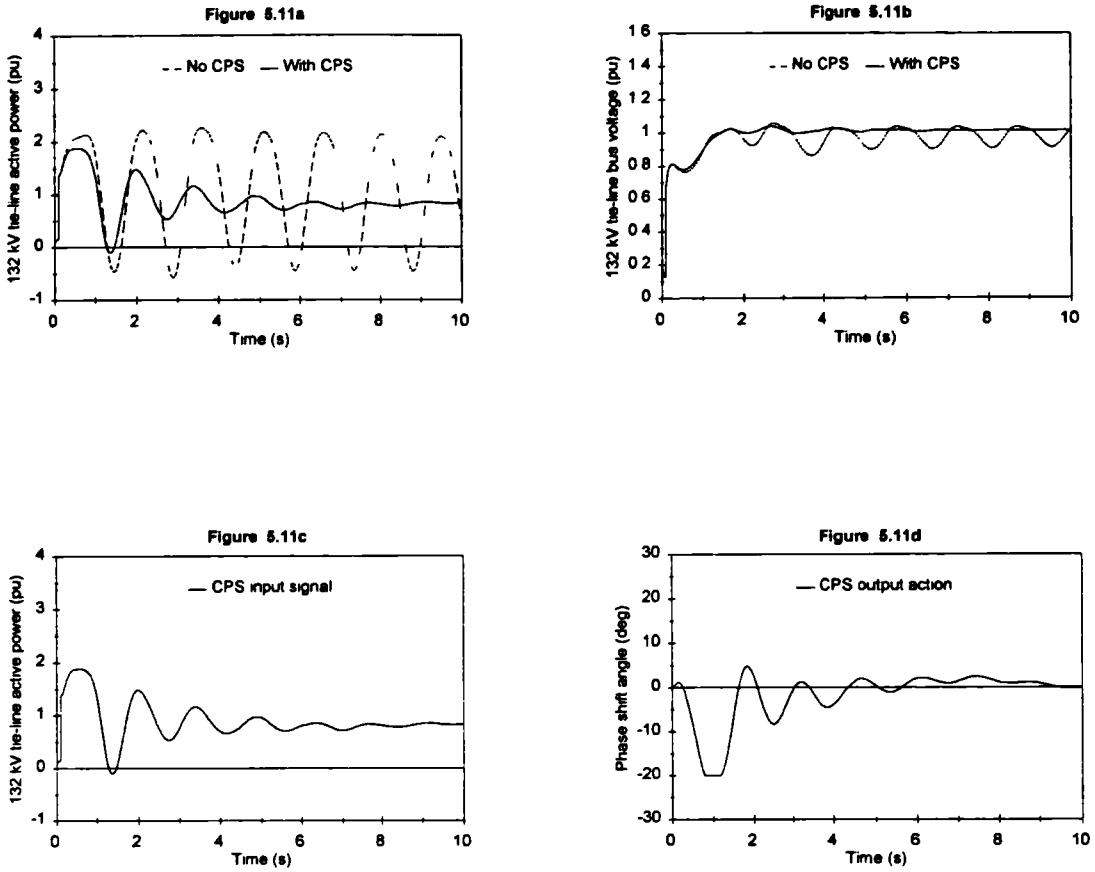


Figure 5.11 Tie-line active power and voltage responses to a large disturbance with CPS

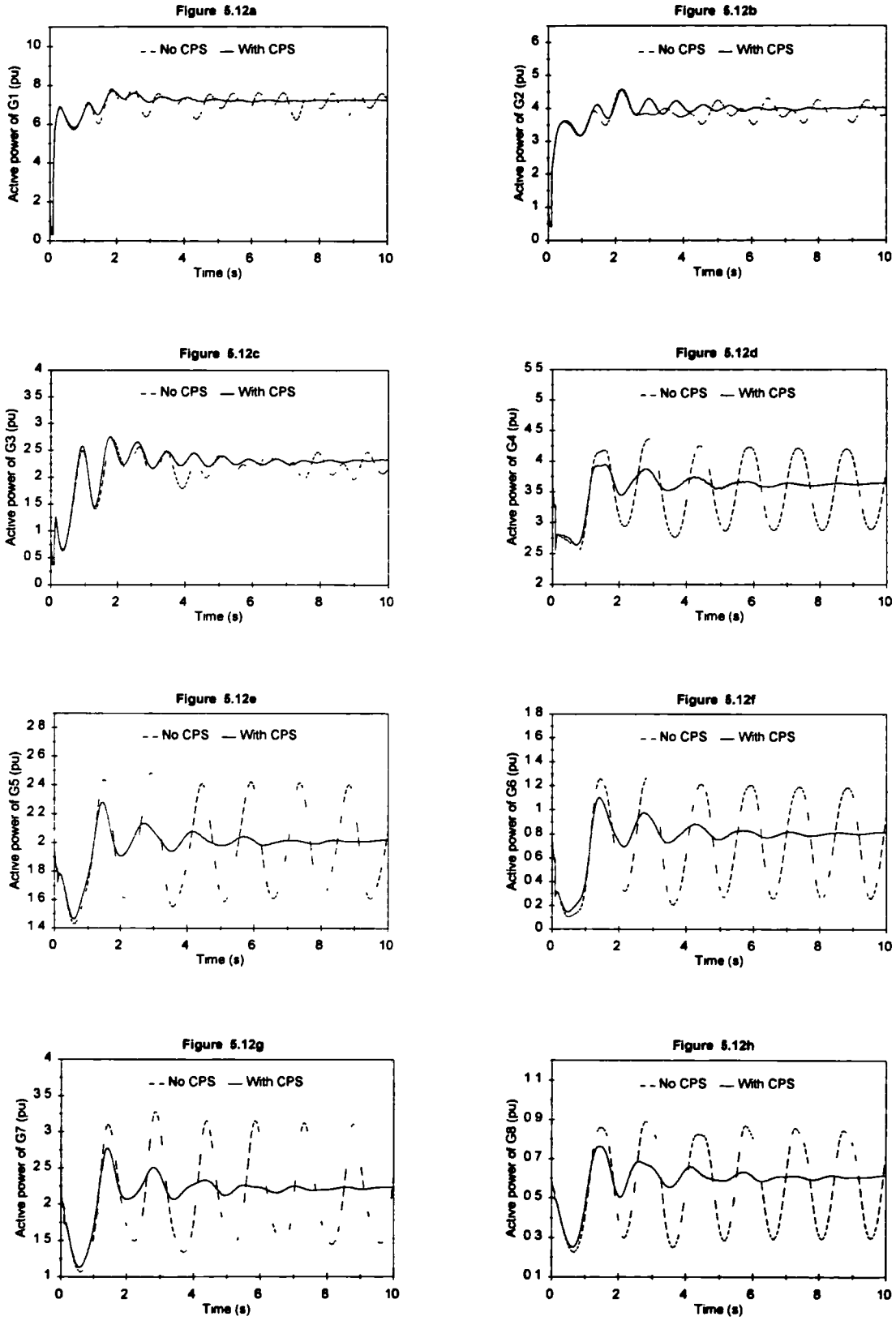


Figure 5.12 Generators' active power output responses to a large disturbance with CPS

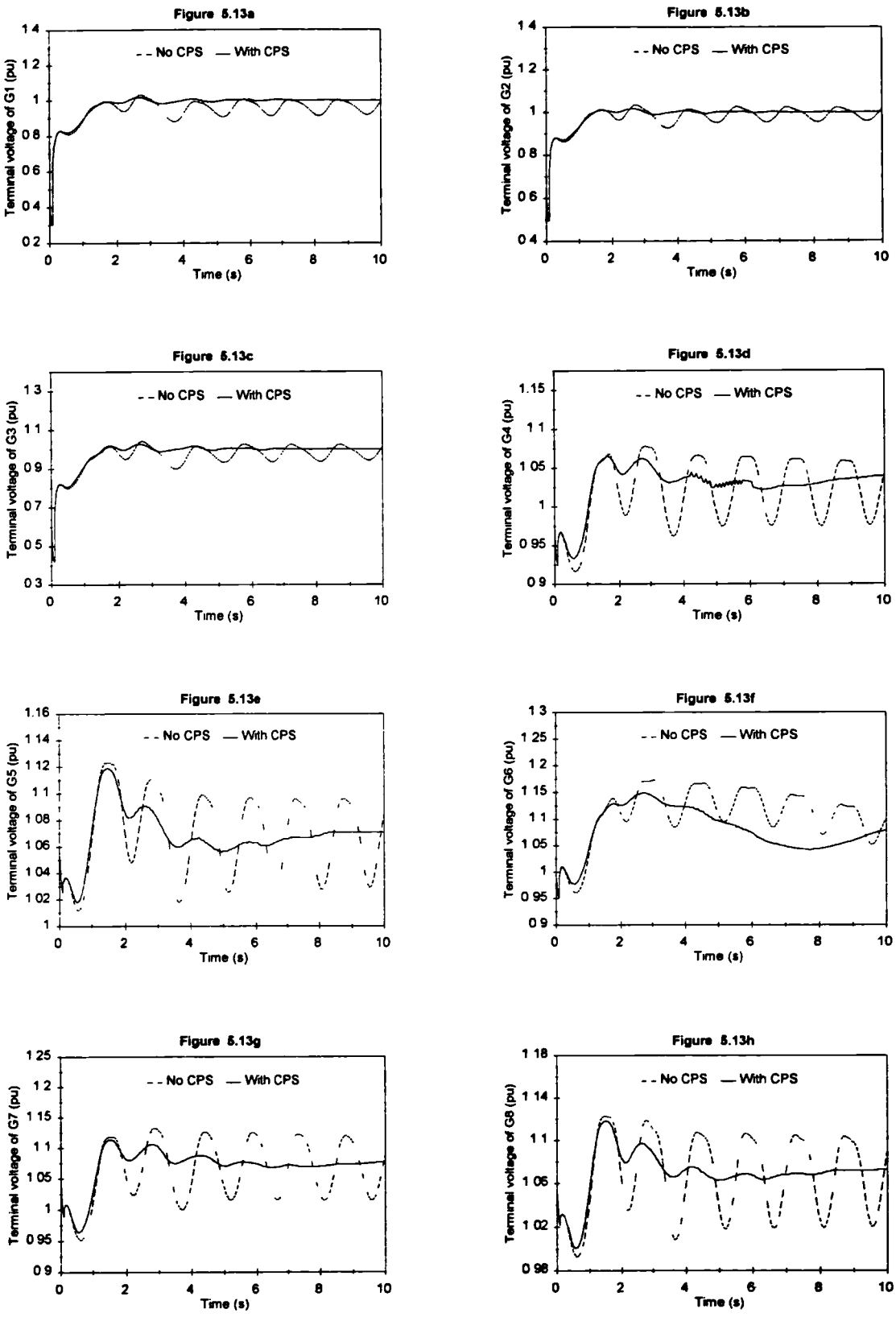
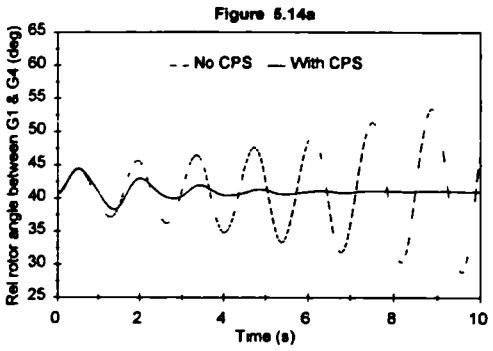
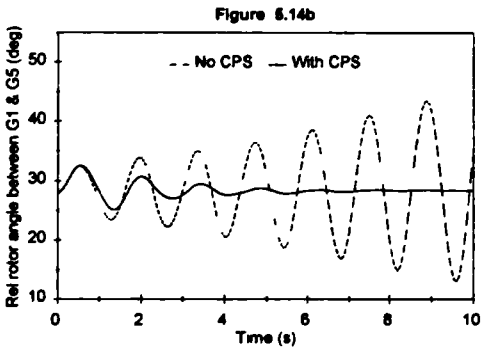
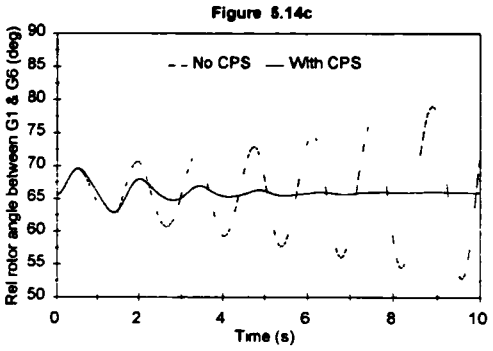
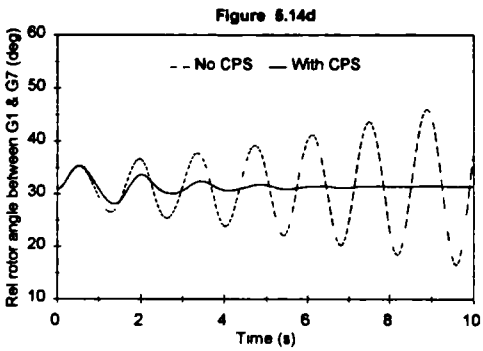


Figure 5.13 Generators' terminal voltage responses to a large disturbance with CPS









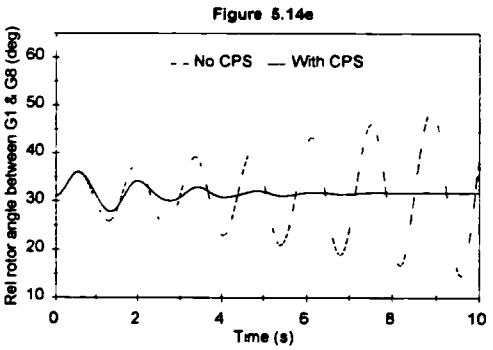


Figure 5.14 Dynamic responses of rotor angle swings following a small disturbance of line switching with CPS

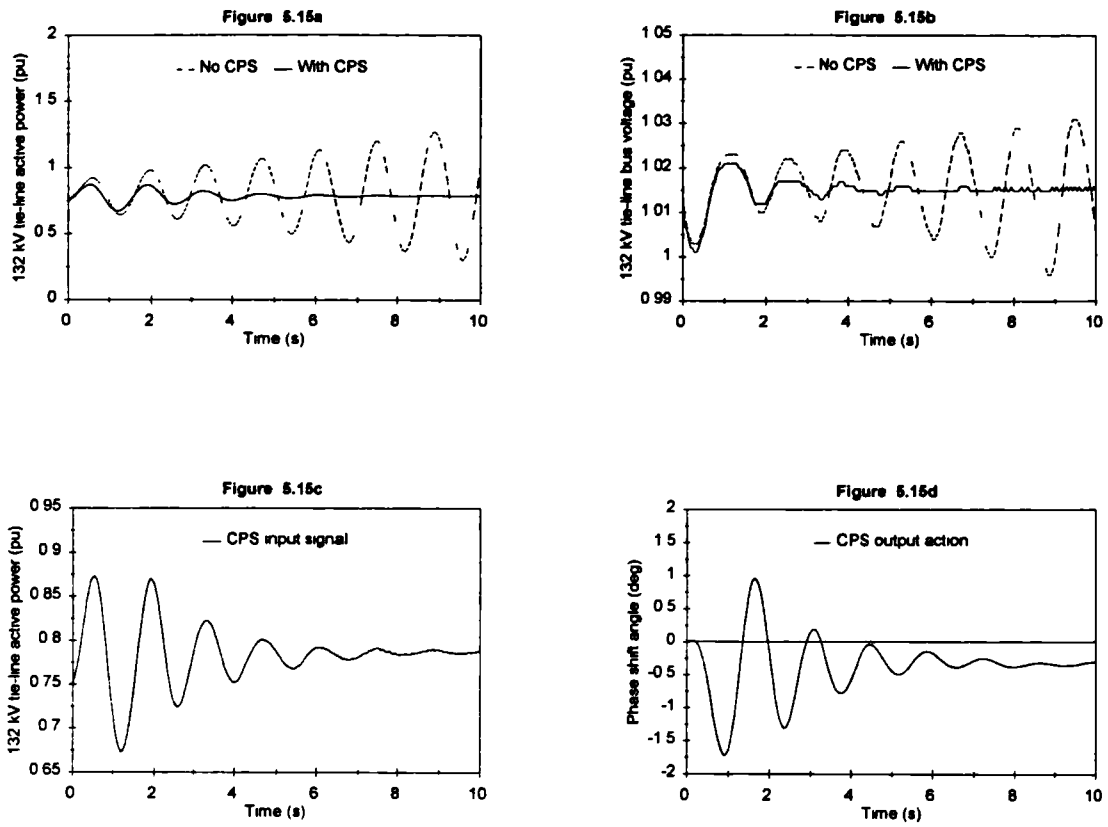


Figure 5.15 Dynamic responses of tie-line active power and voltage following a small disturbance of line switching with CPS

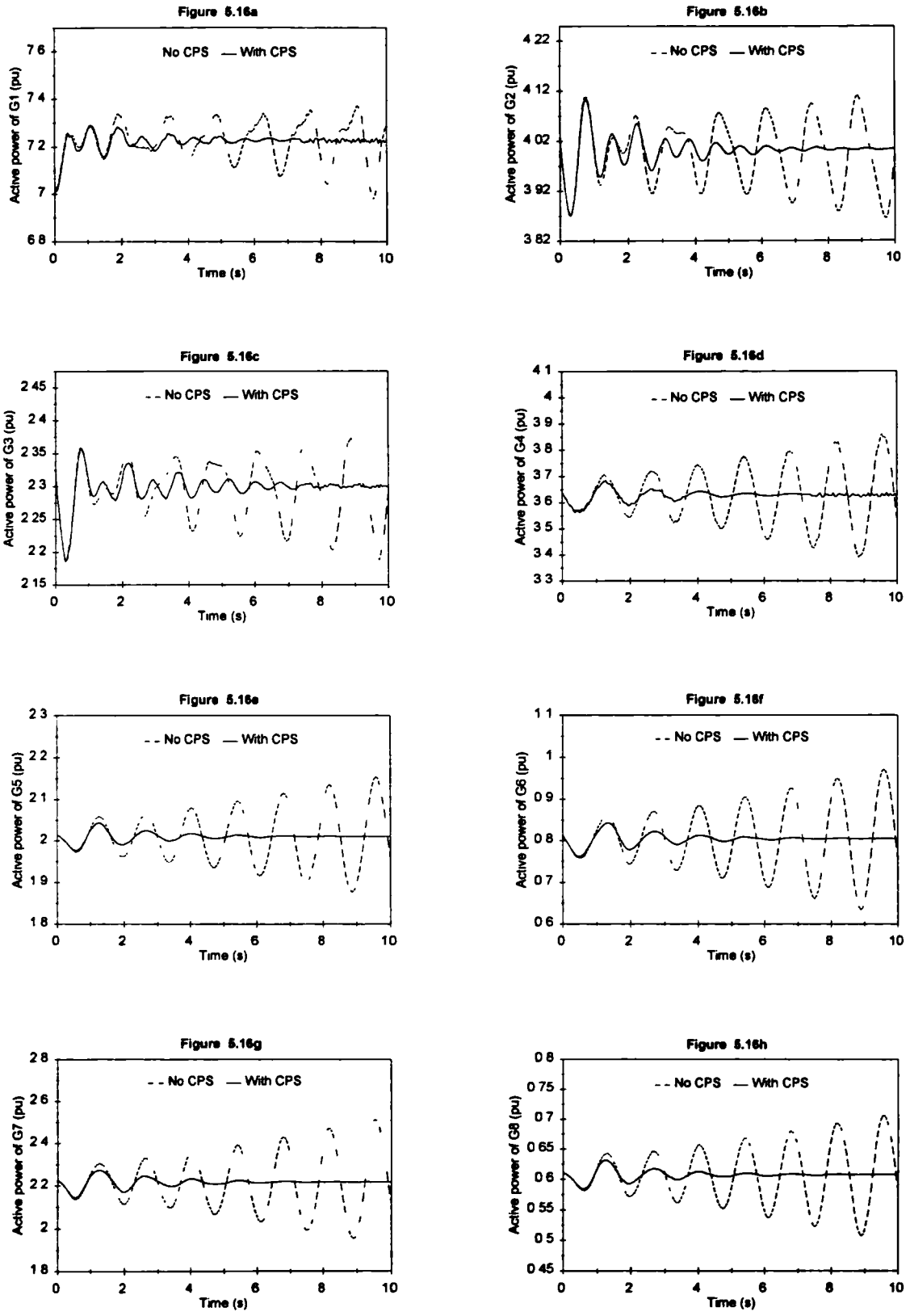


Figure 5.16 Dynamic responses of generators' active power output following a small disturbance of line switching with CPS

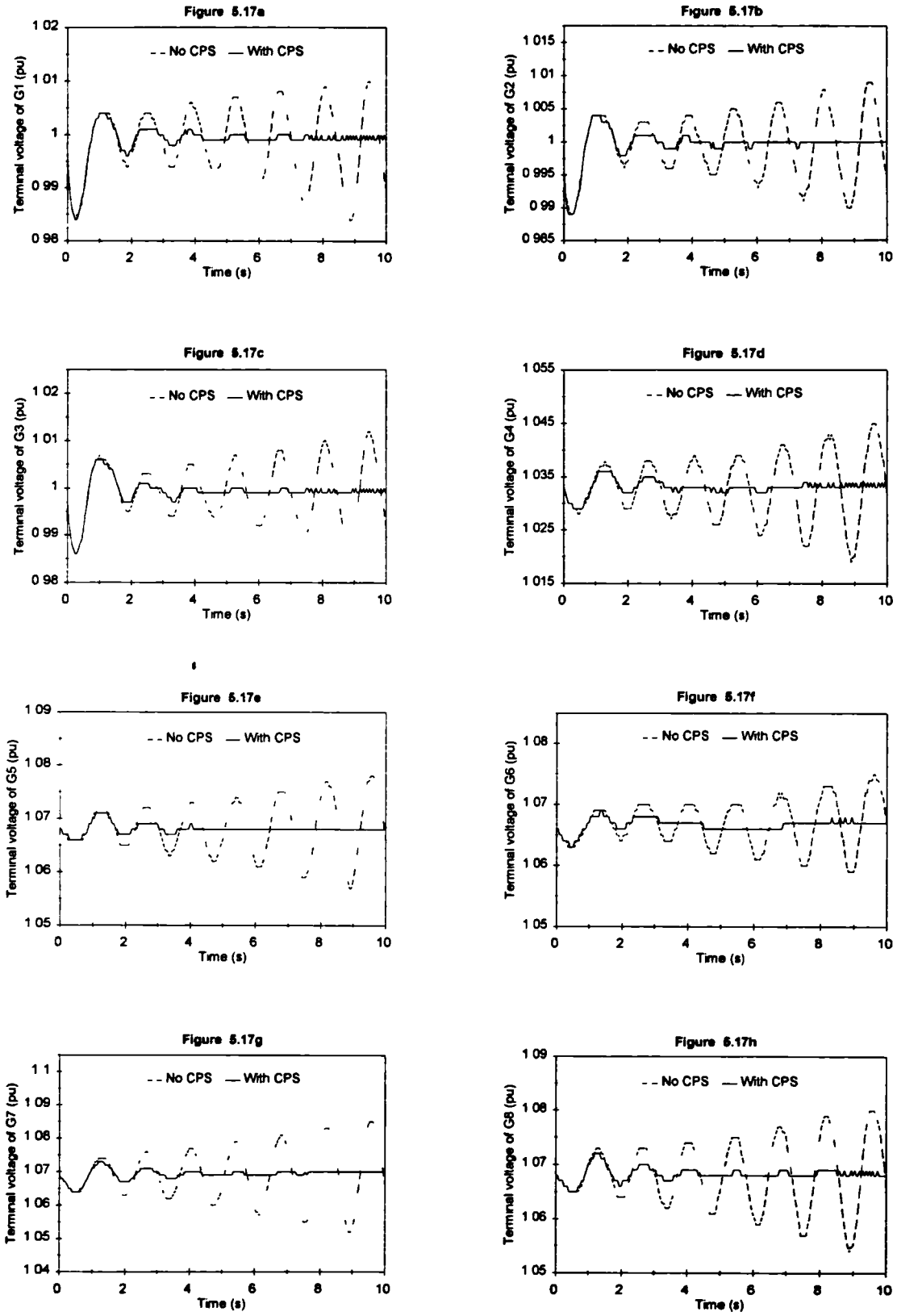


Figure 5.17 Dynamic responses of generators' terminal voltage following a small disturbance of line switching with CPS

CHAPTER SIX

CONCLUSIONS

6.1 GENERAL CONCLUSIONS

In this research, an analytical study of the factors affecting the damping characteristics of low frequency inter-area oscillations in an interconnected system has been presented. The simulation of a CPS to enhance the dynamic stability of an interconnected system was also made. In particular, the controller characteristics of this device were evaluated in order to damp inter-area oscillations under dynamic or transient disturbance conditions.

A linearized model of an interconnected multimachine system in state space form was developed in which synchronous machines and CPS were considered as dynamic subsystems interacting through the interconnected network. Interaction characteristics between dynamic subsystems were used to investigate the impact of CPS on the dynamic behaviour of the interconnected system. The linearized system model was useful for analyzing the dynamic stability problem, for identifying the best CPS installation location and for designing a decentralized output feedback CPS controller. For this dynamic stability study, machine stator, CPS and network transients were neglected and hence the number of state variables in the linearized system model were reduced. Thus a saving in computational time and memory space can be achieved.

Both eigenvalue analysis and time domain simulations were used, in a complementary way, to diagnose the dynamic stability problem. Eigenvalue analysis has been shown to be a powerful tool for identifying system oscillatory modes and analyzing system damping characteristics. The results showed that the dominant mode of oscillation was an undamped inter-area mode having a frequency of 0.76 Hz. The inter-area mode shape indicated that the machines in Area 2 (the receiving end) swung with a higher amplitude against those in Area 1 (the sending end). The participation factors showed that the machine G7 in Area 2 and the machine G1 in Area 1 had high participation in the inter-area mode of oscillation. This is to be expected, since these two units are heavily loaded during the oscillation. It was shown that the damping characteristics of

the inter-area mode were strongly related to the level of power transfer through the tie, weakness of the tie, type of excitation system, load characteristics, machine loading and generation dispatch. Studies on these results showed that the dynamic instability of the interconnected system was caused by a combination of the following factors:

(a) A high level of power transfer across the relatively weak interconnection.

(b) Fast response excitation systems of the generating units in Area 1, i.e. mismatch of excitation characteristics between the two areas.

(c) Unusual load characteristics in the system at the time of the oscillations, i.e. high domestic load with little industrial motor load.

(d) High loading of the machine G1.

The studies also revealed that the damping of the inter-area mode could be improved by reducing the tie-line transfer, increasing the number of tie-line circuits, reducing the excitation system gain of the machine G1 by 33%, increasing the induction motor load in the system by 30%, running the machine G1 at 0.85 power factor lagging, and relocating part of generation from the machine G1 to the other machine. These findings give an insight into the nature of inter-area oscillations, leading to the understanding of their characteristics and the development of practical remedial and interim measures. The findings and understandings form a useful basis for analysis of more complex interconnected systems.

To verify some of the results of eigenvalue analysis with regard to the effects on the damping of inter-area oscillations, time domain simulations were carried out. To study inter-area post-fault oscillations in the system, a 100 ms three-phase fault applied to an EHV transmission line followed by permanent tripping of the line was simulated. To examine the dynamic response of the system, a small disturbance of switching off an EHV transmission line or increasing the reference voltage input of the machine G1 by 1% for 200 ms was simulated. Results of time domain simulations correlated well with those of the eigenvalue analysis.

Because of the emergence of an undamped inter-area mode in the system, it was decided to use a power system device to enhance the inter-area mode damping. Traditionally, inter-area modes have been damped using PSS on generators in multimachine systems. However, when it comes to damp low frequency inter-area oscillations, damping by use of PSS would often require tuning and coordination of a large number of devices, often belonging to different utilities. Recently, the advent in high power thyristors has led to the possibility of CPS. A CPS is a promising power system device in the context of FACTS. The ability of the CPS to control the power flow rapidly can improve the dynamic stability of the interconnected system. The objective of the research was to demonstrate the capability of a CPS to provide additional damping to the inter-area mode without affecting the damping of other local modes.

For higher reliability and lower cost, only local signals were used as inputs to the CPS controller. Many authors have demonstrated that for damping inter-area oscillations, a local signal such as active power or frequency deviation, or a combination of both, was a suitable feedback signal for a series device installed in the tie line. Here, the tie-line active power deviation was selected because it is observable in the inter-area mode of interest, sensitive to inter-area mode oscillations on the machines and tie lines of interest, but not sensitive to local mode oscillations. This type of decentralized controller is of practical interest as the feedback control signal is locally available and thus no remote data transmission is required.

The principle of using a CPS controller for power system damping is based on its ability to modulate the power flow on the transmission line. Therefore to effectively damp out the dominant inter-area oscillatory mode, the CPS should be located at an inter-area connecting point where the change of phase shifting action can effectively modulate the dominant power swing mode. To determine which tie line to be the optimum CPS installation location, a method based on the analysis of participation factors and mode controllability was proposed. Participation factors have been recognised as a good screening tool for site selection [22]. However, they do not contain any information useful in the design of a controller nor do they guarantee the effectiveness of the controller. The entry of the mode controllability matrix (called the controllability index) gives a measure of controllability of the inter-area mode using the CPS input. Although the controllability index does not directly identify the state variable

corresponding to the inter-area mode, unlike the participation factor, it does indicate how effective the input is in controlling the inter-area mode. Therefore by analysis of the magnitudes of the controllability indices for different CPS locations, the best location for installing the CPS could be identified. Simulation results showed that the CPS controller located in the 132 kV tie line, where the participation factor and controllability index were much higher, could increase the damping of the inter-area mode. They also showed that the improper selection of CPS location (i.e. the CPS located in the 66 kV tie line) could significantly reduce its performance.

A compensation-based phase shifter model was developed and included in the transmission system model. By using compensation injected currents at terminal buses to simulate a phase shifter the symmetry property of the bus admittance matrix was maintained. A systematic approach for mathematical modelling of a compensation-based phase shifter was outlined. Based on this approach, a steady-state model, a small-signal dynamic model and a large-signal dynamic model of a compensated-based phase shifter were developed. With the addition of appropriate control systems, the combined model can be used for power flow, dynamic stability and transient stability studies with no modification of the bus admittance matrix required at each iteration. This compensation method has the advantages of fast computational speed and low computer storage compared with that of modifying the bus admittance matrix method.

An output feedback CPS controller based on eigenvalue sensitivity techniques has been designed using the linearized interconnected system model. A computationally inexpensive and meaningful expression of the eigenvalue sensitivities has been presented. By considering the CPS effect on the inter-area mode, sensitivity coefficients of CPS parameters were calculated, from which the correct direction of change of each CPS parameter could be inferred. The design criterion was to maximise the inter-area mode damping without reducing the damping of other local modes. The CPS setting would be optimum when the sensitivities of all CPS parameters were small. Analysis using eigenvalue techniques showed that the CPS controller with the optimized setting located in the 132 kV tie line could significantly improve the damping of the inter-area mode. The inter-area mode shape with CPS indicated no oscillations between the two areas of generators. The controller designed has been shown to be robust to changes in tie-line power transfers, indicating that increasing the inter-

area mode damping could result in increasing the level of power transfer across the tie lines. The damping effectiveness of the proposed controller has been ascertained by non-linear time domain simulations. The simulation results showed that, with the proposed decentralized control strategy based on tie-line power deviation feedback and utilizing a fast-acting CPS to continuously modulate the tie-line power flow during system disturbances, the inter-area mode of oscillation was well damped and the enhancement of system dynamic performance was satisfactory. These results are fully consistent with those of the eigenvalue analysis.

The studies showed that with proper selection of CPS location and controller, just one CPS would suffice to introduce sufficient damping. In practice it may not be economic to locate a CPS in the system for the purpose of improving system damping performance. However, it is observed that the staged development of the tie lines between the two areas in the study system has resulted in a load sharing problem, i.e. one tie line could be at full load before the other. A CPS located in the 132 kV tie line can not only be used to alleviate the load sharing problem in steady state conditions but can also be used to solve the dynamic stability problem under dynamic or transient disturbance conditions. At the moment the CPS, which are in development especially the concept of retrofitting existing mechanical phase shifters with thyristors switches [112], are seen to be more costly but that may change if their capabilities are more fully appreciated.

The above study is based on a particular network topology of the system. The power network is, from time to time, subject to change, and it may therefore be necessary to install more than one CPS to cope with different network topologies.

The methodologies developed in this research can be applied to other practical systems with similar effectiveness.

6.2 SUGGESTIONS FOR FUTURE WORK

In the author's opinion, the following issues remain open for further research:

(1) The methodologies developed in this research should be evaluated further on large interconnected systems to determine the extent to which they can be successfully applied. Inter-area oscillations in large interconnected systems are complex to study, and to control. Large interconnected systems usually exhibit several dominant inter-area modes, each involving a large number of generators.

(2) In the study, the state matrix method has been used to calculate all the eigenvalues and the corresponding eigenvectors of the system. However, the computational time gets longer when the state matrix size becomes larger. Faster and more efficient techniques are needed to calculate and identify system oscillation modes, and to speed up computation. Techniques that take into account the sparse nature of state representation should be used. The identification of critical modes and their relation to state variables is of great importance in deriving control actions.

(3) The proposed eigenvalue sensitivity techniques offer an effective approach to controller design for multimachine systems. The application in this research is confined to the case of installing a single CPS in the system distinguished by one poorly damped inter-area mode. Further research into developing multi-CPS or multi-FACTS design methodologies as applied to general multi-area interconnected systems seems worth considering. Attention should be given to the interaction among controllers, or between controllers and the power system.

(4). In the design of CPS controller with linear theory, a linearized system model is used and therefore the controller performance depends on a particular system operating point. If best control effect is to be achieved, the CPS controller should be adaptive to a wide range of system operating conditions. Further research could use adaptive control as a starting point but could also look into the possibility of fuzzy control with gain scheduling technique which is practical from the engineering point of view.

(5) The choice of feedback signal is crucial to the design of a CPS controller to aid in the damping of inter-area oscillations. In this study, only a feedback signal using tie-line power deviation has been evaluated. It is therefore suggested that the performance of the controller designed using different feedback signals should be evaluated. The area frequency difference of synthesized remote voltages on each side of the controller has been recommended as a suitable feedback signal for damping inter-area oscillations [37]. A feedback signal using the difference between the voltage angles across the controller, suggested by Noroozian, Angquist, Ghandhari and Andersson [40], has been shown to be effective in damping power swings.

(6) The use of UPFC has attracted the attention of utility system planners, manufacturers and researchers. Several system studies [113-115] have been conducted stating the performance of UPFC, reporting that these devices can improve the dynamic performance of power systems. Further research work could simulate a UPFC and compare its performance with the CPS by eigenvalue and time domain simulation studies.

APPENDIX A

SYNCHRONOUS MACHINE AND CONTROLLERS REPRESENTATION

A.1 SYNCHRONOUS MACHINE MODEL

The linearization of equations (3.15), (3.16), (3.17), (3.18), (3.19), (3.20), (3.23), (3.24) and (2.27) about a system operating point, after some manipulations, gives

$$\frac{d(\Delta E'_q)}{dt} = \frac{1}{T'_{do}}(\Delta E_{fd} - (X_d - X'_d)\Delta I_d - \Delta E'_q) \tag{A.1}$$

$$\frac{d(\Delta E''_q)}{dt} = \frac{1}{T''_{do}}(\Delta E'_q - (X'_d - X''_d)\Delta I_d - \Delta E''_q) \tag{A.2}$$

$$\frac{d(\Delta E''_d)}{dt} = \frac{1}{T''_{qo}}((X_q - X''_q)\Delta I_q - \Delta E''_d) \tag{A.3}$$

$$\frac{d(\Delta \omega)}{dt} = \frac{1}{2H}(\Delta P_m - \Delta P_e - D\Delta \omega) \tag{A.4}$$

$$\frac{d(\Delta \delta)}{dt} = \omega_o \Delta \omega \tag{A.5}$$

$$\Delta P_e = I_d^o \Delta E''_d + E''^o_d \Delta I_d + I_q^o \Delta E''_q + E''^o_q \Delta I_q \tag{A.6}$$

$$\begin{bmatrix} \Delta I_d \\ \Delta I_q \end{bmatrix} = \frac{1}{R_a^2 + X''_d X''_q} \begin{bmatrix} R_a & X''_q \\ -X''_d & R_a \end{bmatrix} \left\{ \begin{bmatrix} \Delta E''_d \\ \Delta E''_q \end{bmatrix} - \begin{bmatrix} \Delta V_d \\ \Delta V_q \end{bmatrix} \right\} \tag{A.7}$$

$$\begin{bmatrix}\Delta V_d\\ \Delta V_q\end{bmatrix}=\begin{bmatrix}-V_D^o\sin^o\delta + V_Q^o\cos^o\delta\\ -V_D^o\cos^o\delta - V_Q^o\sin^o\delta\end{bmatrix}[\Delta\delta] + \begin{bmatrix}\cos^o\delta & \sin^o\delta\\ -\sin^o\delta & \cos^o\delta\end{bmatrix}\begin{bmatrix}\Delta V_D\\ \Delta V_Q\end{bmatrix} \quad (A.8)$$

$$\begin{bmatrix}\Delta I_D\\ \Delta I_Q\end{bmatrix}=\begin{bmatrix}-I_d^o\sin^o\delta - I_q^o\cos^o\delta\\ I_d^o\cos^o\delta - I_q^o\sin^o\delta\end{bmatrix}[\Delta\delta] + \begin{bmatrix}\cos^o\delta & -\sin^o\delta\\ \sin^o\delta & \cos^o\delta\end{bmatrix}\begin{bmatrix}\Delta I_d\\ \Delta I_q\end{bmatrix} \quad (A.9)$$

By substituting equation (A.8) into equation (A.7) and then equations (A.7) and (A.6) into equations (A.1), (A.2), (A.3) and (A.4), the following linearized state equation of the *i*-th generator can be obtained

$$\Delta\dot{x}_{ggi} = [A_{ggi}]\Delta x_{ggi} + [C_{ggi}]\Delta V_{gi} \quad (A.10)$$

where

$\Delta x_{ggi} = \left[\Delta E'_{qi}\ \Delta E''_{qi}\ \Delta E''_{di}\ \Delta\omega_i\ \Delta\delta_i\right]^T$ = the *i*-th generator states

$\Delta V_{gi} = \left[\Delta V_{gDi}\ \Delta V_{gQi}\right]^T$ = the *i*-th generator terminal voltage deviations

$$[A_{ggi}]=\begin{bmatrix}\frac{-1}{T'_{do}} & -C_1X''_q & -C_1R_a & 0 & C_1(R_aV_q^o - X''_qV_d^o)\\ \frac{1}{T''_{do}} & -(C_2X''_q+\frac{1}{T''_{do}}) & -C_2R_a & 0 & C_2(R_aV_q^o - X''_qV_d^o)\\ 0 & C_3R_a & -(C_3X''_d+\frac{1}{T''_{qo}}) & 0 & C_3(R_aV_d^o + X''_dV_q^o)\\ 0 & A_{g42} & A_{g43} & \frac{-D}{2H} & A_{g45}\\ 0 & 0 & 0 & \omega_o & 0\end{bmatrix}$$

and

$$[C_{ggi}]=\begin{bmatrix} C_1(R_a\cos^o\delta - X''_q\sin^o\delta) & C_1(R_a\sin^o\delta + X''_q\cos^o\delta) \\ C_2(R_a\cos^o\delta - X''_q\sin^o\delta) & C_2(R_a\sin^o\delta + X''_q\cos^o\delta) \\ C_3(R_a\sin^o\delta + X''_d\cos^o\delta) & -C_3(R_a\cos^o\delta - X''_d\sin^o\delta) \\ C_{g41} & C_{g42} \\ 0 & 0 \end{bmatrix}$$

with

$$Y_g = \frac{1}{R_a^2 + X''_d X''_q}$$

$$C_1 = \frac{Y_g\,(X_d - X'_d)}{T'_{do}}$$

$$C_2 = \frac{Y_g\,(X'_d - X''_d)}{T''_{do}}$$

$$C_3 = \frac{Y_g\,(X_q - X''_q)}{T''_{qo}}$$

$$A_{g42} = -\frac{1}{2H}(E''^{o}_{d}\,Y_g\,X''_q + I^o_q + E''^{o}_{q}\,Y_g\,R_a)$$

$$A_{g43} = -\frac{1}{2H}(I^o_d + E''^{o}_{d}\,Y_g\,R_a - E''^{o}_{q}\,Y_g\,X''_d)$$

$$A_{g45} = -\frac{1}{2H}[-E''^{o}_{d}\,Y_g(V^o_q\,R_a - V^o_d\,X''_q) + E''^{o}_{q}\,Y_g(V^o_q\,X''_d + V^o_d\,R_a)]$$

$$C_{g41} = -\frac{1}{2H}[-E''^{o}_{d} Y_g (R_a \cos^o \delta - X''_q \sin^o \delta) + E''^{o}_{q} Y_g (X''_d \cos^o \delta + R_a \sin^o \delta)]$$

$$C_{g42} = -\frac{1}{2H}[-E''^{o}_{d} Y_g (R_a \sin^o \delta + X''_q \cos^o \delta) + E''^{o}_{q} Y_g (X''_d \sin^o \delta - R_a \cos^o \delta)]$$

Similarly, the interface *i*-th generator-network equation expressed in the D-Q reference frame is obtained from substituting equation (A.8) into equation (A.7) and then equation (A.7) into equation (A.9)

$$\Delta I_{gi} = [W_{ggi}] \Delta x_{ggi} + [N_{ggi}] \Delta V_{gi} \tag{A.11}$$

where

$\Delta I_{gi} = [\Delta I_{gDi} \;\; \Delta I_{gQi}]^T$ = the *i*-th generator current injections into the network

$$[W_{ggi}] = \begin{bmatrix} 0 & Y_g (X''_q \cos^o \delta - R_a \sin^o \delta) & Y_g (R_a \cos^o \delta + X''_d \sin^o \delta) & 0 & W_{15} \\ 0 & Y_g (X''_q \sin^o \delta + R_a \cos^o \delta) & Y_g (R_a \sin^o \delta - X''_d \cos^o \delta) & 0 & W_{25} \end{bmatrix}$$

and

$$[N_{ggi}] = Y_g \begin{bmatrix} -[R_a + (X''_d - X''_q) \cos^o \delta \sin^o \delta] & -(X''_q \cos^{2o} \delta + X''_d \sin^{2o} \delta) \\ (X''_q \sin^{2o} \delta + X''_d \cos^{2o} \delta) & -[R_a - (X''_d - X''_q) \cos^o \delta \sin^o \delta] \end{bmatrix}$$

with

$$W_{15} = -[Y_g (R_a V^o_Q - X''_q V^o_d \cos^o \delta + X''_d V^o_q \sin^o \delta) + I^o_Q]$$

$$W_{25} = [Y_g (R_a V^o_D + X''_q V^o_d \sin^o \delta + X''_d V^o_q \cos^o \delta) + I^o_D]$$

A.2 EXCITATION SYSTEM MODELS

Upon linearization of equations (3.34) through (3.46) about a system operating point, the block-diagonal elements of matrices $[A_{egi}]$ and $[C_{egi}]$ as defined in equation (3.47) are

Fast Exciter Model

$$[A_{egi}]=\begin{bmatrix} -\frac{1}{T_t} & 0 & 0 & 0 & 0 & 0 & 0 \\ -\frac{1}{T_2}(1-\frac{T_1}{T_2}) & -\frac{1}{T_2} & 0 & 0 & 0 & 0 & 0 \\ -\frac{G_a}{T_a}\frac{T_1}{T_2} & \frac{G_a}{T_a} & -\frac{1}{T_a} & 0 & 0 & 0 & 0 \\ 0 & 0 & \frac{G_o}{T_o} & -\frac{1}{T_o} & -K_f\frac{G_o}{T_o}\frac{T_3}{T_4} & -\frac{G_o}{T_o} & 0 \\ 0 & 0 & 0 & \frac{G_c}{T_c} & -\frac{1}{T_c} & 0 & 0 \\ 0 & 0 & 0 & 0 & \frac{K_f}{T_4}(1-\frac{T_3}{T_4}) & -\frac{1}{T_4} & 0 \\ 0 & 0 & 0 & \frac{G_c}{T_c} & (\frac{1}{T_g}-\frac{1}{T_c}) & 0 & -\frac{1}{K_g T_g} \end{bmatrix}$$

and

$$[C_{egi}]=\begin{bmatrix} \frac{G_t}{T_t}\frac{V_D^o}{V_t^o} & \frac{G_t}{T_t}\frac{V_Q^o}{V_t^o} \\ 0 & 0 \\ 0 & 0 \\ 0 & 0 \\ 0 & 0 \\ 0 & 0 \\ 0 & 0 \end{bmatrix}$$

Slow Exciter Model

$$[A_{egi}]=\begin{bmatrix} -\frac{1}{T_t} & 0 & 0 & 0 \\ -\frac{G_a}{T_a} & -\frac{1}{T_a} & 0 & 0 \\ 0 & 0 & -\frac{1}{T_f} & \frac{K_f}{T_f^2} \\ 0 & \frac{G_o}{T_f} & \frac{G_o}{T_f} & -\frac{1}{T_f}(1+\frac{G_o K_f}{T_f}) \end{bmatrix}$$

and

$$[C_{egi}]=\begin{bmatrix} \frac{G_t}{T_t}\frac{V_D^o}{V_t^o} & \frac{G_t}{T_t}\frac{V_Q^o}{V_t^o} \\ 0 & 0 \\ 0 & 0 \\ 0 & 0 \end{bmatrix}$$

Since

$$V_t^2 = V_D^2 + V_Q^2 \tag{A.12}$$

then

$$\Delta V_t = \frac{V_D^o}{V_t^o}\Delta V_D + \frac{V_Q^o}{V_t^o}\Delta V_Q \tag{A.13}$$

A.3 SPEED-GOVERNING SYSTEM MODEL

Upon linearization of equations (3.48) and (3.49) about a system operating point, the block-diagonal elements of the matrix $[A_{sgi}]$ as defined in equation (3.50) are

$$[A_{sgi}] = \begin{bmatrix} -\frac{1}{T_1} & 0 \\ \frac{1}{T_2}(1-\frac{T_3}{T_1}) & -\frac{1}{T_2} \end{bmatrix}$$

APPENDIX B

CONTROLLABLE PHASE SHIFTER REPRESENTATION

The linearization of equations (2.8), (3.73), (3.74), (3.75), (3.76) and (3.77) about a system operating point, after some manipulations, gives

$$\Delta P_{ik} = \left[(V^o_{cDi} V^o_{cDk} + V^o_{cQi} V^o_{cQk}) \frac{\sec^{2o}\phi}{x} \right] [\Delta\phi]$$

$$+ \frac{\tan^o\phi V^o_{cDk} - V^o_{cQk}}{x} \Delta V_{cDi} + \frac{\tan^o\phi V^o_{cQk} + V^o_{cDk}}{x} \Delta V_{cQi}$$

$$+ \frac{\tan^o\phi V^o_{cDi} + V^o_{cQi}}{x} \Delta V_{cDk} + \frac{\tan^o\phi V^o_{cQi} - V^o_{cDi}}{x} \Delta V_{cQk} \qquad \text{(B.1)}$$

$$\Delta \dot{C}_1 = -\frac{1}{T_m} \Delta P_{ik} - \frac{1}{T_m} \Delta C_1 \qquad \text{(B.2)}$$

$$\Delta \dot{C}_2 = \frac{1}{T_w} \Delta C_1 - \frac{1}{T_w} \Delta C_2 \qquad \text{(B.3)}$$

$$\Delta \dot{C}_3 = \frac{K_g}{T_g} \Delta C_1 - \frac{K_g}{T_g} \Delta C_2 - \frac{1}{T_g} \Delta C_3 \qquad \text{(B.4)}$$

$$\Delta \dot{C}_4 = \frac{1}{T_2}(1 - \frac{T_1}{T_2}) \Delta C_3 - \frac{1}{T_2} \Delta C_4 \qquad \text{(B.5)}$$

$$\Delta \dot{\phi} = \frac{K_g}{T_g} \frac{T_1}{T_2} \frac{T_3}{T_4} \Delta C_1 - \frac{K_g}{T_g} \frac{T_1}{T_2} \frac{T_3}{T_4} \Delta C_2$$

$$+ [\frac{T_1}{T_2} \frac{1}{T_4}(1 - \frac{T_3}{T_g}) + \frac{1}{T_2} \frac{T_3}{T_4}(1 - \frac{T_1}{T_2})] \Delta C_3 + \frac{1}{T_4}(1 - \frac{T_3}{T_2}) \Delta C_4 - \frac{1}{T_4} \Delta\phi \qquad \text{(B.6)}$$

By substituting equation (B.1) into equation (B.2) and then assembling equations (B.2), (B.3), (B.4), (B.5) and (B.6) in equation (3.78), the following open-loop state equation in linearized form for the i-th CPS can be obtained

$$\Delta \dot{x}_{ci} = [A_{ci}]\Delta x_{ci} + [C_{ci}]\Delta V_{ci} + [B_1]\Delta u_{ci} \tag{B.7}$$

or

$$\begin{bmatrix} \Delta \dot{C}_{1i} \\ \Delta \dot{C}_{2i} \\ \Delta \dot{C}_{3i} \\ \Delta \dot{C}_{4i} \\ \Delta \dot{\phi}_i \end{bmatrix} = \begin{bmatrix} -\frac{1}{T_m} & 0 & 0 & 0 & 0 \\ \frac{1}{T_w} & -\frac{1}{T_w} & 0 & 0 & 0 \\ \frac{K_g}{T_g} & -\frac{K_g}{T_g} & -\frac{1}{T_g} & 0 & 0 \\ 0 & 0 & \frac{1}{T_2}(1-\frac{T_1}{T_2}) & -\frac{1}{T_2} & 0 \\ A_{51} & A_{52} & A_{53} & \frac{1}{T_4}(1-\frac{T_3}{T_2}) & 0 \end{bmatrix} \begin{bmatrix} \Delta C_{1i} \\ \Delta C_{2i} \\ \Delta C_{3i} \\ \Delta C_{4i} \\ \Delta \phi_i \end{bmatrix}$$

$$+ \begin{bmatrix} C_{11} & C_{12} & C_{13} & C_{14} \\ 0 & 0 & 0 & 0 \\ 0 & 0 & 0 & 0 \\ 0 & 0 & 0 & 0 \\ 0 & 0 & 0 & 0 \end{bmatrix} \begin{bmatrix} \Delta V_{ciDi} \\ \Delta V_{ciQi} \\ \Delta V_{ciDk} \\ \Delta V_{ciQk} \end{bmatrix} + \begin{bmatrix} B_{11} \\ 0 \\ 0 \\ 0 \\ B_{51} \end{bmatrix} [\Delta \phi_i]$$

where

$$A_{51} = \frac{K_g}{T_g}\frac{T_1}{T_2}\frac{T_3}{T_4}$$

$$A_{52} = -\frac{K_g}{T_g}\frac{T_1}{T_2}\frac{T_3}{T_4}$$

$$A_{53} = \frac{T_1}{T_2}\frac{1}{T_4}(1-\frac{T_3}{T_g}) + \frac{1}{T_2}\frac{T_3}{T_4}(1-\frac{T_1}{T_2})$$

$$C_{11} = -\frac{1}{T_m}(\frac{\tan^o\phi V^o_{cDk} - V^o_{cQk}}{x})$$

$$C_{12} = -\frac{1}{T_m}(\frac{\tan^o\phi V^o_{cQk} + V^o_{cDk}}{x})$$

$$C_{13} = -\frac{1}{T_m}(\frac{\tan^o\phi V^o_{cDi} + V^o_{cQi}}{x})$$

$$C_{14} = -\frac{1}{T_m}(\frac{\tan^o\phi V^o_{cQi} - V^o_{cDi}}{x})$$

$$B_{11} = -\frac{1}{T_m}(V^o_{cDi}V^o_{cDk} + V^o_{cQi}V^o_{cQk})\frac{\sec^{2o}\phi}{x}$$

$$B_{51} = -\frac{1}{T_4}$$

Alternatively, in closed-loop representation

$$\Delta \dot{x}_{ci} = [A_{ci}]\Delta x_{ci} + [C_{ci}]\Delta V_{ci} \tag{B.8}$$

or

$$\begin{bmatrix} \Delta \dot{C}_{1i} \\ \Delta \dot{C}_{2i} \\ \Delta \dot{C}_{3i} \\ \Delta \dot{C}_{4i} \\ \Delta \dot{\phi}_i \end{bmatrix} = \begin{bmatrix} -\frac{1}{T_m} & 0 & 0 & 0 & B_{11} \\ \frac{1}{T_w} & -\frac{1}{T_w} & 0 & 0 & 0 \\ \frac{K_g}{T_g} & -\frac{K_g}{T_g} & -\frac{1}{T_g} & 0 & 0 \\ 0 & 0 & \frac{1}{T_2}(1-\frac{T_1}{T_2}) & -\frac{1}{T_2} & 0 \\ A_{51} & A_{52} & A_{53} & \frac{1}{T_4}(1-\frac{T_3}{T_2}) & B_{51} \end{bmatrix} \begin{bmatrix} \Delta C_{1i} \\ \Delta C_{2i} \\ \Delta C_{3i} \\ \Delta C_{4i} \\ \Delta \phi_i \end{bmatrix}$$

$$+ \begin{bmatrix} C_{11} & C_{12} & C_{13} & C_{14} \\ 0 & 0 & 0 & 0 \\ 0 & 0 & 0 & 0 \\ 0 & 0 & 0 & 0 \\ 0 & 0 & 0 & 0 \end{bmatrix} \begin{bmatrix} \Delta V_{ciDi} \\ \Delta V_{ciQi} \\ \Delta V_{ciDk} \\ \Delta V_{ciQk} \end{bmatrix}$$

Similarly, by linearizing equations (3.69) through (3.72), the following interface i-th CPS-network equation in open-loop representation can be obtained

$$\Delta I_{ci} = [W_{ci}]\Delta x_{ci} + [N_{ci}]\Delta V_{ci} + [B_2]\Delta u_{ci} \tag{B.9}$$

or

$$\begin{bmatrix} \Delta I_{ciDi} \\ \Delta I_{ciQi} \\ \Delta I_{ciDk} \\ \Delta I_{ciQk} \end{bmatrix} = \begin{bmatrix} 0 & 0 & 0 & 0 & 0 \\ 0 & 0 & 0 & 0 & 0 \\ 0 & 0 & 0 & 0 & 0 \\ 0 & 0 & 0 & 0 & 0 \end{bmatrix} \begin{bmatrix} \Delta C_{1i} \\ \Delta C_{2i} \\ \Delta C_{3i} \\ \Delta C_{4i} \\ \Delta \phi_i \end{bmatrix}$$

$$+ \begin{bmatrix} 0 & -\frac{\tan^{2o}\phi}{x} & -\frac{\tan^{o}\phi}{x} & 0 \\ \frac{\tan^{2o}\phi}{x} & 0 & 0 & -\frac{\tan^{o}\phi}{x} \\ \frac{\tan^{o}\phi}{x} & 0 & 0 & 0 \\ 0 & \frac{\tan^{o}\phi}{x} & 0 & 0 \end{bmatrix} \begin{bmatrix} \Delta V_{ciDi} \\ \Delta V_{ciQi} \\ \Delta V_{ciDk} \\ \Delta V_{ciQk} \end{bmatrix}$$

$$+ \begin{bmatrix} -(2\tan^{o}\phi V^{o}_{cQi} + V^{o}_{cDk})\frac{\sec^{2o}\phi}{x} \\ (2\tan^{o}\phi V^{o}_{cDi} - V^{o}_{cQk})\frac{\sec^{2o}\phi}{x} \\ V^{o}_{cDi}\frac{\sec^{2o}\phi}{x} \\ V^{o}_{cQi}\frac{\sec^{2o}\phi}{x} \end{bmatrix} \begin{bmatrix} \Delta \phi_i \end{bmatrix}$$

Alternatively, in closed-loop representation

$$\Delta I_{ci} = [W_{ci}]\Delta x_{ci} + [N_{ci}]\Delta V_{ci} \tag{B.10}$$

or

$$\begin{bmatrix} \Delta I_{ciDi} \\ \Delta I_{ciQi} \\ \Delta I_{ciDk} \\ \Delta I_{ciQk} \end{bmatrix} = \begin{bmatrix} 0 & 0 & 0 & 0 & -(2\tan^o\phi V^o_{cQi} + V^o_{cDk})\dfrac{\sec^{2o}\phi}{x} \\ 0 & 0 & 0 & 0 & (2\tan^o\phi V^o_{cDi} - V^o_{cQk})\dfrac{\sec^{2o}\phi}{x} \\ 0 & 0 & 0 & 0 & V^o_{cDi}\dfrac{\sec^{2o}\phi}{x} \\ 0 & 0 & 0 & 0 & V^o_{cQi}\dfrac{\sec^{2o}\phi}{x} \end{bmatrix} \begin{bmatrix} \Delta C_{1i} \\ \Delta C_{2i} \\ \Delta C_{3i} \\ \Delta C_{4i} \\ \Delta\phi_i \end{bmatrix}$$

$$+ \begin{bmatrix} 0 & -\dfrac{\tan^{2o}\phi}{x} & -\dfrac{\tan^o\phi}{x} & 0 \\ \dfrac{\tan^{2o}\phi}{x} & 0 & 0 & -\dfrac{\tan^o\phi}{x} \\ \dfrac{\tan^o\phi}{x} & 0 & 0 & 0 \\ 0 & \dfrac{\tan^o\phi}{x} & 0 & 0 \end{bmatrix} \begin{bmatrix} \Delta V_{ciDi} \\ \Delta V_{ciQi} \\ \Delta V_{ciDk} \\ \Delta V_{ciQk} \end{bmatrix}$$

APPENDIX C

LOAD REPRESENTATION

C.1 STATIC LOAD MODELS

Assuming loads as current sources, the elements of the matrix $[N_L]$ as described in equation (3.86) are

$$[N_L 11] = \frac{1}{V_L^2}\left\{P_L + (K_p - 2)\frac{V_{LD}^2}{V_L^2}P_L + (K_q - 2)\frac{V_{LD}V_{LQ}}{V_L^2}Q_L\right\} \tag{C.1}$$

$$[N_L 12] = \frac{1}{V_L^2}\left\{Q_L + (K_q - 2)\frac{V_{LQ}^2}{V_L^2}Q_L + (K_p - 2)\frac{V_{LD}V_{LQ}}{V_L^2}P_L\right\} \tag{C.2}$$

$$[N_L 21] = -\frac{1}{V_L^2}\left\{Q_L + (K_q - 2)\frac{V_{LD}^2}{V_L^2}Q_L - (K_p - 2)\frac{V_{LD}V_{LQ}}{V_L^2}P_L\right\} \tag{C.3}$$

$$[N_L 22] = \frac{1}{V_L^2}\left\{P_L + (K_p - 2)\frac{V_{LQ}^2}{V_L^2}P_L - (K_q - 2)\frac{V_{LD}V_{LQ}}{V_L^2}Q_L\right\} \tag{C.4}$$

C.2 INDUCTION MOTOR MODEL

Matrices $[A_{mi}]$, $[C_{mi}]$, $[W_{mi}]$ and $[N_{mi}]$ as defined in equations (3.98) and (3.99) are expressed in the following way

$$[A_{mi}]=\begin{bmatrix} -\dfrac{(1+X'(X_o-X')Y_m)}{T'_o} & \omega_o S^o+\dfrac{R_1(X_o-X')Y_m}{T'_o} & \omega_o E'^o_{mQ} \\ -A_{m12} & A_{m11} & -\omega_o E'^o_{mD} \\ A_{m31} & A_{m32} & \dfrac{T^o_m(b+2cS^o)}{2H} \end{bmatrix} \quad \text{(C.5)}$$

where

$$A_{m31}=-\frac{1}{2H\omega_o}[I^o_{mD}-(R_1E'^o_{mD}-X'E'^o_{mQ})Y_m]$$

$$A_{m32}=-\frac{1}{2H\omega_o}[I^o_{mQ}-(X'E'^o_{mD}+R_1E'^o_{mQ})Y_m]$$

$$Y_m=\frac{1}{R_1^2+X'^2}$$

$$[C_{mi}]=\begin{bmatrix} \dfrac{X'(X_o-X')Y_m}{T'_o} & -\dfrac{R_1(X_o-X')Y_m}{T'_o} \\ -C_{m12} & C_{m11} \\ -\dfrac{(R_1E'^o_{mD}-X'E'^o_{mQ})Y_m}{2H\omega_o} & -\dfrac{(X'E'^o_{mD}+R_1E'^o_{mQ})Y_m}{2H\omega_o} \end{bmatrix} \quad \text{(C.6)}$$

$$[W_{mi}] = -Y_m \begin{bmatrix} R_1 & X' & 0 \\ -X' & R_1 & 0 \end{bmatrix} \tag{C.7}$$

$$[N_{mi}] = Y_m \begin{bmatrix} R_1 & X' \\ -X' & R_1 \end{bmatrix} \tag{C.8}$$

REFERENCES

1. **Schleif F.R. and White J.H.,** "Damping for the Northwest-Southwest tieline oscillations - an analog study", IEEE Transactions on Power Apparatus and Systems, Vol. PAS-85, No. 12, December 1966, pp. 1239-1247.

2. **Cresap R.L. and Hauer J.F.,** "Emergence of a new swing mode in the western power system", IEEE Transactions on Power Apparatus and Systems, Vol. PAS-100, No. 4, April 1981, pp. 2037-2045.

3. **Fairney W., Myles A., Whitelegg T.M. and Murray N.S.,** "Low frequency oscillations on the 275 kV interconnectors between Scotland and England", CIGRE Paper 31-08, Paris, September 1982.

4. **Bolden R.L., Wallace P.J. and Grainger A.W.,** "Considerations in the improvement of system damping on the south east Australian interconnected system", CIGRE Paper 31-05, Paris, September 1982.

5. **Hsu Y.Y., Shyue S.W. and Su C.C.,** "Low frequency oscillations in longitudinal power systems: experience with dynamic stability of Taiwan power system", IEEE Transactions on Power Systems, Vol. PWRS-2, No. 1, February 1987, pp. 92-100.

6. **Yusof S.B., Alden R.T.H., Rogers G.J. and Kundur P.,** "Small signal stability analysis for damping control of TNB (Malaysia)/PUB (Singapore) interconnected power system", in Proceedings of the International Power Engineering Conference, Singapore, 18-19 March 1993, pp. 272-277.

7. **Yang X., Feliachi A. and Adapa R.,** "Damping enhancement in the western U.S. power system: a case study", IEEE Transactions on Power Systems, Vol. 10, No. 3, August 1995, pp. 1271-1278.

8. **Klein M., Rogers G.J. and Kundur P.,** "A fundamental study of inter-area oscillations in power systems", IEEE Transactions on Power Systems, Vol. 6, No. 3, August 1991, pp. 914-921.

9. **So P.L. and Macdonald D.C.,** "Analytical study of low frequency inter-area oscillations in power systems", in Proceedings of the 30th Universities Power Engineering Conference, University of Greenwich, London, 5-7 September 1995, pp. 854-857.

10. **So P.L. and Macdonald D.C.,** "Analysis and control of inter-area oscillations for system security enhancement", in Proceedings of the 4th IEE International Conference on Power System Control and Management, Savoy Place, London, 16-18 April 1996, pp. 65-70.

11. **So P.L. and Macdonald D.C.,** "Analysis of inter-area oscillations and their stabilization through excitation systems", in Proceedings of the IASTED International Conference on High Technology in the Power Industry, Banff, Alberta, Canada, 6-8 June 1996, pp. 154-158.

12. **IEEE System Oscillations Working Group,** "Inter-area oscillations in power systems", IEEE Power Engineering Society, IEEE Catalog Number: 95 TP 101, October 1994.

13. **EPRI Research Report TR-103704,** "Analysis of stressed interconnected power networks", Report of Research Project 8010-28, Prepared by Iowa State University, March 1994.

14. **Vittal V., Bhatia N. and Fouad A.A.,** "Analysis of the inter-area mode phenomenon in power systems following large disturbances", IEEE Transactions on Power Systems, Vol. 6, No. 4, November 1991, pp. 1515-1521.

15. **Arcidiacono V., Ferrari E., Marconato R. and Saccomanno F.,** "Analysis of factors affecting the damping of low-frequency oscillations in multimachine systems", CIGRE Paper 32-19, Italy, 1976.

16. **Barbier C., Ferrari E. and Johansson K.E.,** "Questionnaire on electromechanical oscillation damping in power systems: report on the answers", ELECTRA, Vol. 64, 1979, pp. 59-90.

17. **Larsen E.V. and Swann D.A.,** "Applying power system stabilizers, Part I, II and III", IEEE Transactions on Power Apparatus and Systems, Vol. PAS-100, No. 6, June 1981, pp. 3017-3046.

18. **Kundur P.,** "Power system stability and control", Book, McGraw-Hill, 1994.

19. **Hurley J. and Keay F.,** "Overview of power system stability concepts", IEEE Tutorial Course on Power System Stabilization Via Excitation Control, 81 EHO 175-0 PWR, 1981, pp. 2.1-2.16.

20. **Veal C.M.J.,** "The damping of power system oscillations by generator control", Ph.D. Thesis, Imperial College, University of London, August 1989.

21. **Kundur P., Klein M., Rogers G.J. and Zywno M.S.,** "Application of power system stabilizers for enhancement of overall system stability", IEEE Transactions on Power Systems, Vol. PWRS-4, No. 2, May 1989, pp. 614-626.

22. **Klein M., Rogers G.J., Moorty S. and Kundur P.,** "Analytical investigation of factors influencing power system stabilizers performance", IEEE Transactions on Energy Conversion, Vol. 7, No. 3, September 1992, pp. 382-390.

23. **Yang X. and Feliachi A.,** "Stabilization of inter-area oscillation modes through excitation systems", Paper No. 93 WM 206-3 PWRS, presented at the IEEE/PES 1993 Winter Meeting, Columbus, OH, January 31 - February 5, 1993.

24. **Lee K.C.,** "Analysis of power system stabilizers application for controlling poorly damped oscillations in the Alcan/B.C. Hydro power systems", IEEE Transactions on Power Systems, Vol. 8, No. 1, February 1993, pp. 255-263.

25. **Veal C.M.J. and Macdonald D.C.,** "A digital power system stabilizer location and design procedure for the damping of inter-area oscillations",

in Proceedings of the 10th Power Systems Computation Conference, Graz, Austria, 19-24 August 1990, pp. 127-134.

26. **IEEE Committee Report,** "HVDC controls for system dynamic performance", IEEE Transactions on Power Systems, Vol. 6, No. 2, May 1991, pp. 743-752.

27. **Brucoli M., Torelli F. and Trovato M.,** "A decentralized control strategy for dynamic shunt Var compensation in interconnected power systems", IEE Proceedings, Vol. 132, Pt. C, No. 5, September 1985, pp. 229-236.

28. **Hingorani N.G.,** "Power electronics in electric utilities: role of power electronics in future power systems", in Proceedings of the IEEE, Vol. 76, No. 4, April 1988, pp. 481-482.

29. **Hingorani N.G.,** "The future of transmission Switching to Silicon" EPRI Journal, June 1989, pp. 5-13.

30. **Hingorani N.G.,** "FACTS - flexible ac transmission system", in Proceedings of the 5th IEE International Conference on AC and DC Power Transmission, Savoy Place, London, 17-20 September 1991, pp. 1-7.

31. **Moore P. and Ashmole P.,** "Flexible ac transmission systems", IEE Power Engineering Journal, Vol. 9, No. 6, December 1995, pp. 282-286.

32. **IEEE Special Stability Controls Working Group,** "Static Var compensator models for power flow and dynamic performance simulation", Paper No. 93 WM 173-5 PWRS, presented at the IEEE/PES 1993 Winter Meeting, Columbus, OH, January 31 - February 5, 1993.

33. **Larsen E.V., Clark K., Miske A.S. and Urbanek J.,** "Characteristics and rating considerations of thyristor controlled series compensation", Paper No. 93 SM 433-3 PWRD, presented at the IEEE/PES 1993 Summer Meeting, Vancouver, B.C., Canada, 18-22 July 1993.

34. **Iravani M.R. and Maratukulam D.,** "Review of semiconductor-controlled (static) phase shifters for power system applications", Paper No. 94 WM 182-6 PWRS, presented at the IEEE/PES 1994 Winter Meeting, New York, New York, January 30 - February 3, 1994.

35. **Gyugyi L.,** "Unified power-flow control concept for flexible ac transmission systems", IEE Proceedings, Vol. 139, Pt. C, No. 4, July 1992, pp. 323-331.

36. **Gyugyi L.,** " Dynamic compensation of ac transmission lines by solid-state synchronous voltage sources", Paper No. 93 SM 434-1 PWRD, presented at the IEEE/PES 1993 Summer Meeting, Vancouver, B.C., Canada, 18-22 July 1993.

37. **Larsen E.V., Sanchez-Gasca J.J. and Chow J.H.,** "Concepts for design of FACTS controllers to damp power swings", IEEE Transactions on Power Systems, Vol. 10, No. 2, May 1995, pp. 948-956.

38. **Noroozian M. and Andersson G.,** "Damping of power system oscillations by use of controllable components" IEEE Transactions on Power Delivery, Vol. 9, No. 4, October 1994, pp. 2046-2054.

39. **Arabi S. and Kundur P.,** "A versatile FACTS device model for power flow and stability simulations" IEEE Transactions on Power Systems, Vol. 11, No. 4, November 1996, pp. 1944-1950.

40. **Noroozian M., Angquist L., Ghandhari M. and Andersson G.,** "Series-connected FACTS devices control strategy for damping of electromechanical oscillations", in Proceedings of the 12th Power Systems Computation Conference, Dresden, Germany, 19-23 August 1996, pp. 1090-1096.

41. **Wang H.F. and Swift F.J.,** "A unified model for the analysis of FACTS devices in damping power system oscillations PART I: Single-machine infinite-bus power systems", Paper No. 96 SM 464-8 PWRD, presented at the IEEE/PES 1996 Summer Meeting, Denver, Colorado, July 28 - August 1, 1996.

42. **Noroozian M. and Andersson G.,** "Damping of inter-area and local modes by use of controllable components" Paper No. 95 WM 267-5 PWRD, presented at the IEEE/PES 1995 Winter Meeting, New York, New York, January 29 - February 2, 1995.

43. **Lyman W.J.,** "Controlling power flow with phase shifting equipment", AIEE Transactions, Vol. 49, July 1930, pp. 825-831.

44. **Lyman W.J. and North J.R.,** "Application of large phase-shifting transformer on an interconnected system loop", AIEE Transactions, Vol. 57, October 1938, pp. 579-587.

45. **Blume L.F.,** "Phase-angle control", in Transformer Engineering, John Wiley & Sons Inc., 1951.

46. **Humphries M.B.,** "Stretching transmission capacity in the UK", IEEE Power Engineering Review, Vol. 16, No. 11, November 1996, pp. 11-12.

47 **Eilts L.E.,** "Phase shifters within the Western interconnection", Current Activity in Flexible AC Transmission Systems, IEEE 92 TH 0465-5 PWR, April 1992, pp. 53-59.

48. **Dobsa J.,** "Transformers for in-phase, phase-angle and quadrature phase regulation", Brown Boveri Review, Vol. 8, 1972, pp. 376-383.

49. **Arrillaga J. and Duke R.M.,** "Thyristor-controlled quadrature boosting", IEE Proceedings, Vol. 126, No. 6, June 1979, pp. 493-498.

50. **Mathur R.M. and Basati R.S.,** "A thyristor controlled static phase-shifter for ac power transmission", IEEE Transactions on Power Apparatus and Systems, Vol. PAS-100, No. 5, May 1981, pp. 2650-2655.

51. **Han Z.X.,** "Phase shifter and power flow control", IEEE Transactions on Power Apparatus and Systems, Vol. PAS-101, No. 10, October 1982, pp. 3790-3795.

52. **Xing K. and Kusic G.,** "Application of thyristor-controlled phase shifters to minimize real power losses and augment stability of power systems", IEEE Transactions on Energy Conversion, Vol. 3, No. 4, December 1998, pp. 792-798.

53. **Noroozian M. and Andersson G.,** "Power flow control by use of controllable series components", IEEE Transactions on Power Delivery, Vol. 8, No. 3, July 1993, pp. 1420-1429.

54. **Baker R., Guth G., Egli W. and Eglin P.,** "Control algorithm for a static phase shifting transformer to enhance transient and dynamic stability of large power systems", IEEE Transactions on Power Apparatus and Systems, Vol. PAS-101, No. 9, September 1982, pp. 3532-3542.

55. **Sharaf A.M. and Doraiswami R.,** "Stabilizing an ac link by using static phase shifters", IEEE Transactions on Power Apparatus and Systems, Vol. PAS-102, No. 4, April 1983, pp. 788-796.

56. **Sharaf A.M. and Doraiswami R.,** "Dynamic simulation of stability enhancement tools and comparison of control strategies", IEEE Transactions on Power Apparatus and Systems, Vol. PAS-102, No. 6, June 1983, pp. 1886-1893.

57. **Sharaf A.M. and Sivakumar S.,** "Stabilizing interconnected power systems using static phase shifters", Electric Power Systems Research, Vol. 8 (1984/85), pp. 249-259.

58. **La Scala M., Sbrizzai R., Torelli F. and Trovato M.,** "Enhancement of interconnected power system stability using a control strategy involving static phase shifters", International Journal of Electrical Power & Energy Systems, Vol. 15, No. 6, 1993, pp. 387-396.

59. **Iravani M.R., Dandeno P.L. and Maratukulam D.,** "Applications of static phase shifters in power systems", Paper No. 94 WM 068-7 PWRD, presented at the IEEE/PES 1994 Winter Meeting, New York, New York, January 30 - February 3, 1994.

60. **Gronquist J.F., Sethares W.A., Alvarado F.L. and Lasseter R.H.,** "Power oscillation damping control strategies for FACTS devices using locally measurable quantities" Paper No. 95 WM 185-9 PWRS, presented at the IEEE/PES 1995 Winter Meeting, New York, New York, January 29 - February 2, 1995.

61. **So P.L. and Macdonald D.C.,** "Stabilization of inter-area modes by controllable phase shifter", in Proceedings of the 4th IEEE AFRICON International Conference, Stellenbosch, South Africa, 24-27 September 1996, pp. 419-424.

62. **Kaizu H. and Taniguchi T.,** "Synthesis of a stabilizing control problem for a multimachine power system with phase shifter", Int. J. Control, Vol. 43, No. 2, 1986, pp. 689-703.

63. **Iravani M.R. and Mathur R.M.,** "Damping subsynchronous oscillations in power systems using a static phase-shifter", IEEE Transactions on Power Systems, Vol. PWRS-1, No. 2, May 1986, pp. 76-83.

64. **Iravani M.R. and Mathur R.M.,** "Two countermeasures for damping torsional interactions and transient torques of turbine-generators", IEEE Transactions on Power Systems, Vol. PWRS-2, No. 2, May 1987, pp. 406-412.

65. **O'Kelly D. and Musgrave G.,** "Improvement of power-system transient stability by phase-shift insertion", IEE Proceedings, Vol. 120, No. 2, February 1973, pp. 247-252.

66. **Arnold C.P., Duke R.M. and Arrillaga J.,** "Transient stability improvement using thyristor controlled quadrature voltage injection", IEEE Transactions on Power Apparatus and Systems, Vol. PAS-100, No. 3, March 1981, pp. 1382-1388.

67. **Abdel-Aty Edris,** "Enhancement of first-swing stability using a high-speed phase shifter", IEEE Transactions on Power Systems, Vol. 6, No. 3, August 1991, pp. 1113-1118.

68. **Stemmler H. and Guth G.,** "The thyristor-controlled static phase shifter - a new tool for power flow control in ac transmission systems", Brown Boveri Review, Vol. 3, 1982, pp. 73-78.

69. **Angquist L., Lundin B. and Samuelsson J.,** "Power oscillation damping using controlled reactive power compensation - a comparison between series and shunt approaches" IEEE Transactions on Power Systems, Vol. 8, No. 2, May 1993, pp. 687-700.

70. **Gyugyi L.,** "Fundamentals of thyristor-controlled static Var compensators in electric power system applications", IEEE Special Symposium on Application of Static Var Systems for System Dynamic Performance, IEEE Publication 87TH0187-5-PWR, 1987.

71. **Laughton M.A.,** "Matrix analysis of dynamic stability in synchronous multimachine systems", IEE Proceedings, Vol. 113, No. 2, February 1966, pp. 325-326.

72. **Undrill J.M.,** "Dynamic stability calculations for an arbitrary number of interconnected synchronous machines", IEEE Transactions on Power Apparatus and Systems, Vol. PAS-87, No. 3, March 1968, pp. 835-844.

73. **Demello F.P. and Concordia C.,** "Concepts of synchronous machine stability as affected by excitation control", IEEE Transactions on Power Apparatus and Systems, Vol. PAS-88, No. 4, April 1969, pp. 316-329.

74. **Moussa H.A.M. and Yu Y.N.,** "Dynamic interaction of multi-machine power system and excitation control", IEEE Transactions on Power Apparatus and Systems, Vol. PAS-93, 1974, pp. 1150-1158.

75. **Byerly R.T., Sherman D.E. and McLain D.K.,** "Normal modes and mode shapes applied to dynamic stability analysis", IEEE Transactions on Power Apparatus and Systems, Vol. PAS-94, No. 2, March/April 1975, pp. 224-229.

76. **Elrazaz Z. and Sinha N.K.,** "Dynamic stability evaluation for multimachine system: an efficient eigenvalue approach", IEE Proceedings, Vol. 128, Pt. D, No. 6, November 1981, pp. 268-274.

77. **Gross G., Imparato C.F. and Look P.M.,** "A tool for the comprehensive analysis of power system dynamic stability", IEEE Transactions on Power Apparatus and Systems, Vol. PAS-101, No. 1, January 1982, pp. 226-234.

78. **Lim C.M. and Elangovan S.,** "Design of stabilizers in multi-machine power systems", IEE Proceedings, Vol. 132, Pt. C, No. 3, May 1985, pp. 146-153.

79. **Tse C.T. and Tso S.K.,** "Approach to the study of small-perturbation stability of multimachine systems", IEE Proceedings, Vol. 135, Pt. C, No. 5, September 1988, pp. 396-405.

80. **Brucoli M., Torelli F. and Trovato M.,** "State space representation of interconnected power systems for dynamic interaction studies", Electric Power Systems Research, Vol. 5, 1982, pp. 315-330.

81. **Rogers G.J. and Kundur P.,** "Small signal stability of power systems", IEEE Symposium on Eigenanalysis and Frequency Domain Methods for System Dynamic Performance, IEEE Publication 90TH0292-3-PWR, 1989, pp. 5-12.

82. **Kundur P., Rogers G.J., Wong D.Y., Wang L. and Lauby M.G.,** "A comprehensive computer program package for small signal stability analysis of power systems", IEEE Transactions on Power Systems, Vol. 5, No. 4, November 1990, pp. 1076-1083.

83. **Arabi S., Rogers G.J., Wong D.Y., Kundur P. and Lauby M.G.,** "Small signal stability program analysis of SVC and HVDC in ac power systems", IEEE Transactions on Power Systems, Vol. 6, No. 3, August 1991, pp. 1147-1153.

84. **Dommel H.W. and Sato N.,** "Fast transient stability solutions", IEEE Transactions on Power Apparatus and Systems, Vol. PAS-91, No. 4, July/August 1972, pp. 1643-1650.

85. **Roman-Messina A. and Cory B.J.,** "Enhancement of dynamic stability by coordinated control of static Var compensators", International Journal of Electrical Power & Energy Systems, Vol. 15, No. 2, 1993, pp. 85-93.

86. **Martins N.,** "Efficient eigenvalue and frequency response methods applied to power system small-signal stability studies", IEEE Transactions on Power Systems, Vol. PWRS-1, No. 1, February 1986, pp. 217-226.

87. **Perez-Arriaga I.J., Verghese G.C. and Scweppe F.C.,** "Selective modal analysis with applications to electric power systems, Part I: heuristic introduction", IEEE Transactions on Power Apparatus and Systems, Vol. PAS-101, No. 9, September 1982, pp. 3117-3125.

88. **Hauer J.F.,** "Introduction to the 1989 IEEE/PES Symposium on eigenanalysis and frequency domain methods for system dynamic performance ", IEEE Symposium on Eigenanalysis and Frequency Domain Methods for System Dynamic Performance, IEEE Publication 90TH0292-3-PWR, 1989, pp. 1-4.

89. **Lou G.J., Xu X.H., Long S.Q. and Li Q.C.,** "Low frequency oscillations on the interconnectors between Hong Kong and Guangdong", in Proceedings of the Chinese Society of Electrical Engineering, Vol. 6, No. 1, January 1986, pp. 29-35.

90. **Park R.H.,** "Two-reaction theory of synchronous machines. Generalized method of analysis - Part I", AIEE Transactions, Vol. 48, July 1929, pp. 716-730.

91. **Park R.H.,** "Two-reaction theory of synchronous machines. Part II", AIEE Transactions, Vol. 52, June 1933, pp. 352-355.

92. **Cooper C.B. and Howells E.D.,** "The calculation of power system stability with particular reference to the Victorian system", Electrical

Engineering Transactions, The Institution of Engineers, Australia, September 1965, pp. 75-84.

93. **Alden R.T.H. and Zein El-Din H.M.,** "Multi-machine dynamic stability calculations", IEEE Transactions on Power Apparatus and Systems, Vol. PAS-95, No. 5, September/October 1976, pp. 1529-1534.

94. **Yu Y.N.,** "Electric power system dynamics", Book, Academic Press, New York, 1983.

95. **Roman-Messina A.,** "Coordination of static Var compensators to damp power and voltage oscillations", Ph.D. Thesis, Imperial College, University of London, November 1990.

96. **Taranto G.N., Pinto L.M.V.G. and Pereira M.V.F.,** "Representation of FACTS devices in power system economic dispatch", IEEE Transactions on Power Systems, Vol. 7, No. 2, May 1992, pp. 572-576.

97. **Milanovic J.V. and Hiskens I.A.,** "Effects of load dynamics on power system damping", IEEE Transactions on Power Systems, Vol. 10, No. 2, May 1995, pp. 1022-1028.

98. **Makarov Y.V., Maslennikov V.A. and Hill D.J.,** "Revealing loads having the biggest influence on power system small disturbance stability", IEEE Transactions on Power Systems, Vol. 11, No. 4, November 1996, pp. 2018-2023.

99. **Dovan T., Dillion T.S., Berger C.S. and Forward K.E.,** "A micro-computer based on-line identification approach to power system dynamic load modelling", IEEE Transactions on Power Systems, Vol. 2, No. 3, August 1987, pp. 529-536.

100. **Arrillaga J., Arnold C.P. and Harker B.J.,** "Computer modelling of electrical power systems", Book, John Wilely & Sons, 1983.

101. **Roa-Sepulveda C.A.,** "Dynamic simulation of voltage instability phenomena", Ph.D. Thesis, Imperial College, University of London, November 1992.

102. **Taylor D.G.,** "Analysis of synchronous machines connected to power-system networks", IEE Proceedings, Vol. 109, Pt. C, July 1962, pp. 606-610.

103. **Mitten R. and Lee Y.B.,** "Interconnected operation of the China Light power system", IEE International Conference on APSCOM, Hong Kong, November 1991, pp. 530-533.

104. **Tse C.T. and Tso S.K.,** "Modal and eigenvalue sensitivity analyses of power oscillations in interconnected systems", IEE International Conference on APSCOM, Hong Kong, November 1991, pp. 808-814.

105. **Shih L.J., Lee S.Y., Chen K.K. and Lin C.Y.,** "Experience with low frequency oscillation in Taiwan power system", in Proceedings of the International Power Engineering Conference, Singapore, 18-19 March 1993, pp. 332-337.

106. **Hsu Y.Y. and Chen C.L.,** "Identification of optimum location for stabilizer applications using participation factors", IEE Proceedings, Vol. 134, Pt. C, No. 3, May 1987, pp. 238-224.

107. **Lal J. and Fleming R.J.,** "Discussion by J. Lal and R.J. Fleming on Coordinated application of stabilizers in multimachine power systems", IEEE Transactions on Power Apparatus and Systems, Vol. PAS-99, No. 3, May/June 1980, pp. 892-901.

108. **Rouco L. and Pagola F.L.,** "An eigenvalue sensitivity approach to location and controller design of controllable series capacitors for damping power system oscillations" Paper No. PE-547-PWRS-0-01-1997, presented at the IEEE/PES 1997 Winter Meeting, New York, 2-6 February 1997.

109. **Nagata M., Yokoyama A. and Sekine Y.,** "Stabilization of inter-area and/or oscillatory modes in large-scale power system by VIPS apparatus

based on decentralized control scheme" Paper No. SPT PS 09-01-0087, presented at the IEEE/KTH Stockholm Power Tech Conference, Stockholm, Sweden, 18-22 June 1995, pp. 262-267.

110. **Van Ness J.E., Boyle J.M. and Imad F.P., ,** "Sensitivities of large, multiple-loop control systems", IEEE Transactions on Automatic Control, Vol. AC-10, July 1965, pp. 308-315.

111. **Tse C.T. and Tso S.K.,** "Design optimisation of power system stabilisers based on modal and eigenvalue-sensitivity analyses", IEE Proceedings, Vol. 135, Pt. C, No. 5, September 1988, pp. 406-415.

112. **Eilts L.E. and Easton R.H.,** "Example system study for liberty phase-shifter retrofit with thyristor switches", FACTS Applications, Report prepared by the FACTS Application Task Force of the FACTS Working Group, IEEE Power Engineering Society, IEEE Catalog Number: 96 TP 116-0, 1996, pp. 8-9 ~ 8-11.

113. **Nabavi-Niaki and Iravani M.R.,** "Steady-state and dynamic models of unified power flow controller (UPFC) for power system studies", IEEE Transactions on Power Systems, Vol. 11, No. 4, November 1996, pp. 1937-1943.

114. **Edris A., Gyugyi L., Rietman T.R., Schauder C.D., Torgerson D.R. and Williams S.L.,** "The unified power flow controller: a new approach to power transmission control", FACTS Applications, Report prepared by the FACTS Application Task Force of the FACTS Working Group, IEEE Power Engineering Society, IEEE Catalog Number: 96 TP 116-0, 1996, pp. 8-29 ~ 8-38.

115. **Schauder C.D., Gyugyi L., Lund M.R., Hamai D.M., Rietman T.R., Torgerson D.R. and Edris A.,** "Operation of the unified power flow controller (UPFC) under practical constraints" Paper No. PE-511-PWRD-0-11-1996, presented at the IEEE/PES 1997 Winter Meeting, New York, 2-6 February 1997.

BIBL. LO